

University of Windsor

Scholarship at UWindor

Electronic Theses and Dissertations

Theses, Dissertations, and Major Papers

1982

Component magnetization of the iron formation and deposits at the Griffith Mine near Red Lake, Ontario.

Ikramuddin Ahmad. Osmani
University of Windsor

Follow this and additional works at: <https://scholar.uwindsor.ca/etd>

Recommended Citation

Osmani, Ikramuddin Ahmad., "Component magnetization of the iron formation and deposits at the Griffith Mine near Red Lake, Ontario." (1982). *Electronic Theses and Dissertations*. 1503.
<https://scholar.uwindsor.ca/etd/1503>

This online database contains the full-text of PhD dissertations and Masters' theses of University of Windsor students from 1954 forward. These documents are made available for personal study and research purposes only, in accordance with the Canadian Copyright Act and the Creative Commons license—CC BY-NC-ND (Attribution, Non-Commercial, No Derivative Works). Under this license, works must always be attributed to the copyright holder (original author), cannot be used for any commercial purposes, and may not be altered. Any other use would require the permission of the copyright holder. Students may inquire about withdrawing their dissertation and/or thesis from this database. For additional inquiries, please contact the repository administrator via email (scholarship@uwindsor.ca) or by telephone at 519-253-3000ext. 3208.

CANADIAN THESES ON MICROFICHE

I.S.B.N.

THESES CANADIENNES SUR MICROFICHE



National Library of Canada
Collections Development Branch

Canadian Theses on
Microfiche Service

Ottawa, Canada
K1A 0N4

Bibliothèque nationale du Canada
Direction du développement des collections

Service des thèses canadiennes
sur microfiche

NOTICE

The quality of this microfiche is heavily dependent upon the quality of the original thesis submitted for microfilming. Every effort has been made to ensure the highest quality of reproduction possible.

If pages are missing, contact the university which granted the degree.

Some pages may have indistinct print especially if the original pages were typed with a poor typewriter ribbon or if the university sent us a poor photocopy.

Previously copyrighted materials (journal articles, published tests, etc.) are not filmed.

Reproduction in full or in part of this film is governed by the Canadian Copyright Act, R.S.C. 1970, c. C-30. Please read the authorization forms which accompany this thesis.

THIS DISSERTATION
HAS BEEN MICROFILMED
EXACTLY AS RECEIVED

AVIS

La qualité de cette microfiche dépend grandement de la qualité de la thèse soumise au microfilmage. Nous avons tout fait pour assurer une qualité supérieure de reproduction.

S'il manque des pages, veuillez communiquer avec l'université qui a conféré le grade.

La qualité d'impression de certaines pages peut laisser à désirer, surtout si les pages originales ont été dactylographiées à l'aide d'un ruban usé ou si l'université nous a fait parvenir une photocopie de mauvaise qualité.

Les documents qui font déjà l'objet d'un droit d'auteur (articles de revue, examens publiés, etc.) ne sont pas microfilmés.

La reproduction, même partielle, de ce microfilm est soumise à la Loi canadienne sur le droit d'auteur, SRC 1970, c. C-30. Veuillez prendre connaissance des formules d'autorisation qui accompagnent cette thèse.

LA THÈSE A ÉTÉ
MICROFILMÉE TELLE QUE
NOUS L'AVONS REÇUE

COMPONENT MAGNETIZATION OF THE IRON FORMATION
AND DEPOSITS AT THE GRIFFITH MINE
NEAR RED LAKE, ONTARIO

by



Ikramuddin Ahmad Osmani

A Thesis

submitted to the Faculty of Graduate Studies through
the Department of Geology in Partial Fulfillment
of the requirements for the degree of
Master of Science at
The University of Windsor

Windsor, Ontario, Canada
1982

© Ikramuddin Ahmad Osmani 1982
All Rights Reserved

777781

TABLE OF CONTENTS

ABSTRACT.	iv
ACKNOWLEDGEMENTS.	vii
LIST OF FIGURES	xi
LIST OF TABLES.	xv
LIST OF APPENDICES.	xvi
CHAPTER	
I. INTRODUCTION.	1
1.1 Problem and Proposal.	1
1.2 Previous Similar Work and Location of the Area.	2
1.3 History of the Mine	2
II. GEOLOGY	6
2.1 Regional Geology.	6
2.1.1 Metavolcanics.	6
2.1.2 Iron Formation	9
2.1.3 Metasediments.	10
2.1.4 Mafic to Intermediate Intrusive Rocks	10
2.1.5 Intermediate to Felsic Intrusive Rocks	11
2.1.6 Hornblende-Biotite Quarz- diorite and Hornblende- Biotite Diorite.	12
2.1.6a Bruce Lake Pluton	12
2.1.6b Pakwash Lake Pluton	12
2.1.7 Muscovite-Biotite Granodiorite	13
2.1.8 Pleistocene Deposits	13
2.1.9 Recent Deposits.	14
2.1.10 Structure.	14
2.2 Mine Geology.	15
2.2.1 Geological Setting	15
2.2.2 Stratigraphy of the IF	15
2.2.3 Structure.	17
III. EXPERIMENTAL METHODS.	20
3.1 Sampling.	20
3.2 Sample Preparation.	20
3.3 Sample Treatment.	23
3.3.1 Specific Gravity	23
3.3.2 Magnetic Susceptibility.	23

3.3.3	Anisotropy of Magnetic Susceptibility	23
3.3.4	Natural Remanent Magnetization.	24
3.3.5	AF Demagnetization.	24
3.3.6	Thermal Demagnetization	25
3.3.7	Stability Tests	25
3.4	Computations	33
3.5	Magnetic Model	34

IV. RESULTS

4.1	Specific Gravity	35
4.2	Magnetic Susceptibility.	35
4.3	Anisotropy of Magnetic Susceptibility.	39
4.4	Natural Remanent Magnetization	41
4.4.1	Iron Formation.	41
4.4.1a	NRM Intensity	41
4.4.1b	Koenigsberger Ratio (Q)	41
4.4.1c	NRM- k_{\perp} Relationship	50
4.4.1d	Storage Test.	52
4.4.1e	Shock Test.	52
4.4.2	Host Rock NRM	52
4.4.2a	NRM Intensity	52
4.4.2b	Koenigsberger Ratio	52
4.4.2c	Storage Test.	56
4.5	Statistical Analysis	56
4.5.1	Statistical Analysis of IF.	56
4.5.2	Statistical Analysis of HR.	59
4.6	AF Demagnetization of IF	60
4.6.1	Pilot Specimens	60
4.6.2	Remaining Specimens	64
4.6.2a	Conventional Analysis	64
4.6.2b	Modal Analysis of the Paleomagnetic Data.	64
4.7	Fold Test After AF Cleaning.	69
4.8	Thermal Demagnetization of IF Pilot Specimens	80
4.8a	Modal Analysis of Pilot Specimens at 450°C, 500°C, and 550°C	81
4.8b	Fold Test of Thermally Cleaned IF Pilot Specimens.	87
4.9	AF Demagnetization of the Host Rock.	87
4.9.1	Pilot Specimens	87
4.9.2	Remaining Specimens	91
4.9.2a	Conventional Analysis	91
4.9.2b	Modal Analysis of the Paleomagnetic Data.	94
4.9.3	Fold Test After AF Cleaning	99
4.10	Thermal Demagnetization of HR Pilot Specimens.	103

4.11	Dike-HR Baked Contact Test.	108
4.12	Paleomagnetic Ages of the Isolated Remanent Components.	109
4.13	Magnetic Model.	119
4.13.1	Dipping Sheet of Infinite Strike Length.	119
V.	CONCLUSION AND RECOMMENDATIONS.	125
	APPENDICES	129
	REFERENCES	134
	VITAE AUCTORIS	137

ABSTRACT

The magnetic characteristics and the ore genesis of the Algoman-type iron formation (IF) and host rock (HR) at the Griffith Mine Near Red Lake, Ontario, were determined from a study of 175 IF blocks and 54 HR sites. The mean specific gravity (SG) of the IF specimens is 3.36 g/cm^3 , i.e., mixed ore and lean IF. The low field magnetic susceptibility perpendicular to bedding (K_{\perp}) for the IF gives a lognormal mean of $4.0 \times 10^{-2} \text{ cgs/cm}^3$ which is $\lll K_{\perp HR}$ such that the HR values can be neglected in the magnetic anomaly computation. The relationship $K_{\perp} = 0.1159 \text{ SG} - 0.312$ gives a correlation coefficient of $+ .95$ and gives $K_{\perp IF} = 0.15 \text{ cgs/cm}^3$ for economic iron ore. The IF shows anisotropy of susceptibility with $K_{\min} = K_{\perp}$ and $K_{\parallel} = 1.45 K_{\perp}$. Both the HR and IF natural remanent magnetization (NRM) intensities are lognormally distributed with means of 1.47×10^{-5} and $2.1 \times 10^{-2} \text{ emu/cm}^3$ respectively, giving Koenigsberger ratios (Q) of 0.051 and 0.66. In computing the magnetic anomaly for the ore zone the HR NRM and induced magnetization can be neglected and the IF NRM augments the induced magnetization (J_{\perp}) by 14%. Stability tests show that IF NRM's are unstable with significant viscous (VRM) components. Shock tests show that blasting may have reduced the NRM intensity by 40% in

certain specimens close to where blasting had occurred.

After AF and thermal cleaning, the remanence of 27% of the IF samples survive statistical screening tests. Smoothing and contouring of IF, AF and thermal data at the population level isolated two pre-folding and two post-folding remanence components. The pre-folding A, B remanence components are directed at (118°, 71°, 6°) and (208°, 37°, 4°) (declination, inclination, cone of 95% confidence) respectively. The A and B components give apparent paleomagnetic ages (APA) that likely represent a primary and the secondary remanence respectively that IF acquired prior to deformation during Kenoran orogeny. The B component pole falls near the APW path. Its location gives an APA of ~2.7 Ga. The A component pole diverges significantly from the A component poles of Sherman, Moose Mountain and Adams Mine IF. Microplate tectonics prior to the acquisition of the B components between various "greenstone belts" within the Superior Province may be an explanation for this discordance. The Griffith Mine is located within the Uchi greenstone belt whereas the other IF studied and pole positions for the apparent polar wander (APW) path are derived from within the Abitibi greenstone belt. The post-folding C component is directed at (12°, 35°, 8°) which indicates an age of ~2.6 Ga and is likely associated with the intrusion of Bruce Lake pluton. The

postfolding D component is directed at (214°, 72°, 15°). It indicates an age of ~2.0 Ga and is, perhaps, related to a post Kenoran event. Smoothing and contouring of HR AF data at the population level isolated, E, F, G, and H components. The E component is directed at (241°, -28°, 3°), the F component at (225°, 4°, 3°), the G component at (164°, -27°, 4°), and the H component at (200°, 82°, 4°). The paleomagnetic ages for these components are similar to those obtained for IF.

The location of the dike poles suggest paleomagnetic ages ranging between ~1.7 to 1.9 Ga and is likely acquired when dikes intruded the HR during the Hudsonian orogeny.

Using a computer model which incorporates the induced component, anisotropy of susceptibility, NRM components, demagnetization factor of 2π , and assuming an infinite depth extent for the IF, the computed peak value for the North pit aeromagnetic anomaly at the Griffith Mine agrees within 3% of the observed anomaly. Also the computed anomaly half-width ($W_{1/2}$) value agrees within 18% of the observed value. The South pit gives similar results.

ACKNOWLEDGEMENTS

I am most grateful to Dr. D.T.A. Symons for suggesting this project and am indebted to him for his guidance, supervision and funding of this project to the finish.

I am also in debt to Dr. M. Stupavsky for the numerous suggestions, explanations and critical assistance I received from him.

Thanks are also extended to Mr. F. Facca, the Mine Geologist, for his geological advice and help in collecting samples, to Matthew Uza and Brian Philbey for their efforts in sample collecting and preparation, and to Gayna Sinclair for her drafting services.

Leaves ix, x, have been omitted in page numbering

LIST OF FIGURES

Figure

1.	Location of the Griffith Mine.	3
2.	Regional Geology, Host Rock Sample Sites and Location of the Griffith Mine.	7
3.	Typical Cross Section of the North Orebody . . .	18
4a.	Outline of North pit, Griffith Mine, Showing Locations of Block Samples of Iron Formation . .	21
4b.	Outline of South pit, Griffith Mine, Showing Locations of Block Samples of Iron Formation . .	22
5.	Histogram of the Specific Gravities of 452 IF Specimens	36
6.	Lognormal Histogram of k_{\perp} Susceptibility for 453 IF Specimens	37
7.	Lognormal Histogram of k_{\perp} Susceptibility for 444 HR Specimens	38
8.	Regression Line of Specific Gravity versus k_{\perp} Susceptibility for 363 IF Specimens	40
9a.	Histogram of k_{\min} (k_{\perp}) Direction for 453 IF spe- cimen by (a) inclination, and (b) declination. .	42
9b.	Histogram of k_{\min} (k_{\perp}) Direction for 453 IF spe- cimen by (a) inclination, and (b) declination. .	43
10.	Histogram of k_{int} Directions for 453 IF Specimens.	44
11.	Histogram of k_{\max} Directions for 453 IF Specimens.	45
12.	Histogram of k_{int}/k_{\min} for 453 IF Specimens.	46
13.	Histogram of k_{\max}/k_{\min} for 453 IF Specimens.	47
14.	Lognormal Histogram of NRM Intensity for 453 HR Specimens	48
15.	Lognormal Histogram of the Koenigsberger Ratio (Q) for 453 HR Specimens	49

Figure		Page
16.	Regression line of NRM intensity versus k_{\perp} susceptibility for 453 IF specimens.	51
17a.	Histogram of NRM inclination change of IF specimens over four weeks.	53
17b.	Histogram of NRM intensity change of IF specimens over four weeks.	53
18a.	Histogram of NRM intensity change of IF specimens after induced shock.	54
18b.	Histogram of NRM inclination change of IF specimens after induced shock.	54
19.	Lognormal histogram of NRM intensity for 491 HR specimens.	55
20.	Lognormal histogram of the Koenigsberger ratio (Q) for 491 HR specimens.	57
21a.	Histogram of NRM inclination of HR specimens over four weeks	58
21b.	Histogram of NRM intensity change of HR specimens over four weeks.	58
22.	IF AF Demagnetization Curve - Paleomagnetic Stability Index for Directional Changes	62
23.	IF AF Demagnetization Curve - Relative Intensity	63
24.	Directional Changes of AF Demagnetization on an Equal Area Projection for IF Pilot Specimens	65
25a.	Plot of Optimum AF Cleaning Field for IF and HR Specimens.	66
25b.	Relative Intensity of NRM After Cleaning at Optimum AF Field	66
26.	IF AF Cleaned Site Mean Directions on an Equal Area Projection	67
27.	Smoothing and Contouring of AF Cleaned IF specimens Corrected for Bedding Tilt and Plunge of Fold (Down Direction; east Limb of East-West Synclines)	70

Figure	Page
27a. Smoothing and contouring of AF Cleaned IF Specimens Corrected for Bedding Tilt and Plunge of Fold (Down Direction; West Limb of East West Synclines.	71
28. Smoothing and Contouring of AF Cleaned IF Specimens Not Corrected for Bedding Tilt and Plunge of Fold (Down Direction; East and West Limbs of East-West Syncline)	72
29. Smoothing and Contouring of AF Cleaned IF Specimens Corrected for Bedding Tilt and Plunge of Fold (Down Direction; Components of East and West Limbs are Combined).	78
30. Directional Changes of Thermal Demagnetization on an Equal Area Projection for IF Pilot Specimens	82
31. IF Thermal Demagnetization Curve - Relative Intensity	83
32. IF Thermal Demagnetization Curve - Paleomagnetic Stability Index	84
33a. Smoothing and Contouring of Thermally Cleaned IF Pilot Specimens Corrected for Bedding Tilt and Plunge of Fold (Down Direction).	85
33b. Smoothing and Contouring of Thermally Cleaned IF Pilot Specimens not corrected for Bedding Tilt and Plunge of Fold (Down Direction).	86
34. Directional Changes of AF Demagnetization on an Equal Area Projection for HR Pilot Specimens.	89
35. HR AF Demagnetization Curve - Paleomagnetic Stability Index for Directional Changes	90
36. HR AF Demagnetization Curve - Relative Intensity	92
37. HR AF Cleaned Site Mean Directions on an Equal Area Projection	93
38a. Smoothing and Contouring of AF Cleaned HR Specimens Corrected for Bedding Tilt (Down Direction).	95
38b. Smoothing and Contouring of AF Cleaned HR Specimens Corrected for Bedding tilt (Up-Direction).	96

Figure

39a.	Smoothing and countouring of AF cleaned HR Specimens not Corrected for Bedding Tilt (Down Direction).	97
39b.	Smoothing and contouring of AF cleaned HR Specimens not Corrected for Bedding Tilt (Up Direction).	98
40.	Smoothing and contouring of NRM HR Specimens not Corredted for Bedding Tilt (Down Direction) . .	100
41.	HR Thermally Cleaned Pilot Specimen Directions on an Equal Area Projection:	104
42.	Directional Changes of Thermal Demagnetization on an Equal Area Projection for HR Pilot Specimens . .	105
43.	HR Thermal Demagnetization Curve - Paleomagnetic Stability Index for Directionsl Changes	106
44.	HR Thermal Demagnetization Curve - Relative Intensity.	107
45a.	Dike-HR Baked Contact Test.	111
45b.	Dike-HR baked Contact Test.	112
46.	Apparent Polar Wander (APW) Curve (after Seguin, <u>et al.</u> 1982) Showing the Pole Positions	114
47.	Apparent Polar Wander (APW) Curve (after Irving, 1979) Showing Pole Positions.	117
48.	Apparent Polar Wander (APW) Curve (after Irving, 1979), Showing Pole Positions for Dike.	118
49.	Computed Magnetic Anomaly of IF at 147 m Elevation (Total Field Relative to Background Equal to Zero).	120

LIST OF TABLES

<u>Table</u>		<u>Page</u>
1.	Table of Lithologic Units (Shklanka, 1970) . . .	8
2.	Stratigraphy of the IF (Schelske, 1970)	16
3.	Sampling and Remanence Data of IF Sites	26
4.	Sampling and Remanence Data of HR Sites	31
5.	Summary of Remanence Directions and Angular Variance Tests for Corrected versus Uncor- rected Anomalies of East (E) and West (W) Limbs of East-West Synclines.	74
6.	Variance Tests for Corrected and Uncorrected Directions (Components of East and West Limbs Are Combined)	77
7.	Summary of Remanence Directions and Fold Test for IF Thermally Cleaned Pilot Specimens	88
8.	Summary of HR Remanence Directions.	101
9.	Angular Variance Ratio Tests of Host Rock AF Data	102
10.	Results of Dike - HR Baked Contact Test	110
11.	Paleomagnetic Pole Positions of the Griffith Mine	113
12a.	Summary and Comparison of Magnetic Properties of the Iron Formation at the Sherman, Moose Mountain, Adams and Griffith Mines.	122
12b.	Summary and Comparison of Magnetic Properties of the Host Rock at the Sherman, Moose Mountain, Adams and Griffith Mines.	123
13.	Summary of Aeromagnetic Response of IF.	124

LIST OF APPENDICES

Appendix	Page
1. Computer Program for the Calculation of the Magnetic Anomaly Over a Thin Sheet of Infinite Strike and Depth Extent.	124

CHAPTER I

INTRODUCTION

1.1 PROBLEM AND PROPOSAL

The exploration for iron ore deposits in Ontario has been done primarily by airborne and ground magnetic surveys measuring the total magnetic field. The most intense magnetizations are targets for examination. The vertical magnetization in Ontario iron formations (IF) is controlled by: (1) the nature and abundance of the magnetic minerals, (2) the gross geometry of the deposits, (3) the attitude of the bedding relative to the Earth's magnetic field (EMF), (4) the anisotropy of magnetic susceptibility, and (5) the direction and intensity of the natural remanent magnetization (NRM).

The purpose of this study is twofold:

(a) to provide reliable averages for the magnetic properties of the IF and host rock (HR) in the vicinity of the Griffith Mine so that the air and ground magnetic anomalies may be reasonably interpreted, and

(b) to determine the paleomagnetic characteristics of the IF and HR in order to provide information on the age and genesis of the ore.

This information will aid in the exploration for new iron ore deposits by more closely defining their magnetic geophysical parameters and their genetic geological control.

1.2 PREVIOUS SIMILAR WORK AND LOCATION OF THE AREA

Several successful studies on the paleomagnetism of Precambrian IF in Canada have been done (Symons 1966, 1967; Seguin 1972, 1975). Symons and Stupavsky (1979, 1980), and Symons, et al. (1980, 1981) studied both the magnetic properties and the ore genesis of Algoman-type banded IF and associated HR of the Sherman Mine near Temagami, the Moose Mountain Mine near Capreol and the Adams Mine Near Kirkland Lake, Ontario. The present study utilizes similar methods for the Griffith Mine, 50 km south of Red Lake, Ontario (Fig. 1). Wherever possible and relevant, comparison will be made to the results of these previous studies.

1.3 HISTORY OF THE MINE

Bruce (1924) reported on some drilling on the North and South deposits prior to 1922 in search of secondary enriched zones in the IF. From then until 1953, no work is known to have been undertaken. In 1953, L. Dempster, J. Dempster, and A. C. Mosher, working for a syndicate managed by Calmour Mines Ltd., staked the present property. Prospecting, trenching, sampling and dip needle work were

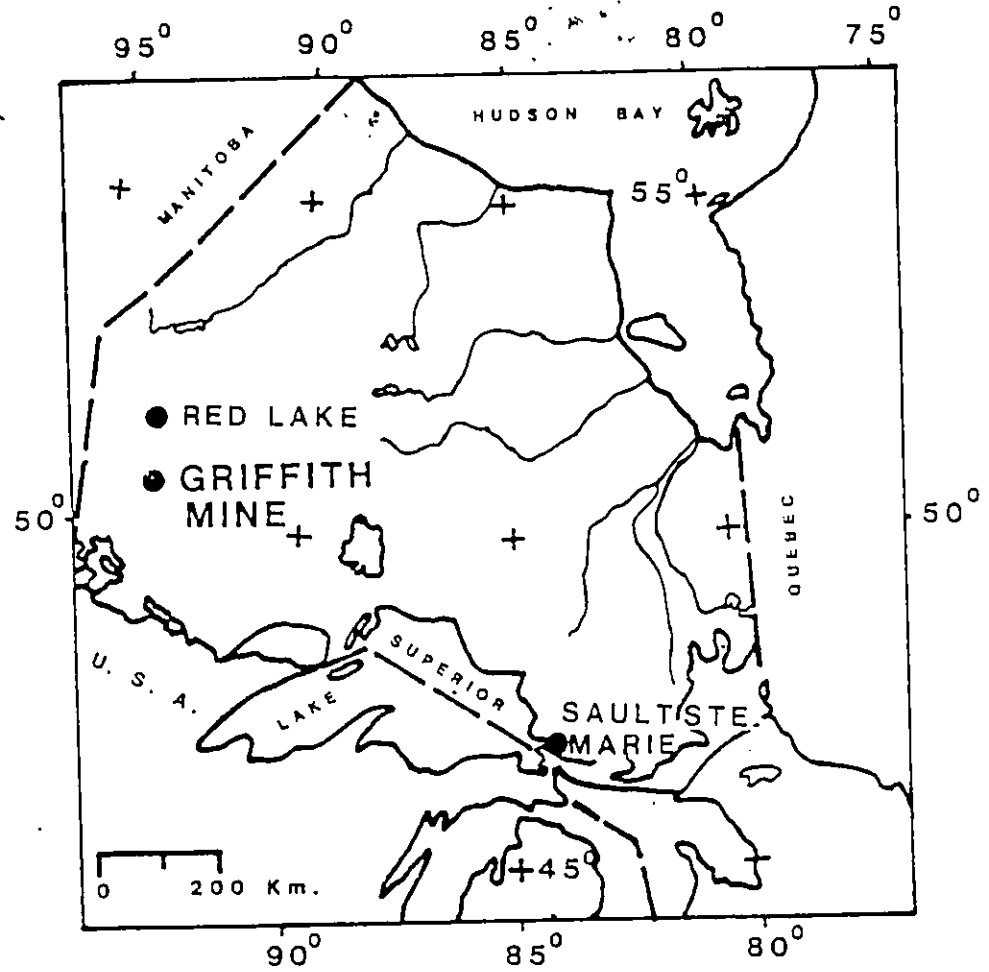


Fig. 1 Location of the Griffith Mine.

carried out in the same year. In 1954, Iron Bay Mines Ltd. was incorporated. In the same year they carried out geo-magnetic and geological surveys and drilled 29 holes for a total length of 3968 m. From 1955 to 1959, pilot plant concentration tests were run on the drill cores. In 1959 and 1960, bulk samples were tested for pelletizing qualities. In 1962, an option agreement with Taconite Lake Iron Company Ltd., was made. That company carried out further concentration tests and drilled an additional 3076 m of core in 1963 and 1964. In 1965, property was assigned to the Steel Company of Canada Ltd. The property was named the Griffith Mine with Pickands Mather and Company as Managing Agents.

There are two major outcroppings of IF at Bruce Lake known as the North ore body and South ore body. Of the two deposits, only the North deposit is presently being mined. Mining is done by the open pit method with the ultimate pit dimensions designed to be approximately 1823 m long, 911 m wide, and 150 m deep. In order to do this, a 1990 m long earth dike has been built out into the lake around the east side of the North deposit. This was followed by dredging of the lake clays and silts to expose the eastern flank of the deposit. Test work on bulk samples and drill core has indicated little variation in the iron content for the North and South deposits. The South deposit grades 32.3% and the

North deposit grades 30.5% total Fe. The pellets grade 66.2% Fe, 4.5% SiO₂ and 0.01% P. Scheduled production is at the rate of 1.4 million tonnes of pellets per year.

CHAPTER II

GEOLOGY

The Geology in the vicinity of the Griffith Mine is shown in Fig. 2. It has been described by Shklanka (1970) from which most of this discussion is taken.

2.1 REGIONAL GEOLOGY

The Bruce Lake map area of the District of Kenora (Patricia portion) is located approximately 50 km south of Red Lake, Ontario. It is bounded by longitudes $93^{\circ}15'W$ and $93^{\circ}30'W$ and latitudes $50^{\circ}45'N$ and $50^{\circ}52'N$. The area is centred around the Griffith Mine.

Table 1 summarizes the lithologic units present along with the available radiometric age data.

2.1.1 Metavolcanics

The metavolcanics are confined to a few limited areas in the northern and northwestern parts of the map area. Outcrops are too scattered to establish any stratigraphic sequence. The metavolcanics are mainly composed of fine to coarse grained tuff, agglomerate, rhyodacite, and mafic metavolcanics.

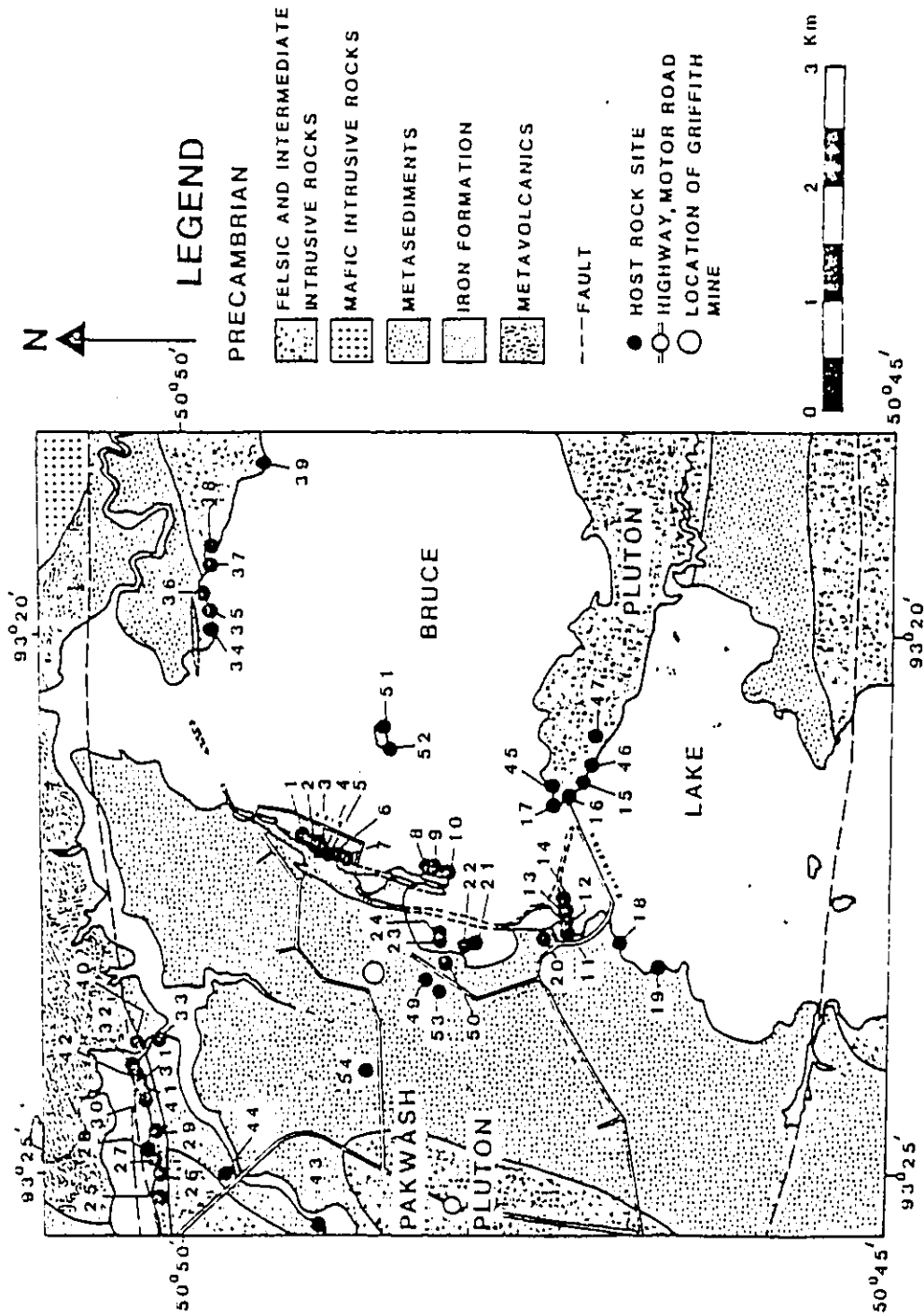


Fig. 2 Regional geology, host rock sample sites and location of the Griffith Mine (modified after Shklanka, 1970).

TABLE 1
Table of lithologic units (Shklanka, 1970)

	Approx. Radiometric Age (Ma)
CENOZOIC	
Recent	
Fluvial and lacustrine deposits, reworked till, swamp deposits	
Pleistocene	
clay, sand, gravel, boulder deposits	
----- Unconformity -----	
PRECAMBRIAN	
FELSIC AND INTERMEDIATE INTRUSIVE ROCKS	
Muscovite-biotite granodiorite	
----- Intrusive contact -----	
Hornblende-biotite quartz diorite, hornblende-biotite diorite	2480 ± 50 ¹
----- Intrusive contact -----	
Biotite granodiorite	
----- Relations uncertain -----	
MAFIC AND INTERMEDIATE INTRUSIVE ROCKS	
Metagabbro, feldspar porphyry, lamprophyre	
----- Intrusive contact -----	
METASEDIMENTS	2734 ± 96 ²
Greywacke, arkosic grit, pebbly greywacke	
Iron formation	
METAVOLCANICS	2738-2791 ± 96 ²
Fine-grained tuff, coarse-grained tuff, rhyodacite, agglomerate, mafic metavolcanics	

Note: ¹Stockwell et al. (1976); ²Nunes and Thurston (1980).

2.1.2 Iron Formation

The IF occurs discontinuously along the northwestern, western and southwestern margins of the Bruce Lake pluton. The IF is interbedded with metasediments and intruded by the pluton. The two known economic deposits, the North and South deposits, are located on the west shore of Bruce Lake.

The IF consists mainly of magnetite-chert interlayered with recrystallized chert, jasper, or locally magnetite-rich biotite schist. The interbedded metasediments include fine-grained greywacke, arkosic grit and pebbly greywacke. Quartz and feldspar are the main minerals in the metasediments and are accompanied by various proportions of biotite, blue-green amphibole, actinolite, garnet, or andalusite. Minor accessory minerals include apatite, sphene, pyrite and magnetite (Shklanka 1970, p. 5)

The IF is complexly folded into anticlines and synclines with numerous minor folds developed within the larger structures. The systematic and regular development of axial planes and plunge angles indicates a tectonic origin for the superimposed folds rather than penecontemporaneous folding. The presence of micas and amphibole in the crestal regions of some folds, parallel to the axial planes, substantiates this interpretation and also further indicates that amphibolite facies metamorphism accompanied the folding.

2.1.3 Metasediments

Metagreywacke is the main metasedimentary rock type in the map area. It occurs in the central part of the area, in the north part where it may also be found interbedded with waterlain tuffs, and in the south part where it is part of the granitic-metasedimentary complex. The rocks are light to dark grey and fine to medium grained. They are composed mainly of quartz and plagioclase. Biotite usually forms about 10% of the rock volume but may form up to 20%. Minor accessory minerals include sphene, apatite, zircon, tourmaline, magnetite, and pyrite. Secondary minerals include chlorite, sericite, or epidote (Shklanka 1970, p. 5).

2.1.4 Mafic to Intermediate Intrusive Rocks

Metagabbro and mafic to intermediate dikes are found in the map area. Metagabbro is inferred to underlie most of the northeastern corner of the area where scattered outcrops correspond to an anomalous area of fairly high uniform magnetic susceptibility (Aeromagnetic Map 861G, ODM-GSC 1960). The gabbro is dark grey to black and medium grained. It consists of blue-green amphibole and plagioclase with minor amounts of pyrrhotite, pyrite, and quartz (Shklanka 1970, p. 6).

Dikes of mafic and intermediate composition are concentrated along the west shore of Bruce Lake cutting the IF, greywacke, and Bruce Lake pluton. They also occur

throughout the north-central part of the area in the meta-sediments and volcanic tuffs. Three distinct type of dikes are found: (a) feldspar porphyry dikes, (b) lamprophyre dikes, and (c) gabbro dikes. Most of the dikes are 30 cm to 50 cm wide. The mafic and intermediate intrusions invade the metasediments and metavolcanics, but their relationships to one another and to the felsic to intermediate intrusions are not clear.

2.1.5 Intermediate to Felsic Intrusive Rocks

Biotite granodiorite is confined mainly to the southeastern part of the area where it forms a distinct pluton. In addition, a few scattered occurrences have been mapped to the north of East Lake. The granodiorite is light to medium grey, fine to medium grained, and foliated. Quartz and plagioclase are the dominant minerals. Biotite is characteristic of these rocks. Magnetite and zircon are the common accessory minerals (Shklanka 1970, p. 8). The biotite granodiorite in the southeastern part of the area clearly predates the muscovite-biotite granodiorite on the basis of the cross-cutting relationships. The biotite granodiorite in the northern part of the area is considered to be of similar age to that in the southwestern part on the basis of their lithological similarities.

2.1.6 Hornblende-Biotite Quartzdiorite and Hornblende-Biotite Diorite

Quartz diorite with dioritic zones forms two plutons that are referred as the Bruce Lake and Pakwash Lake plutons.

2.1.6a Bruce Lake Pluton

The western margin of this granitic batholith underlies the Bruce Lake. On the basis of available geophysical and geological information (Davies and Pryslak 1967; ODM-GSC 1965) this batholith extends east-northeast for approximately 58 km with a width of ~7 km. Exposures in the area are confined mainly to scattered outcrops on islands and along the shore line of the northern part of Bruce Lake. The rocks are medium-grained, light to medium grey, and mainly massive. They are composed of mainly plagioclase with 5 to 18% quartz, and about 15% hornblende and biotite. Sphene, apatite and zircon are minor accessory minerals. Secondary epidote sericite, or chlorite are in less abundance. The pluton intrudes metagreywacke and IF with sharp contacts. Inclusions are not abundant, however, greywacke, IF, and hornblende-rich inclusions are present (Shklanka 1970, p. 9)..

2.1.6b Pakwash Lake Pluton

This pluton is confined to the western part of the map area. It is at least 12 km long and 5 km wide. It is com-

posed of rocks that range from quartz diorite to diorite. Mineralogically, they resemble those of the Bruce Lake pluton, except that quartz is usually in a lower range of 5 to 10%. Contacts of the pluton with the host rocks (HR) are usually sharp and generally conformable. Inclusions other than common amphibole-rich 'clots' are not numerous (Shklanka 1970, p. 10).

2.1.7 Muscovite-Biotite Granodiorite

Muscovite-biotite granodiorite underlies the southwestern and south-central parts of the Bruce Lake area, either alone or as part of a sedimentary complex. The rocks are medium to coarse grained. The usual mineral assemblage is muscovite, biotite, quartz, oligoclase, and microcline. Minor accessory minerals include apatite, tourmaline, and zircon (Shklanka 1970, p. 11).

Associated with the granodiorite are dikes of aplite and pegmatite. The aplites are mainly a few centimeters wide but the pegmatite dikes may attain 3 m or more.

The muscovite-biotite granodiorites are the latest intrusions in the area. Post-granodiorite deformation affected these rocks are sheared in proximity to the east-trending lineament at the south end of Bruce Lake.

2.1.8 Pleistocene Deposits

Pleistocene deposits mantle most of the area except for scattered rock outcrop. However good exposures are

few. The deposits include clay, sand, gravel, and boulders.

2.1.9 Recent Deposits

Reworking of Pleistocene deposits took place at a higher water level than is now present along the shoreline of Bruce Lake. The resulting deposits contain a mixture of clays, sand, gravel and boulders. Recent peat and swamp deposits overlie much of the area particularly in the southern part where the relief is low. Also Recent fluvial, lacustrine and local outwash deposits were formed adjacent to the Hartman moraine.

2.1.10 Structure (Shklanka 1970, p. 14-15)

Foliation in the area include primary bedding and flow layering, and secondary schistocities and slip cleavages.

Bedding is recognizable in most of the sediments and pyroclastics. Flow layering is present in some granitic rocks, especially the muscovite-biotite granodiorite. Two secondary schistocities, corresponding to two metamorphic events, are present. At least one predated the Bruce Lake pluton and one is coincident with its emplacement.

Slip cleavage is most pronounced in proximity to faults. Lineations are both diverse and scattered. They indicate more than one age and mode of origin. Lineations in proximity to the East Lake fault reflect late movement. Linea-

tions in the Pakwash Lake pluton probably reflect the primary flowage direction. Axial line lineations related to folding of the rocks, probably reflect more than one age of deformation. The attitudes of the tuffaceous rocks to the northeast of East Lake suggest an east-west fold with a steeply south-dipping axial plane. Folds in the IF are numerous.

Two faults, referred as the East Lake and Bruce Lake faults, occur in the northern and southern parts of the area respectively. The East Lake fault trends east through East Lake and bifurcates in the western part of the area.

2.2 MINE GEOLOGY

2.2.1 Geological Setting

The metamorphosed Precambrian IF located on the west side of Bruce Lake, is interbedded with graywacke and biotite schists. It is located on the west margin of the large Bruce Lake quartz diorite pluton. The IF occurs as discontinuous bodies with a crescent-shaped distribution which conforms to the contact of the pluton.

2.2.2. Stratigraphy of the IF

The stratigraphic subdivisions of the IF and interbedded sediments are based on diamond drilling and are listed from top to bottom, or in order of increasing age with the approximate thickness for each unit (Schelske 1970, pp. 1279-1280) (Table 2).

TABLE 2
Stratigraphy of the IF (Schelske 1970)

<u>Unit</u>	<u>Approx. thickness (m)</u>
An upper wall rock of biotite schist and graywackes	-
Schistose magnetic IF	4
Banded magnetite-quartz IF	36
Schistose magnetic IF	3-4
Biotite schists and graywackes	22
Schistose magnetic IF	9-12
Banded magnetite-quartz IF	3-6
A lower wall rock of biotite schists and graywackes	-

2.2.3 Structure

Folding is the main structural feature in the ore deposits. Repetition of the units by folding has produced ore widths in the North and South deposits that are far in excess of the true IF thickness, thus making these areas amenable to open pit mining. Figure 3 of the North ore body shows that the IF is folded into two synclines with a central anticline. The structures trend at $N30^{\circ}E$ and plunge at an average of $30^{\circ}SW$. The limbs of the folds are steep and in some places are actually overturned because of secondary or minor folds. The South ore body is an overturned syncline on the east side with an anticline on the west. The structure trends at $S27^{\circ}W$ and plunges at an average of $59^{\circ}SE$.

The similarity in plunge among the numerous minor folds and the development of mineral orientation at the crestal positions of some folds parallel to the axial planes indicate that folding was tectonic and correspond to the first period of metamorphism (Shklanka 1970, p. 22).

Most folds are tight or isoclinal in nature, but some are open.

Distinct foliations in the rocks include bedding and two schistocities. In addition, a later superimposed slip cleavage was developed locally. The first schistosity is coincident with the first period of metamorphism and parallels the bedding, except along axial regions of the folds

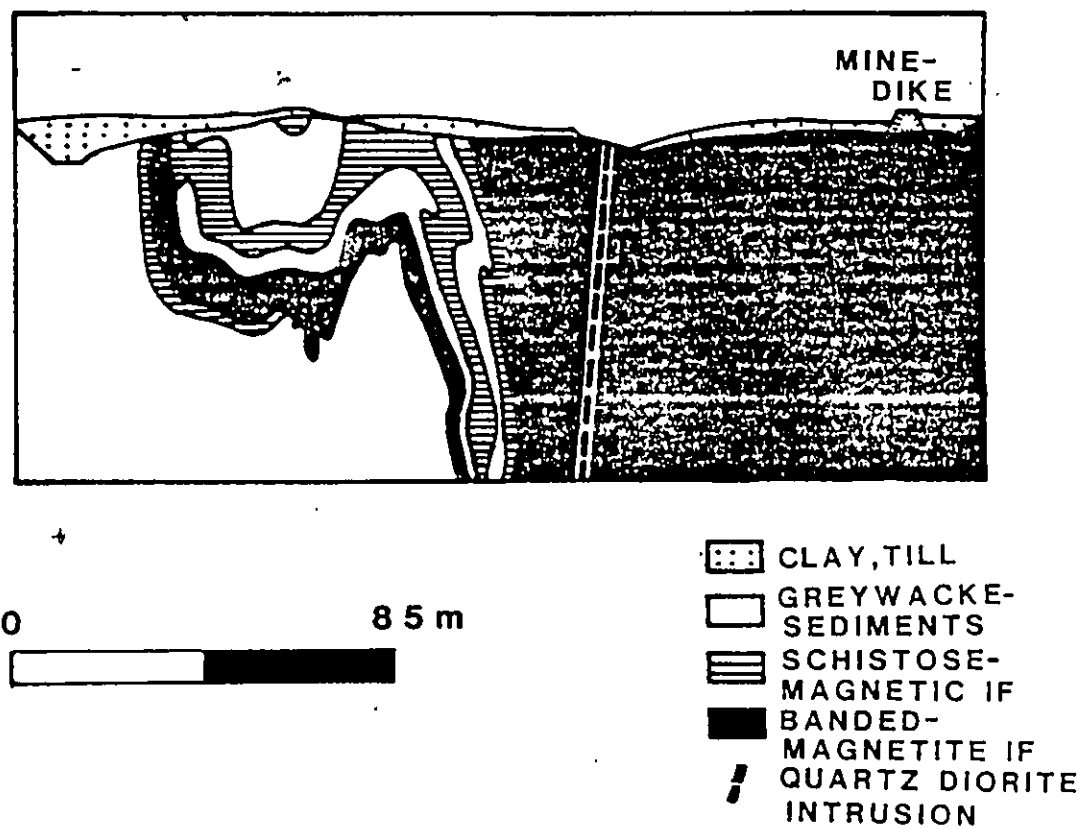


Fig. 3 Typical cross section of the North orebody; modified after Schelske, Fig. 1, p. 1279.

where it is developed as an axial plane cleavage. The superimposed schistosity, coincident with a second period of metamorphism, is readily identifiable in the mafic dikes which postdate folding. The later slip cleavage, not identified megascopically, was due to cataclastic deformation of the rocks and is related to localized zones of slip (Shklanka 1970, p. 21).

CHAPTER III

EXPERIMENTAL METHODS

3.1 SAMPLING

At the Griffith Mine 175 IF oriented samples and 54 field drilled HR sites were collected in a period of twelve days during June, 1980. The samples and sites were distributed as uniformly as possible both from within the pits and from the surrounding HR in order to provide representative data. A total of 175 hand samples of IF including 160 from the North ore body (Fig. 4a) and 15 from the South ore body (Fig. 4b) were collected. They were oriented in situ using a topographic sitings based on mine bench maps and a modified inclinometer. At each HR site (Fig. 2), a minimum of five cores were drilled several meters apart. The cores were oriented in situ using a solar compass with Brunton compass and topographic sitings to an accuracy of $<2^\circ$.

3.2 SAMPLE PREPARATION

Symons and Stupavsky (1979), after considerable experimentation with a variety of drill bit types and sizes, found that 0.95 cm right cylindrical IF specimens can be readily drilled from the IF hand samples despite their

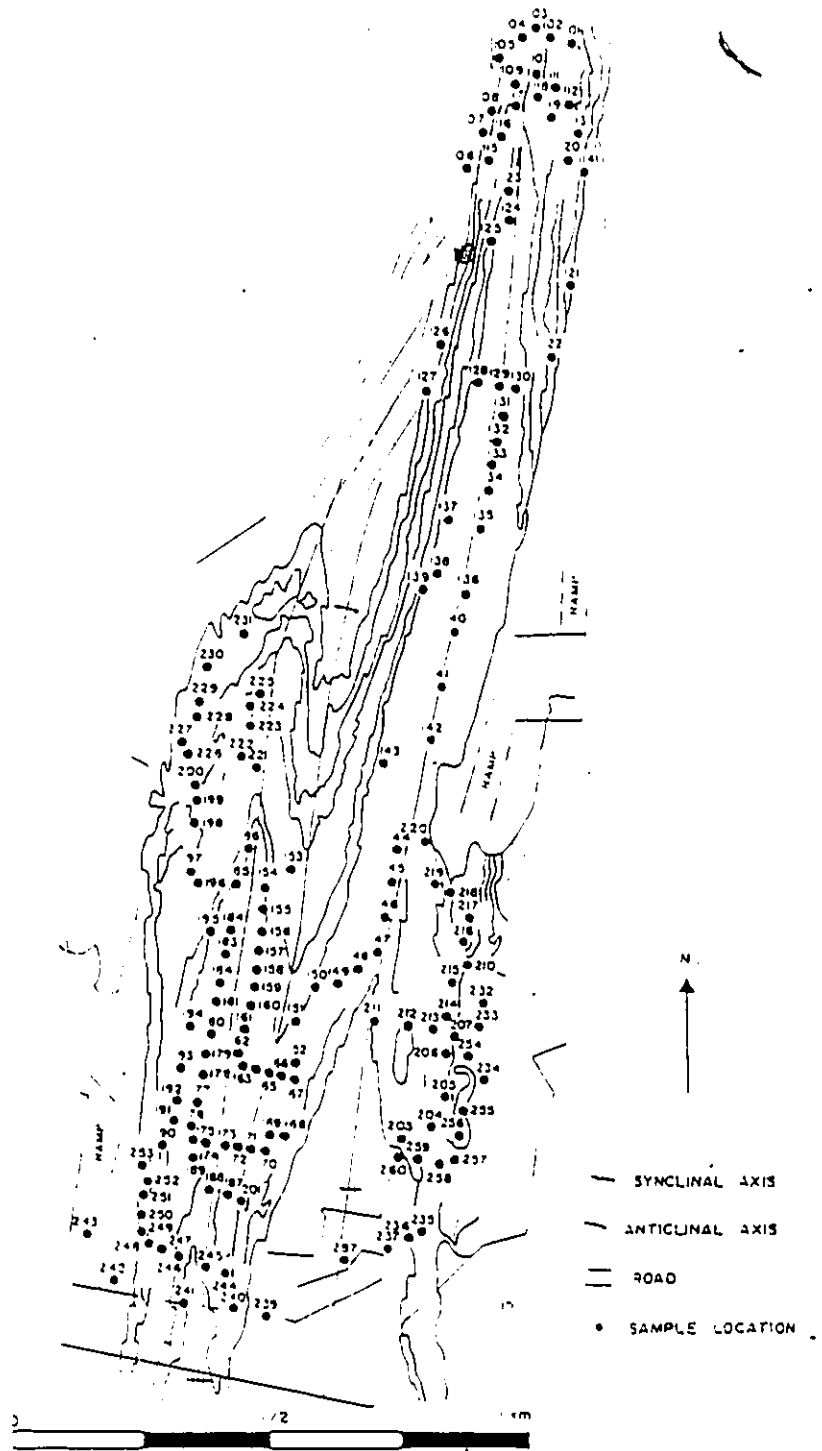


Fig. 4a Outline of North Pit, Griffith Mine, showing locations of block samples of Iron-Formation

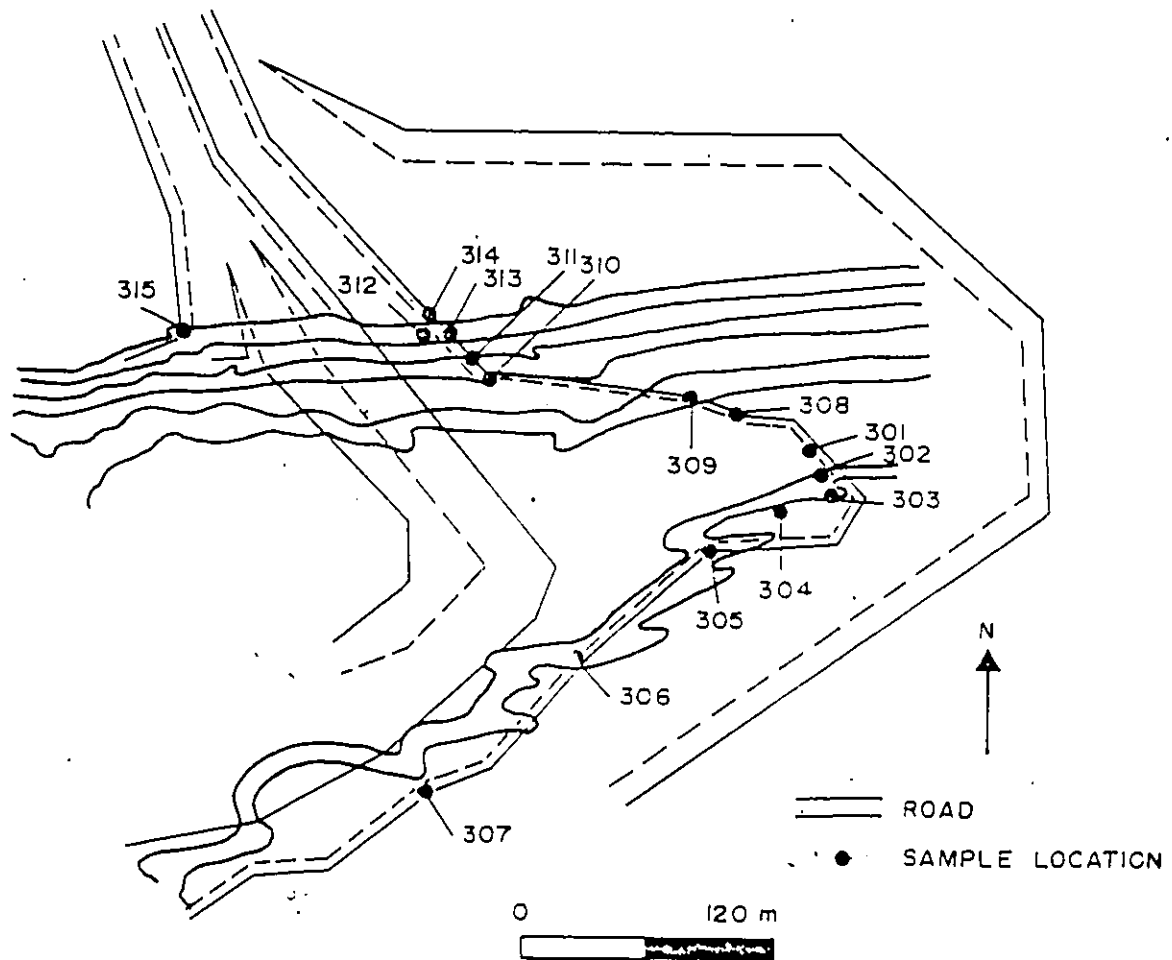



Fig. 4b Outline of South Pit, Griffith Mine, showing locations of block samples of iron-formation.



hardness using Felker thin-wall bits. At least four such specimens were drilled from each hand sample yielding 700 IF specimens for AF cleaning. An additional 370 IF specimens were cut for storage tests, shock tests, and thermal cleaning tests. Thus the total IF data base comes from 1070 specimens.

The drilled HR cores were cut to give two conventional cylindrical specimen of ~2.50 cm diameter and ~2.45 cm length. This yielded ten specimens from each site for AF and thermal cleaning to give a total of 540 HR specimens.

3.3 SAMPLE TREATMENT

3.3.1 Specific Gravity

The specific gravity was measured on the 700 IF specimens using a modified picnometric technique. Individual measurements are repeatable to an accuracy of $\pm 0.01 \text{ gcm}^{-3}$.

3.3.2 Magnetic Susceptibility

The low-field susceptibility perpendicular to bedding (K_{\perp}) was measured on a toroid bridge (Christie and Symons, 1969) for the 500 IF and 540 HR specimens.

3.3.3 Anisotropy of Magnetic Susceptibility

The low-field magnetic susceptibility of the 500 IF specimens was measured on the toroid bridge along 9 directions. The principal axial directions and magnitudes of

the susceptibility ellipsoid were computed from the matrix elements.

3.3.4 Natural Remanent Magnetization

The natural remanent magnetizations (NRM) of the 700 IF specimens and 540 HR specimens were measured using a Schonstedt SSM-1A spinner magnetometer. A "3-spin" measurements technique gave efficient treatment and reliable measurements in all the cases. The NRM direction and intensity for each specimen were computed from the 3 component measurements.

3.3.5 AF Demagnetization

A total of 54 IF pilot specimens with an average NRM direction and intensity for that sample were selected so as to adequately represent the range of IF NRM characteristics. These were step demagnetized in alternating fields (AF) with peak intensities of 5, 10, 15, 20, 30, 40, 50, 60, 80 and 100 mT using a Schonstedt GSD-1 AF demagnetizer. Similarly, one pilot specimen per HR site with an average NRM direction and intensity for that site was step demagnetized in AF field of 5, 10, 15, 20, 30, 40, 50, 60, 80 and 100 mT peak intensity.

The paleomagnetic stability Index (PSI) method of Symons and Stupavsky (1974) for directional analysis and the intensity decay curves for each pilot specimen were used to select the optimum AF intensity for demagnetizing the

remaining specimens from each site and limb (Tables 3 and 4).

3.3.6 Thermal Demagnetization

A total of 48 IF pilot specimens with an average NRM direction and intensity for that sample so as to adequately represent the IF were thermally step demagnetized at temperatures of 100, 200, 300, 400, 450, 500, 550, 575, 600, 625 and 650°C using a furnace having a non-inductive heating element, located in a nested series of five 'mu'-metal shields in a shielded room. The introduction of random acquisition of remanence by the specimens during the cooling caused by incomplete elimination or shielding of the Earth's field was checked by placing the specimens in opposite directions during successive steps. Spurious coherent magnetizations acquired by IF specimens during heating were statistically eliminated by positioning the specimens randomly in the oven. Similarly, one HR specimen per site with an average NRM direction and intensity for that site was thermally step demagnetized at temperatures of 100, 200, 300, 400, 450, 500, 550, 575, 600, 625 and 650°C.

3.3.7 Stability Tests

Storage tests were done to assess the degree of stability of the remanence caused by the acquisition of viscous remanence (VRM) components by IF. First, the NRM of 18 IF and 14 HR specimens were measured. Then the specimens were taken out of the shielded room and exposed to the Earth's magnetic

TABLE 3
Sampling and Remanence Data of Iron Formation Sites

Sample	Limb-Syncline	AF Intensity (mT)	Data Screening			N	Remanent Magnetization			
			a	b	c		Length (R)	Decl. (deg)	Incl. (deg.)	α_{95} (deg.)
101	E-E	50				0				
102	W-E	40	1		1	2	1.998	209.13	22.06	9.57
103	W-E	40				0				
104	W-E	40				0				
105	W-E	40				0				
106	W-E	40	1			3	2.820	190.04	3.08	41.05
107	W-E	40	1			3	2.960	99.19	-17.87	17.52
108	W-E	40	1			3	2.850	7.55	-27.71	39.90
109	W-E	40				0				
110	W-E	40				0				
111	E-E	40				0				
112	E-E	40				4	3.892	219.64	2.68	17.73
113	E-E	20				0				
114	E-E	40	1			3	2.850	264.78	48.95	35.52
115	W-E	*								
116	W-E	30				0				
117	W-E	*								
118	W-E	*								
119	E-E	40				0				
120	E-E	40				0				
121	E-E	40				0				
122	E-E	40				0				
123	W-E	40				0				
124	W-E	40				0				
125	W-E	40			1	3	2.853	108.49	27.87	37.28
126	W-E	40				0				
127	W-E	20				0				
128	W-E	20	1			3	2.897	56.63	22.33	28.72
129	E-E	20	1			3	2.853	228.02	52.89	38.24
130	E-E	30				0				
131	E-E	30				0				
132	E-E	30				0				
133	E-E	30				0				
134	E-E	30	1			3	2.862	277.31	78.16	33.60
135	E-E	30				0				
136	E-E	30			1	3	2.955	326.97	59.15	18.60
137	W-E	30				0				
138	W-E	30				4	3.850	168.96	39.27	27.34
139	W-E	30				0				
140	E-E	30				0				
141	E-E	30				0				

TABLE 3 - continued

Sample	Limb-Syncline	AF Intensity (mT)	Data			N	Remanent Magnetization			
			Screening				Length (R)	Decl. (deg.)	Incl. (deg.)	α_{95} (deg.)
			a	b	c					
142	E-E	40				0				
143	W-E	40				0				
144	W-E	40				0				
145	W-E	40				0				
146	W-E	40	1			3	2.862	204.94	17.94	33.60
147	W-E	40				0				
148	W-E	30	1			3	2.895	65.49	61.54	29.10
149	W-E	30				0				
150	W-E	30				0				
151	W-E	30				0				
152	W-E	30				0				
153	E-W	30				0				
154	E-W	30				0				
155	E-W	30				0				
156	E-W	30				4	3.850	29.73	81.83	21.37
157	E-W	30	1			3	2.925	293.37	23.00	24.30
158	E-W	30	1			0				
159	E-W	30				0				
160	E-W	30				0				
161	E-W	30				0				
162	E-W	30				0				
163	E-W	30				0				
164	E-W	30				4	3.919	204.05	7.52	15.29
165	E-W	30				0				
166	W-E	30				0				
167	W-E	30				0				
168	W-E	*								
169	W-E	30	1			3	2.919	26.73	1.00	25.28
170	W-E	30				0				
171	E-W	*								
172	E-W	30		1		3	2.871	232.15	49.12	32.39
173	E-W	30	1			3	2.962	177.35	61.35	17.19
174	W-W	30				0				
175	W-W	30				4	3.850	186.94	63.57	21.03
176	W-W	30	1			3	2.854	42.83	51.70	34.58
177	W-W	40				0				
178	W-W	40				0				
179	W-W	40	1			3	2.850	195.60	34.45	35.59
180	W-W	30	1			3	2.961	347.80	-7.38	17.44
181	W-W	30	1			3	2.917	50.57	60.23	25.66
182	W-W	30				0				
183	W-W	30				0				

TABLE 3 - continued

Sample	Limb-Syncline	AF. Intensity (mT)	Data			N	Remanent Magnetization			
			Screening a	b	c		Length (R)	Decl. (deg.)	Incl. (deg.)	α_{95} (deg.)
184	W-W	30				0				
185	W-W	30	1			3	2.858	91.43	47.94	34.17
186	W-W	*								
187	E-W	30				0				
188	W-W	30				0				
189	W-W	30				0				
190	W-W	30				0				
191	W-W	30				0				
192	W-W	30				0				
193	W-W	30				0				
194	W-W	30				0				
195	W-W	*								
196	W-W	30	1			3	2.840	290.03	-44.36	36.89
197	W-W	*								
198	W-W	*								
199	W-W	*								
200	W-W	40				3	2.820	45.60	-46.65	39.06
201	E-W	40				4	3.951	215.75	48.01	11.81
202	W-W	*								
203	E-E	30		1		3	2.833	231.82	29.33	30.77
204	E-E	30				0				
205	E-E	30				0				
206	E-E	30				0				
207	E-E	30	1		1	2	1.910	224.65	-7.49	87.90
208	E-E	30	1			3	2.953	29.91	17.43	19.12
209	E-E	30				0				
210	E-E	30	1			3	2.880	59.81	0.12	42.49
211	E-E	30				0				
212	E-E	30				0				
213	E-E	30				0				
214	E-E	30				0				
215	E-E	*								
216	E-E	30	1			3	2.960	218.83	12.58	17.61
217	E-E	30				4	3.969	34.88	20.99	9.27
218	E-E	30				0				
219	E-E	*								
220	E-E	30				0				
221	W-W	30				0				
222	W-W	30		2		2	1.943	181.33	26.67	63.37
223	W-W	30	1			3	2.930	209.44	-25.61	23.44
224	W-W	30				0				
225	W-W	30				0				

TABLE 3 - continued

Sample	Limb-Syncline	AF Intensity (mT)	Data Screening			N	Remanent Magnetization			
			a	b	c		Length (R)	Decl. (deg.)	Incl. (deg.)	α_{95} (deg.)
226	W-W	30	1			3	2.830	155.88	7.12	38.61
227	W-W	30				0				
228	W-W	30				0				
229	W-W	30				0				
230	W-W	30	1	1		2	1.969	59.33	24.62	44.96
231	W-W	*								
232	E-E	30				0				
233	E-E	30				0				
234	E-E	30	1	1		2	1.955	26.05	10.21	55.58
235	E-E	30				4	3.910	341.50	3.15	16.13
236	E-E	30				0				
237	E-E	30				0				
238	E-E	30				0				
239	W-E	*								
240	E-W	30				0				
241	W-W	30				0				
242	W-W	30				1				
243	W-W	30				0				
244	E-W	30				0				
245	E-W	30	1			3	2.865	155.96	25.96	33.14
246	W-W	30				4	3.840	54.91	30.97	27.69
247	W-W	30				0				
248	W-W	30				0				
249	W-W	30				0				
250	W-W	30				0				
251	W-W	40				0				
252	W-W	40				0				
253	W-W	40				0				
254	E-E	20				0				
255	E-E	20				0				
256	E-E	20				0				
257	E-E	30				0				
258	E-E	30				0				
259	E-E	30		1		3	2.952	222.05	30.62	19.31
260	E-E	30				0				
301	S-pit	30				0				
302	S-pit	30				0				
303	S-pit	30				0				
304	S-pit	30				0				
305	S-pit	30		1		3	2.862	182.15	57.81	33.64
306	S-pit	*								
307	S-pit	30	1			3	2.880	216.78	22.32	42.59

TABLE 3 - continued

Sample	Limb-Syncline	AF Intensity (mT)	Data Screening			N	Remanent Magnetization			
			a	b	c		Length (R)	Decl. (deg.)	Incl. (deg.)	χ_{95} (deg.)
308	S-pit	30				0				
309	S-pit	*								
310	S-pit	40				0				
311	S-pit	40				0				
312	S-pit	30	1	1		2	1.995	178.20	29.38	17.52
313	S-pit	30				0				
314	S-pit	30				4	3.810	173.25	28.69	24.02
315	S-pit	30				0				

Notes: R - length of vector resultant

χ_{95} - radius of the cone of 95% confidence (Fisher 1953) in degrees.

* - sample considered to have too low intensity for demagnetization

Data Screening:

a - core rejected as anomalous with respect to remaining cores from the sample,

b - sample considered to contain two direction populations.

c - sample rejected as specimen directions diverge from sample mean direction by more than 20°.

TABLE 4
Sampling and Remanence Data of Host Rock Sites

Sample	Rock Unit	AF Intensity (m)	Data Screening			N	Remanent Magnetization			
			a	b	c		Length (R)	Decl. (deg.)	Incl. (deg.)	α_95 (deg.)
1	QD	30	4	1		0				
2	QD	20	3	1		0				
3	QD	20	1	1		2	1.982	204.43	-19.17	34.64
4	QD	20	2	1		2	1.989	250.05	37.16	25.83
5	QD	40				4	3.785	317.76	48.89	7.61
6	QD	60	2		2	0				
7	DK	30	1	1	1	3	2.833	326.89	27.47	37.22
8	QD	40	1		2	2	1.985	261.93	-15.97	30.81
9	QD	30	5			0				
10	QD	60	2		1	2	1.925	229.83	-33.32	74.74
11	MS	20	1		2	2	1.979	286.34	5.02	37.10
12	MS	80	4	1	1	0				
13	MS	30	2		1	3	2.810	279.12	27.66	40.07
14	MS	40	2		1	2	1.986	247.11	25.41	43.86
15	QD	40	2			3	2.986	168.93	-8.14	10.36
16	QD	100	1			3	2.929	161.53	-15.28	23.74
17	QD	30	4			0				
18	MS	30	5			0				
19	MS	20	4			0				
20	MS	30	5			0				
21	MS	50	5			0				
22	MS	20	2	1		2	1.950	275.75	14.99	59.90
23	MS	20	2	1	1	0				
24	MS	100	4		1	0				
25	MV	80	2			3	2.881	256.01	-40.82	44.57
26	MV	30	1	1	1	2	1.980	230.83	-26.06	38.68
27	MV	40	5			0				
28	MV	40	2			2	1.988	315.02	-30.39	27.51
29	MV	60	1			3	2.927	232.66	-10.81	24.04
30	MV	30		1		3	2.976	224.31	15.53	13.56
31	MV	30		1		3	2.962	241.38	28.87	17.17
32	DK	100	2			4	3.984	314.58	35.04	6.82
33	MS	80	2	1	1	0				
34	QD	20	1			3	2.858	164.33	-29.34	34.14
35	QD	20	2			2	1.999	165.54	-40.27	5.57
36	DK	30		2		2	1.973	168.79	-26.72	41.54
37	DK	40	3			0				
38	QD	30	1			3	2.973	199.70	-24.64	14.43
39	QD	40	1			3	2.981	259.57	2.09	11.96
40	MV/QD	30			1	2	1.969	259.16	41.19	44.99

TABLE 4 - continued

Sample	Rock Unit	AF Intensity (mT)	Data Screening			N	Remanent Magnetization			
			a	b	c		Length (R)	Decl. (deg.)	Incl. (deg.)	α_{95} (deg.)
41	MV	30	1	1		3	2.995	218.69	10.19	5.99
42	MV	40				3	2.978	235.68	21.00	13.14
43	MS	20	5			0				
44	MS	20	1	1	1	2	1.984	108.28	20.29	32.45
45	QD/MS	20	2			2	1.967	173.99	32.16	46.71
46	MS/QD	30	2	1		2	1.997	310.63	42.10	14.58
47	QD	50			1	3	2.963	146.42	29.47	16.90
48	QD	20	1			4	3.917	301.99	40.93	15.49
49	MS	20	5			0				
50	MS	20	5			0				
51	QD	20	1	1		2	1.988	202.60	-52.44	27.96
52	QD	60	1	1		3	2.969	193.79	-42.78	15.42
53	MS	20	1	1		2	1.951	127.28	28.30	58.26
54	MS	30	5			0				

Notes: Rock Unit:

- QD - quartziorite,
- DK - dike
- MS - metasediments
- MV - metavolcanics

Data Screening:

- a - core rejected because the 2 specimen direction diverged by $>20^\circ$
- b - core rejected as sole remaining direction to inadequately represent the site
- c - core rejected as anomalous with respect to remaining cores from the Site.
- R - length of the vector resultant.
- α_{95} - radius of the cone of 95% confidence (Fisher 1953) in degrees.

field (EMF). Half of the specimens were placed perpendicular to the EMF and the other half were placed parallel to the EMF. The specimens were remeasured after storage periods of 7, 14, and 28 days. A shock test was performed on 10 IF specimens to assess how dynamite blasting used in mining the rock could affect the NRM response. After measuring the NRM of the specimens, they were hit 20 times on an aluminum plate and their remanence remeasured. The test was performed first with the specimens oriented parallel to the EMF and then repeated perpendicular to the EMF.

3.4 COMPUTATIONS

In order to handle the 20 quantitative variables for the 1610 specimens, it is mandatory to use a computer for the computations and data analysis. Existing laboratory computer programs, stored on disk in the computer library, were used for this purpose. Input data included specimen identification, longitude and latitude, K_{\perp} susceptibility and specific gravity. These programs calculate and plot the declination, inclination and intensity of the remanence, and the declination, inclination and magnitudes of the axes of the anisotropy of susceptibility ellipsoids as well as their means and confidence limits.

BMDP5D programs (BMDP-77) were used to plot the output in histogram form for analysis. The program has been adapted to calculate the means and confidence limits using both normal

and lognormal statistics for the various output parameters.

The BMDP6D program was used to correlate between two data sets, plot the data and do regression fits with correlation statistics. These statistical tests help define the limits of each of the parameters that are required for the magnetic model to be proposed.

3.5 MAGNETIC MODEL

The magnetic model program was compiled and tested in studies of the Sherman Mine by Symons and Stupavsky (1979), the Moose Mountain Mine by Symons, Walley and Stupavsky (1980), and the Adams Mine by Symons, Quick and Stupavsky (1981). The program (Walley, 1980) incorporates all the important factors for interpreting magnetic anomalies over a magnetic sheet. Most magnetic model computer programs used to calculate the induced magnetic components of a sheet include a variety of thicknesses, magnetite contents, and strike and dips relative to the Earth's varying geomagnetic field. Some programs also incorporate the remanence and/or the demagnetizing factor. No previous programs incorporate all of these plus the effect of magnetic anisotropy. The magnetic model used in this study follows the standard theoretical equations for the induced component. The demagnetizing factor and the anisotropy of susceptibility equations follow Gay (1963) and the remanence equations follow Strangway (1965). See Appendix 1 for the model computations.

CHAPTER IV

RESULTS

4.1 SPECIFIC GRAVITY

The histogram of IF specific gravity (S.G.) (Fig. 5) shows a normal distribution, ranging between barren silica (S.G. 2.65 g/cm^{-3}) and magnetic ore values of 4.04 g/cm^3 . The overall mean value from 452 specimen is 3.36 g/cm^3 (standard deviation = 0.31). This value is lower than the expected ore value because the sampling includes low grade and barren wall-rock samples, i.e., mixed ore and lean IF. The calculated SG of the economic ore at Griffith Mine, with a 31% total Fe, is 3.60 g/cm^3 .

4.2 MAGNETIC SUSCEPTIBILITY

A total of 453 IF specimens show a lognormal distribution for K_{\perp} , with a lognormal mean of $4.0 \times 10^{-2} \text{ cgs/cm}^3$ (Fig. 6). A total of 444 HR specimens show a similar lognormal distribution with a lognormal mean of $3.60 \times 10^{-4} \text{ cgs/cm}^3$ (Fig. 7). Because $K_{\perp} \text{ IF} = 111 K_{\perp} \text{ HR}$, it is reasonable to neglect the $K_{\perp} \text{ HR}$ in calculating the IF magnetic anomaly.

A total of 363 IF specimens show an excellent regression fit between the SG and $K_{\perp} \text{ IF}$ with a correlation coef-

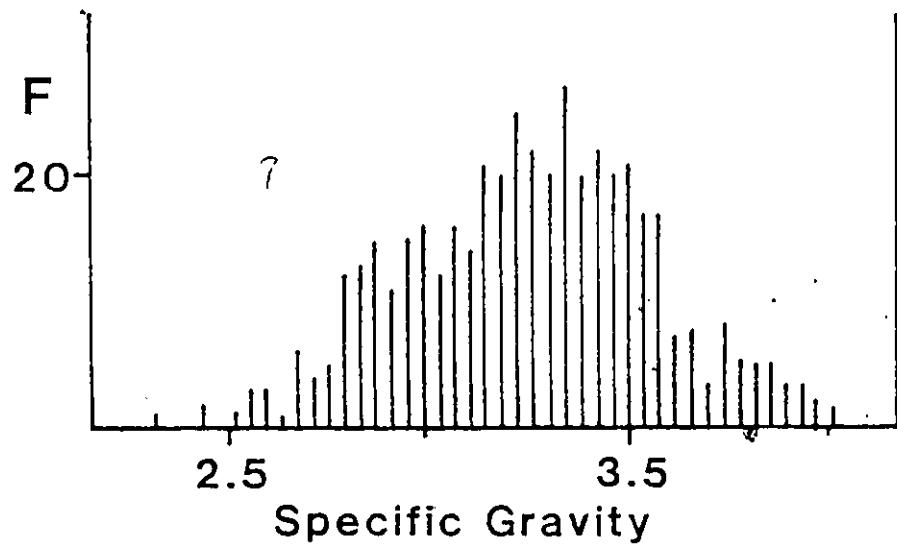


Fig. 5 Histogram of the specific gravities of 452 iron formation specimens.

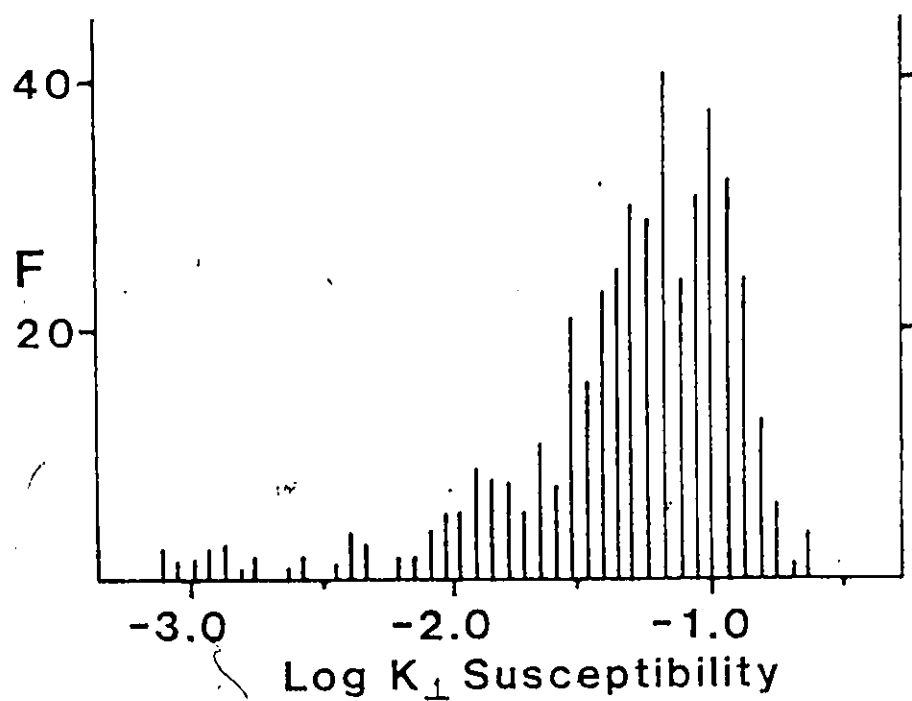


Fig. 6 Lognormal histogram of K_{\perp} susceptibility for 453 IF specimens.

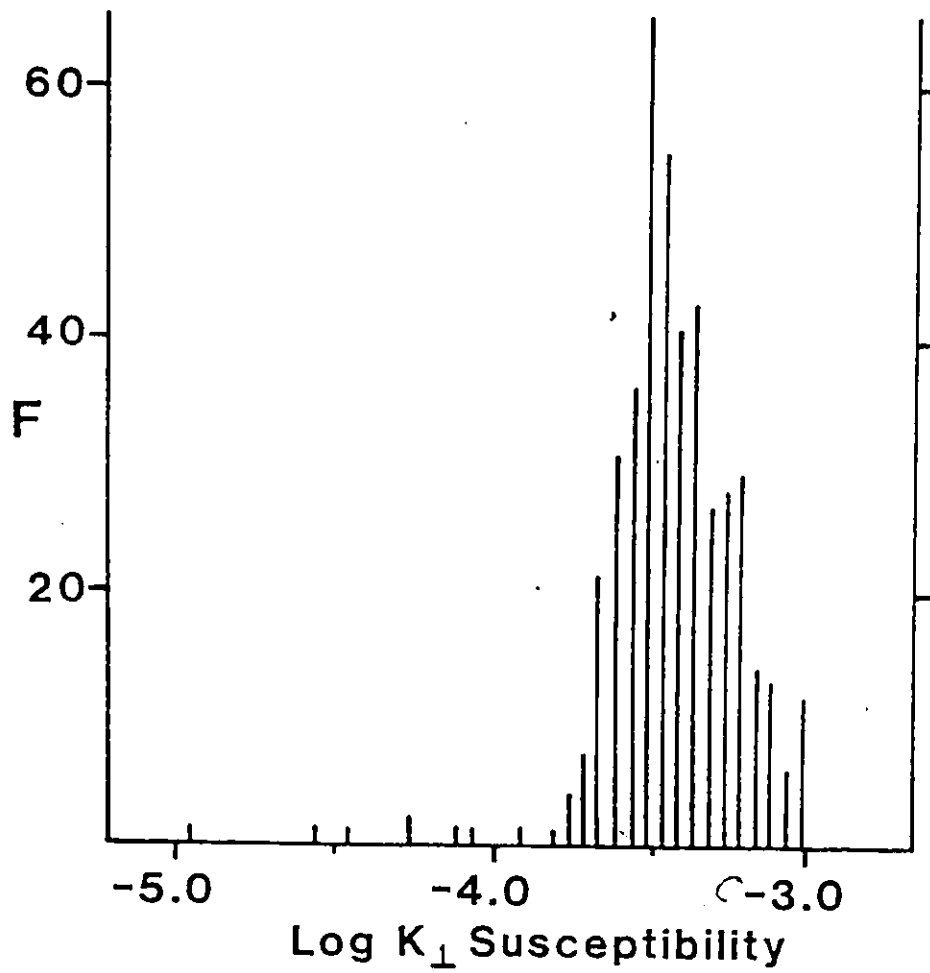


Fig. 7 Lognormal histogram of K_{\perp} susceptibility for 444 HR specimens.

ficient of +.851 (Fig. 8) and give the relationship

$$K_{\perp IF} = 0.1159SG - 0.312.$$

This is similar to the relationships obtained at the Moose Mountain Mine (Symons et al., 1980) and Sherman Mine (Symons and Stupavsky, 1979) but different from the Adams Mine (Quick, 1981):

$$\text{Moose Mountain: } K_{\perp IF} = 0.0912 SG - 0.249$$

$$\text{Sherman Mine : } K_{\perp IF} = 0.906 SG - 0.245$$

$$\text{Adams Mine : } K_{\perp IF} = 0.0698 SG - 0.179$$

Economic ore for the Griffith Mine contains 31% total Fe with 27% Fe in magnetite and 4% Fe in hematite. Thus, the SG of economic ore can be calculated from the equation:

$$\begin{aligned} SG_{\text{ore}} = & \frac{\% \text{Fe in magnetite} \times SG \text{ magnetite}}{\% \text{Fe in formula weight magnetite}} + \\ & \frac{\% \text{Fe in hematite} \times SG \text{ hematite}}{\% \text{Fe in formula weight hematite}} + \\ & \% \text{Silica} \times SG \text{ silica} \end{aligned}$$

The SG of economic ore is thus 3.60 g/cm³ giving mean value of .15 cgs/cm³ for K_{\perp} for iron ore.

4.3 ANISOTROPY OF MAGNETIC SUSCEPTIBILITY

The expected anisotropy of susceptibility pattern for banded IF is that the minimum (K_{\min}) axial direction of the ellipsoid is perpendicular to the bedding plane and the

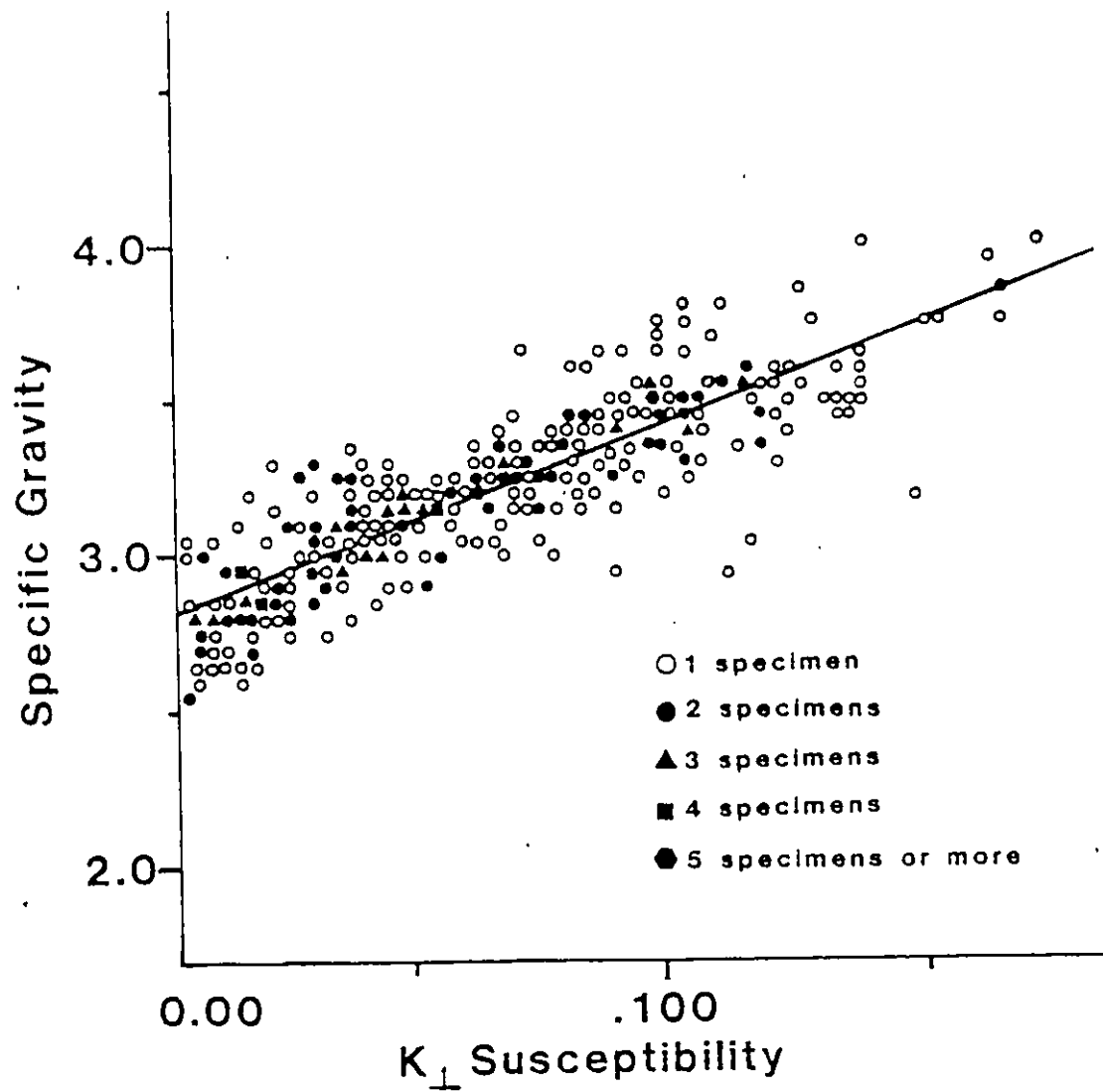


Fig. 8 Regression line of specific gravity versus K_{\perp} susceptibility for 363 IF specimens.

intermediate (k_{int}) and maximum (k_{max}) directions are parallel to the bedding plane. The principal susceptibility axes in this study agree with this pattern. The k_{min} direction is perpendicular to the bedding plane, i.e., k_{\perp} (Fig. 9) with the k_{int} and k_{max} directions in the bedding plane, i.e., k_{\parallel} (Figs. 10 and 11). The mean magnitude ratio of k_{int}/k_{min} is 1.4 (Fig. 12) and k_{max}/k_{min} is 1.5 (Fig. 13). Thus the mean bedding plane susceptibility is:

$$k_{\parallel} = \left[\frac{(k_{int} + k_{max})}{2} \right]$$

$$= 1.45$$

This ratio may be lower than reality because some of the cores may be confined to one band of IF and hence appear less anisotropic than the IF as a whole.

4.4 NATURAL REMANENT MAGNETIZATION

4.4.1 Iron Formation

4.4.1a NRM Intensity

The NRM intensities of 453 IF specimens also show a lognormal distribution (Fig. 14) with lognormal mean of $2.1 \times 10^{-2} \text{ emu/cm}^3$.

4.4.1b Koenigsberger Ratio (Q)

The Q ratio has a lognormal distribution with a mean of 0.66 (Fig. 15). Thus, if the IF NRM directions were

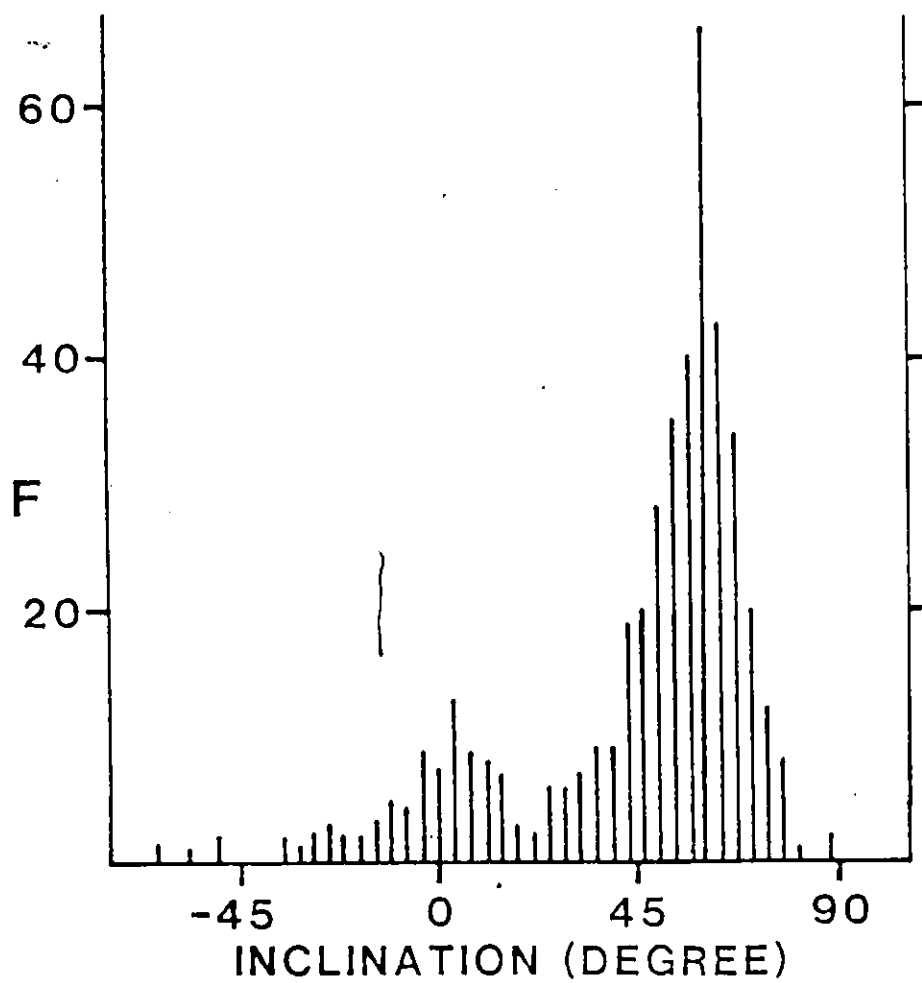


Fig. 9a Histogram of k_{\min} (k_{\perp}) direction for 453 IF specimen by (a) inclination, and (b) declination.

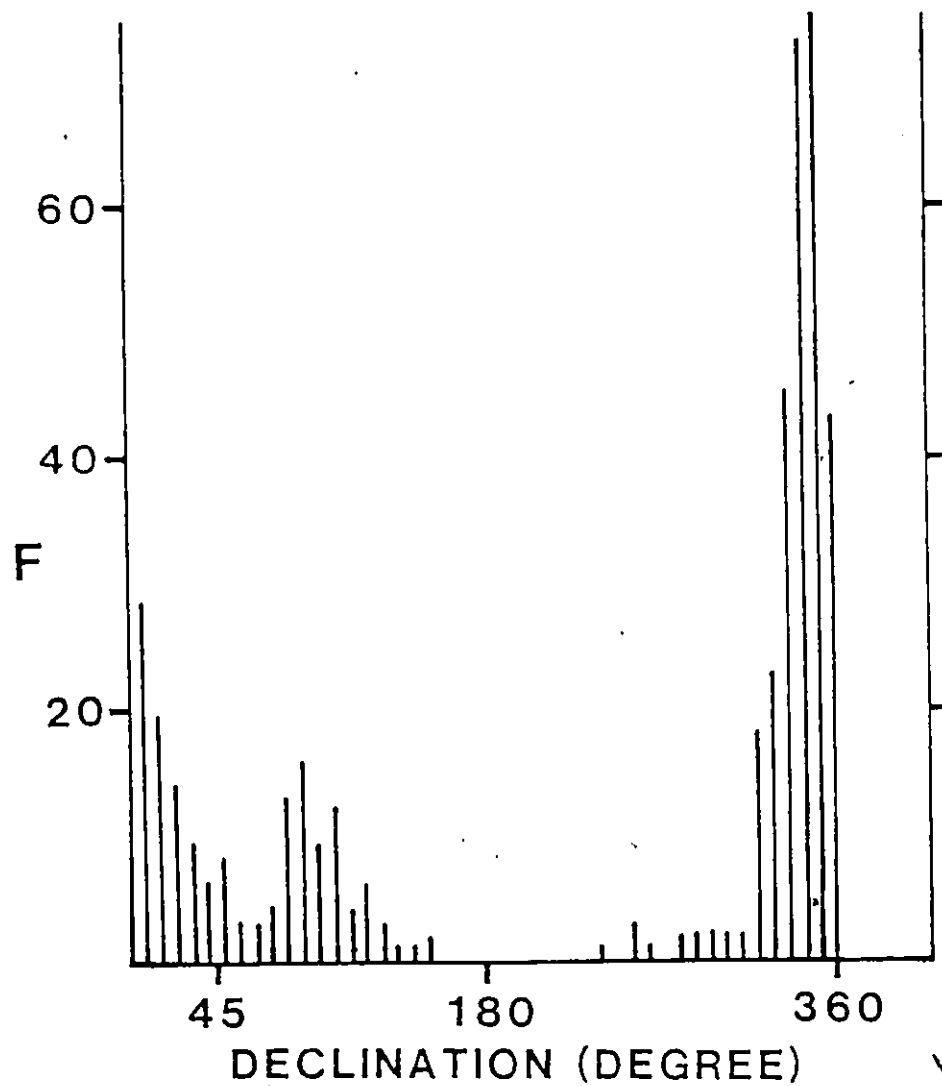


Fig. 9b Histogram of k_{\min} (k_{\perp}) direction for 453 IF specimen by (a) inclination, and (b) declination.

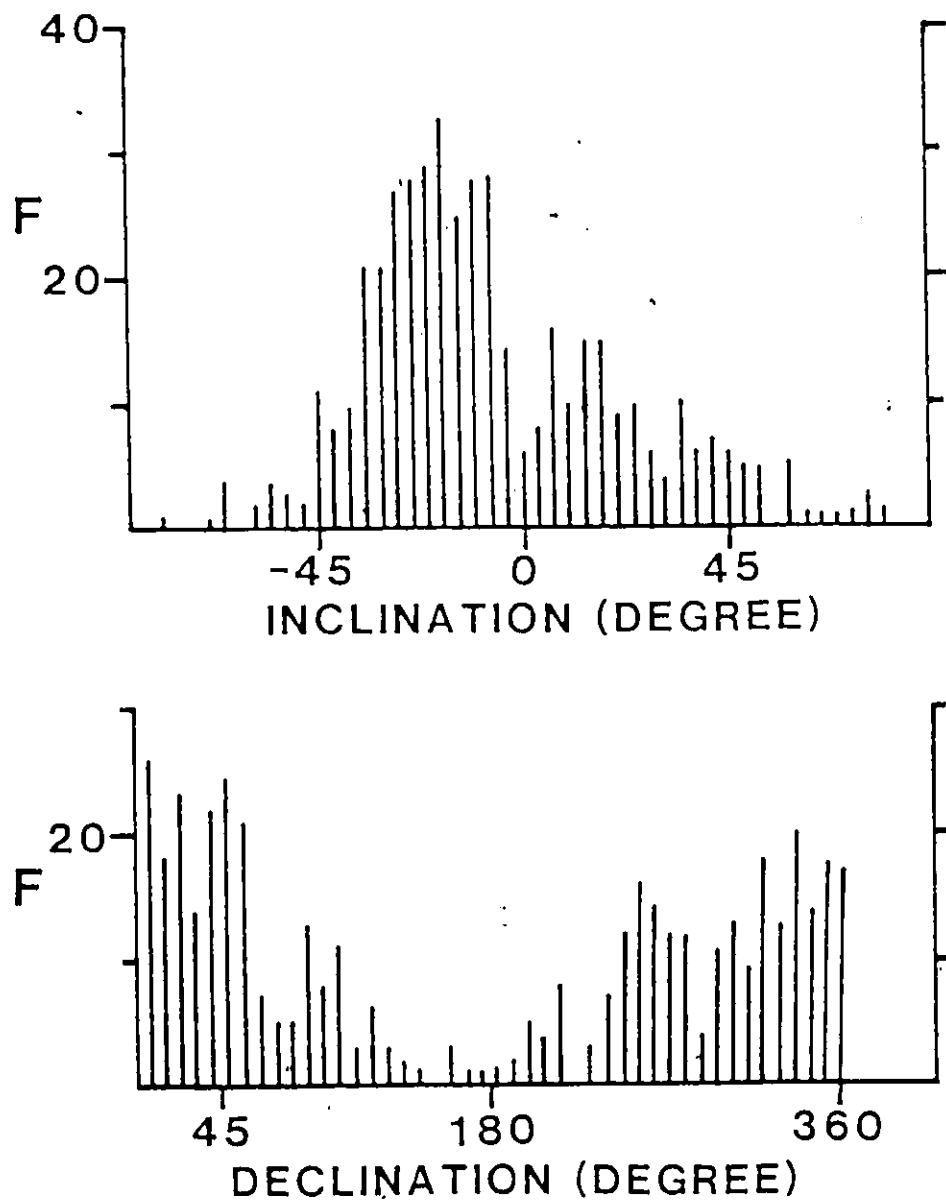


Fig. 10. Histogram of k_{int} directions for 453 IF specimens.

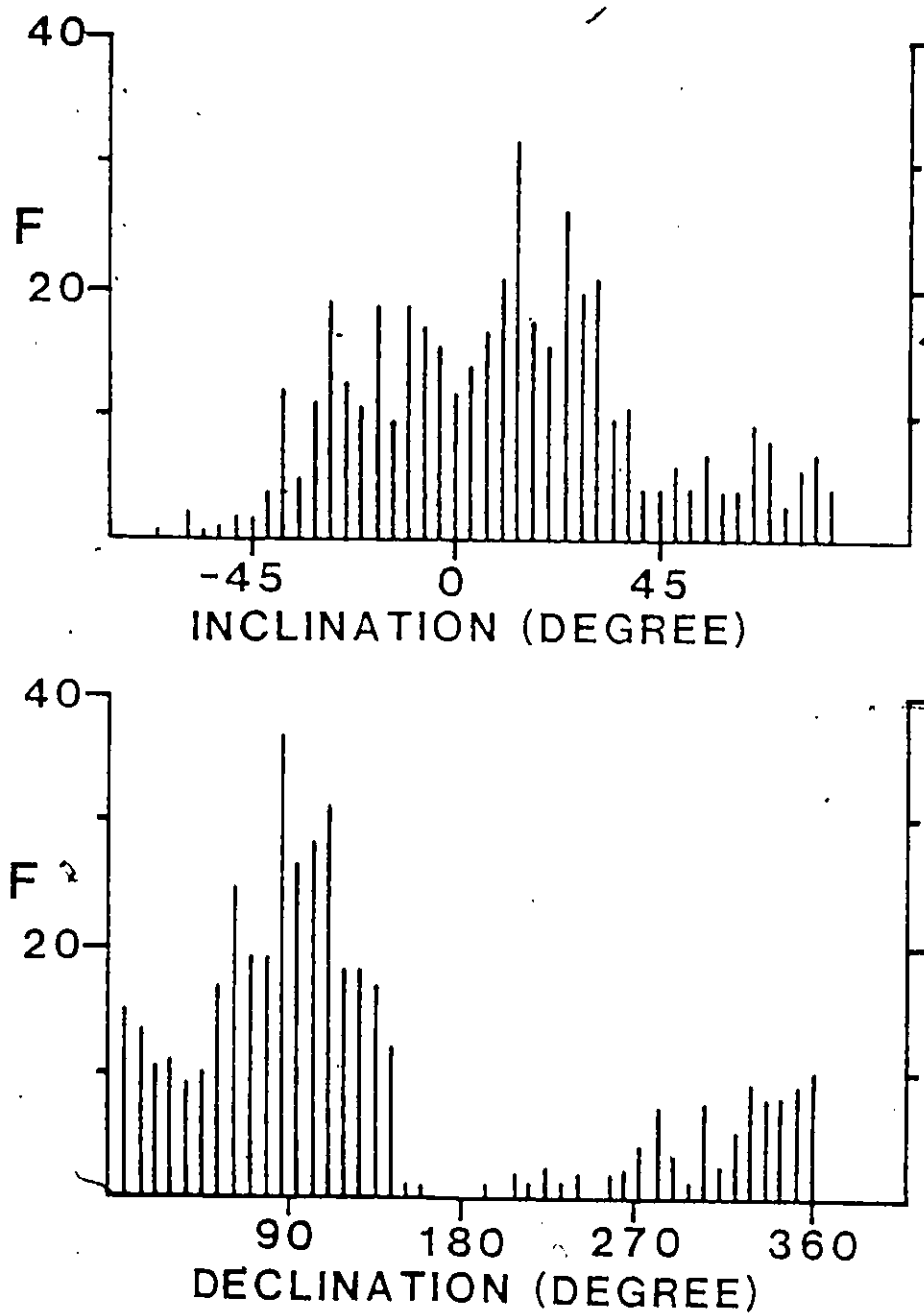


Fig. 11. Histogram of k_{\max} directions for 453 IF specimens.

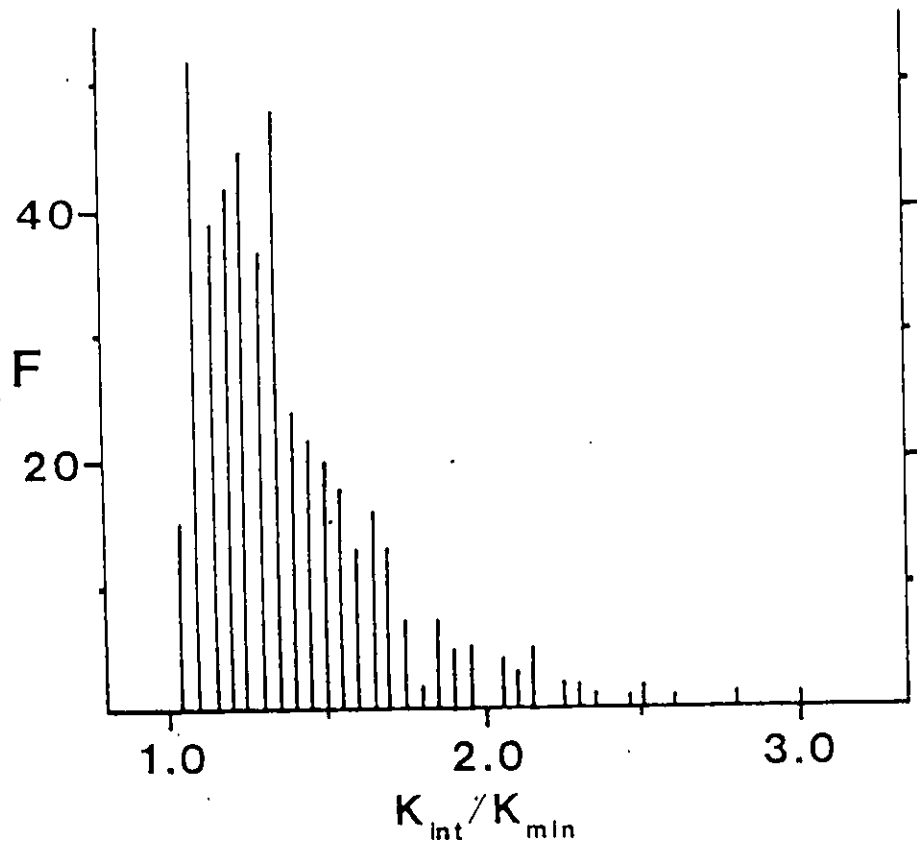


Fig. 12 Histogram of k_{int}/k_{min} for 453 IF specimens

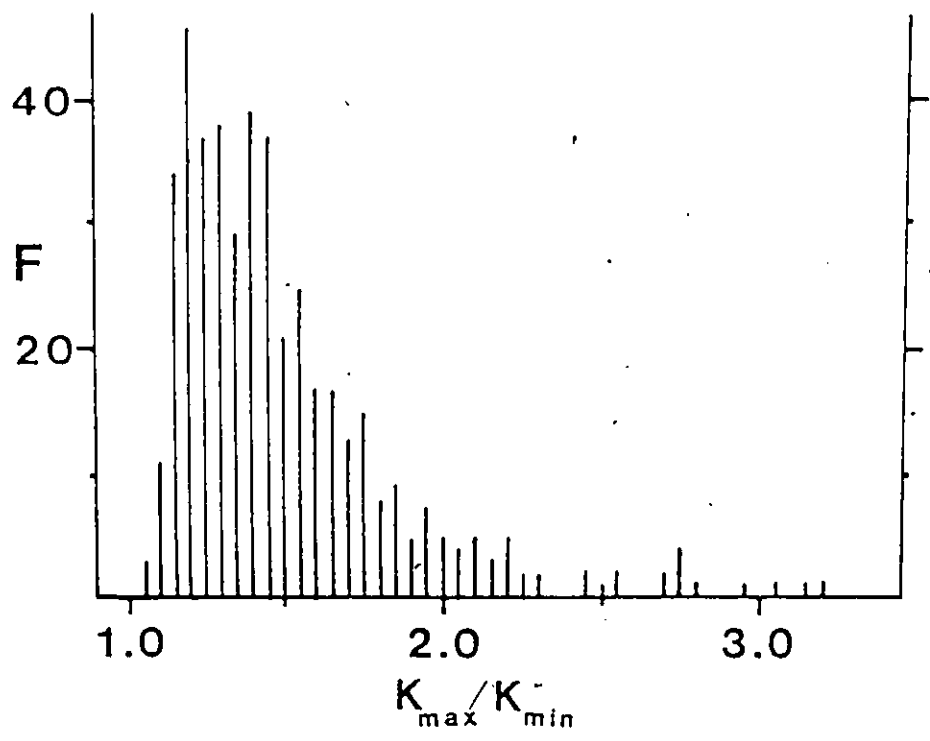


Fig. 13 Histogram of k_{max}/k_{min} for 453 IF specimens.

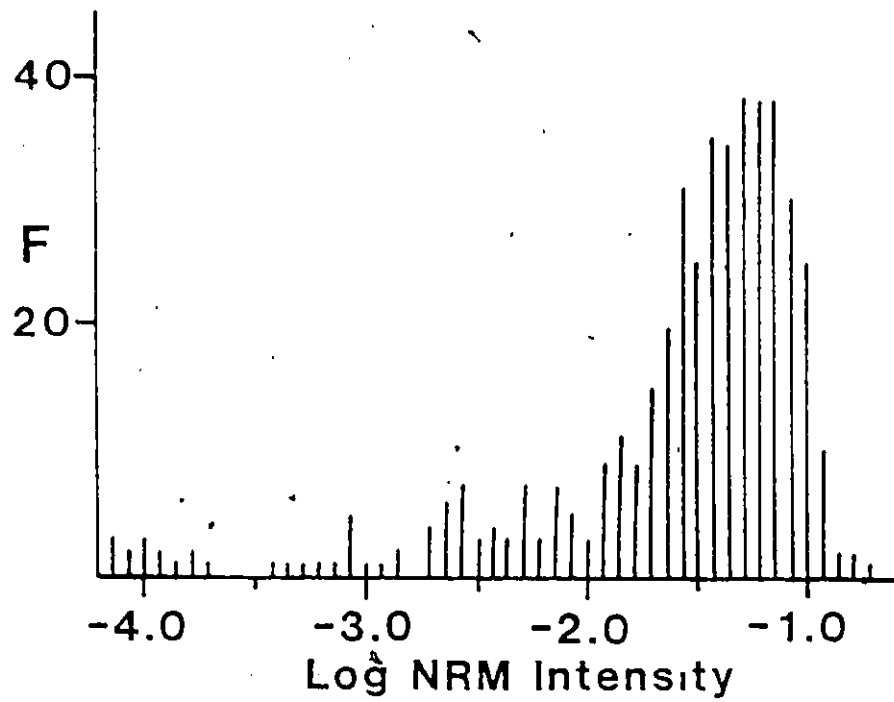


Fig. 14 Lognormal histogram of NRM intensity for 453 IF specimens.

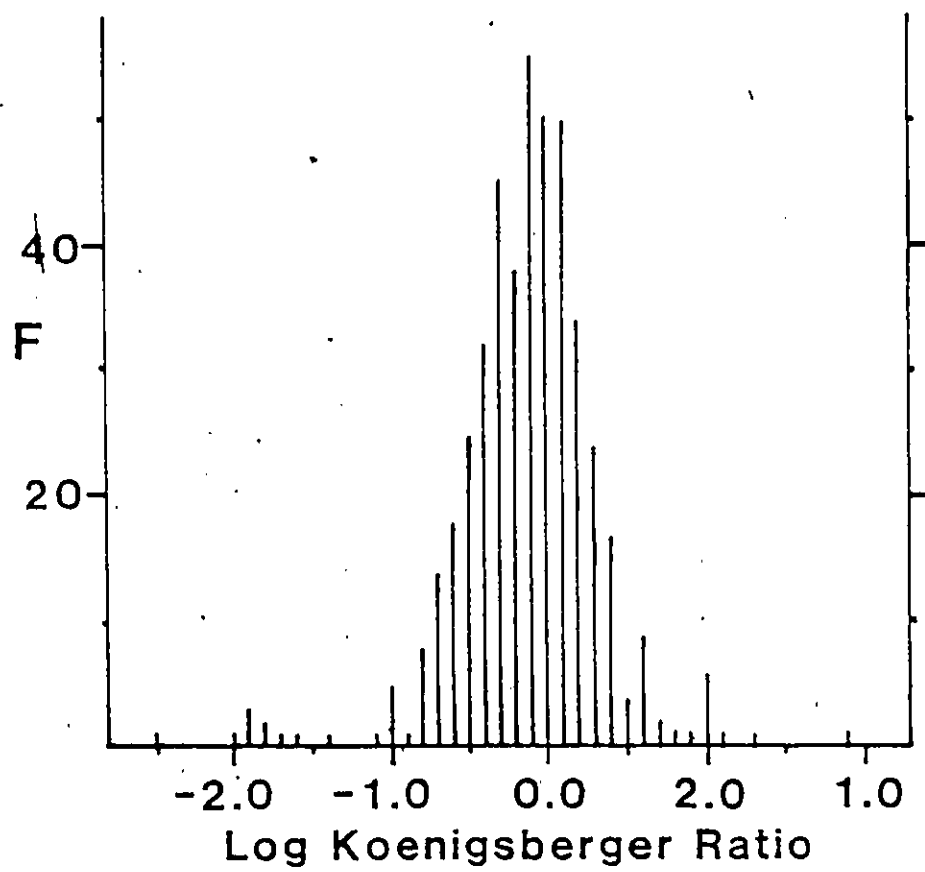


Fig. 15 Lognormal histogram of the Koenigsberger ratio (Q) for 453 IF specimens.

entirely aligned with the Earth's field, then the remanence would increase the induced anomaly by 66%. The mean NRM direction of 33.0° , 76.5° , $\alpha_{95} = 11.5^\circ$ has a deviation angle (θ) of $\sim 8^\circ$ from the EMF direction of 5.5°E , 78.4° . The ratio of the vector resultant ($R = 117.3$) to the number of block mean directions ($N = 541$) in the NRM population gives an effective Koenigsberger ratio (Q_e) of $Q_e = (R/N) \times Q$. Thus the NRM augments the induced magnetic intensity (J_i) by $(Q_e \times \cos \theta) J_i$ to give an augmenting factor of $0.14 J_i$. This value is lower than the values $0.24 J_i$, $0.22 J_i$ and $0.17 J_i$ obtained for the Moose Mountain Mine, Sherman Mine and Adams Mine deposits respectively.

4.4.1c NRM- k_\perp Relationship

The relationship between NRM intensity and k_\perp has a correlation coefficient of $+0.55$ for 453 specimens (Fig. 16). The NRM to k_\perp relationship obtained in the Griffith Mine is:

$$\text{NRM} = 0.372 k_\perp + 0.013$$

This NRM intensity is in close agreement with the values obtained at the Moose Mountain Mines and Sherman Mines but higher than the value obtained at Adams Mine.

Moose Mountain Mine:	$\text{NRM} = 0.439 k_\perp + 0.023$
Sherman Mine	: $\text{NRM} = 0.434 k_\perp + 0.005$
Adams Mine:	: $\text{NRM} = 0.215 k_\perp + 0.016$

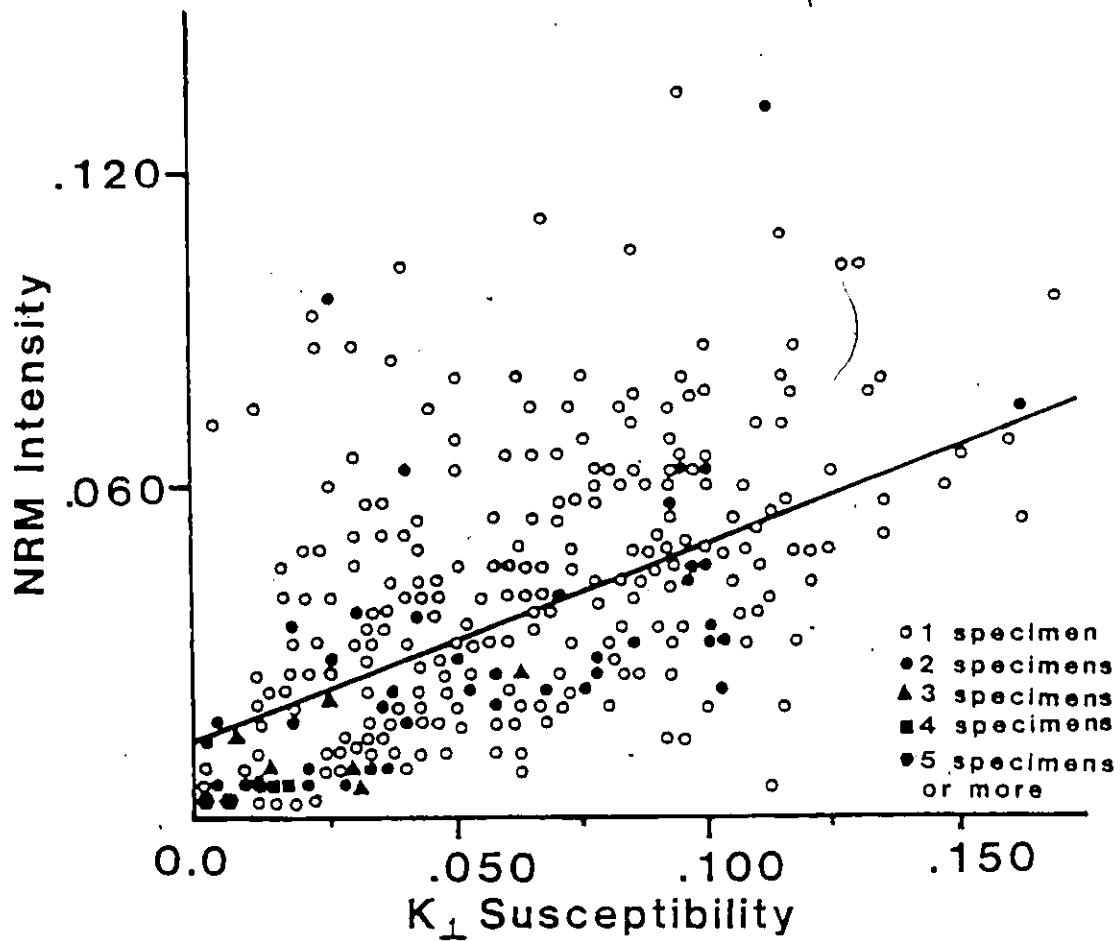


Fig. 16 Regression line of NRM intensity versus K_{\perp} susceptibility for 453 IF specimens.

4.4.1d Storage Test

A storage test run on 18 representative IF specimens show an average NRM change of ~17% in intensity (Fig. 17b) and of 4° in direction over a four week period (Fig. 17a). This suggests that IF NRM's are quite unstable with significant viscous (VRM) components.

4.4.1e Shock Test

The shock test run on 20 IF specimens show a 44% mean reduction in NRM intensity after 20 shocks (Fig. 18a) and a 29° change in direction after 20 shocks (Fig. 18b). These results suggest that the blasting may have affected the NRM in the IF specimen. Shapiro and Ivanov (1966) found that the resulting shock remanence can be erased by low alternating field demagnetization. Cisowski and Fuller (1978) have also shown that partial thermal demagnetization effectively removes shock remanence.

4.4.2 Host Rock NRM

4.4.2a NRM Intensity

The NRM intensities (J_0) of the HR specimens exhibit a lognormal distribution with a broad spectrum of values from 6.31×10^{-8} emu/cm³ to 1.60×10^{-2} emu/cm³ with a log-normal mean from 491 specimens of 1.47×10^{-5} emu/cm³ (Fig. 19).

4.4.2b Koenigsberger Ratio

The Koenigsberger ratio (Q) of the remanent to

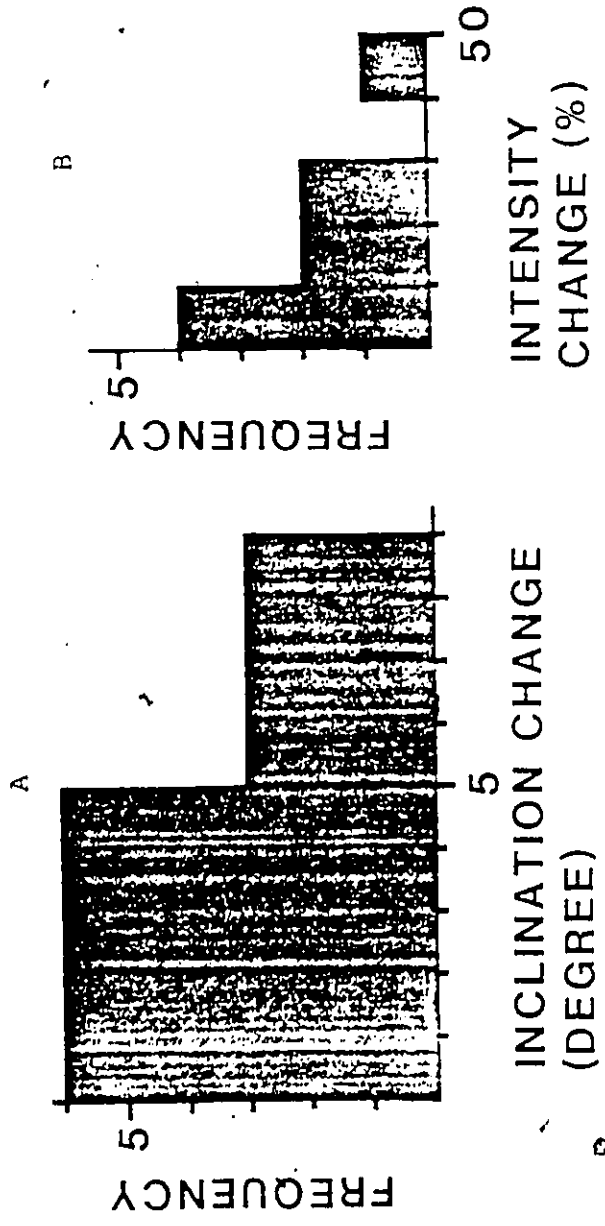


Fig. 17a Histogram of NRM inclination change of IF specimens over four weeks

Fig. 17b Histogram of NRM intensity change of IF specimens over four weeks.

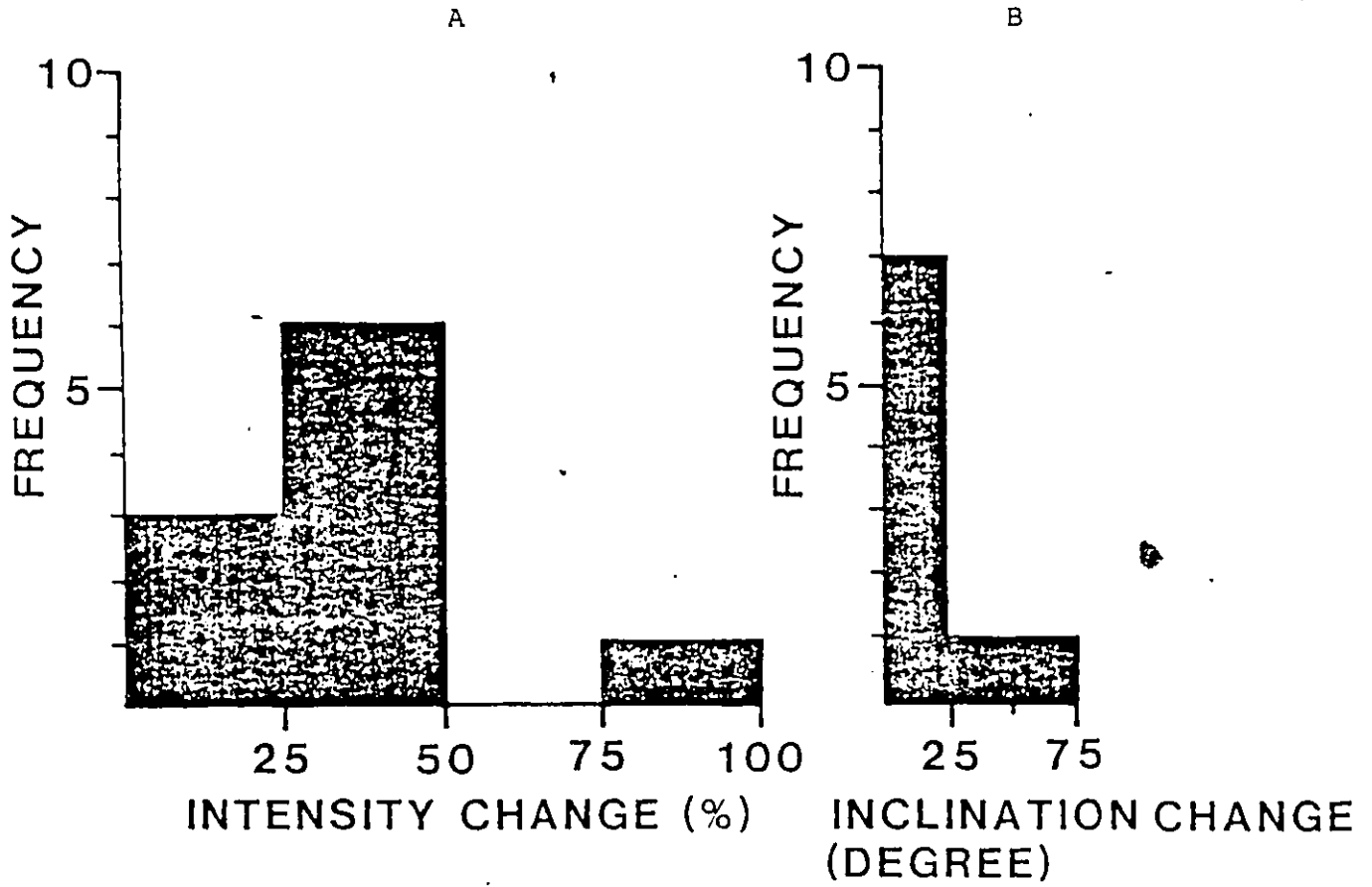


Fig. 18a Histogram of NRM intensity change of IF specimens after induced shock

Fig. 18b Histogram of NRM inclination change of IF specimens after induced shock.

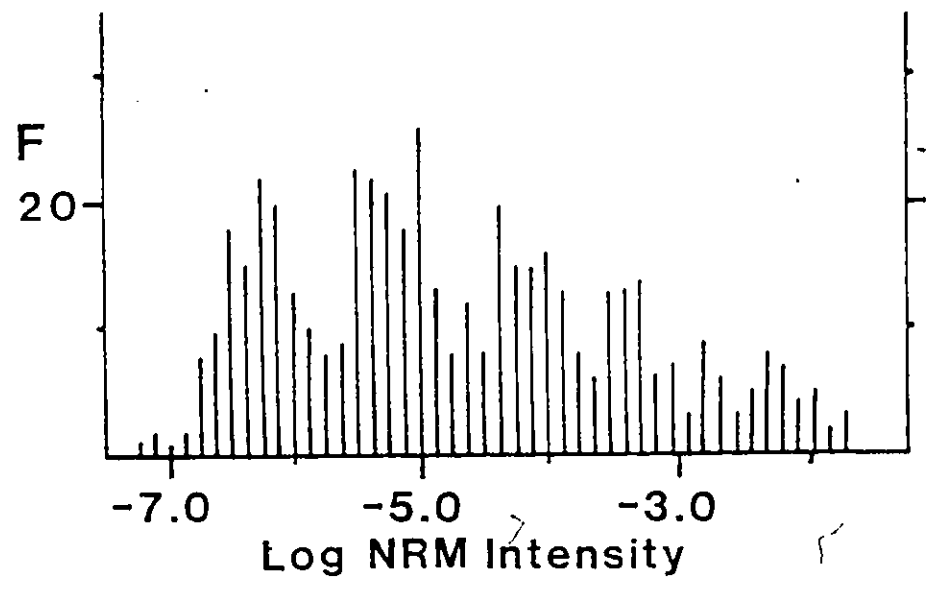


Fig. 19 Lognormal Histogram of NRM intensity for 491 HR specimens.

induced magnetization also has a lognormal distribution with values ranging from 2.5×10^{-4} to 251 with lognormal mean of 0.051 (Fig. 20). The mean induced magnetization of the IF is ~2170 times greater than the mean HR NRM. Thus it is reasonable to omit the HR NRM from anomaly calculations although in a number of places its NRM contribution is important.

4.4.2c Storage Test

A storage test run on 14 ~~HR~~ specimens show an average NRM change of 5% in intensity (Fig. 21a) and of 2.5° in direction over a four week period (Fig. 21b). This suggests that the NRM stability is high and that the viscous (VRM) component is relatively small.

4.5 STATISTICAL ANALYSIS

4.5.1 Statistical Analysis of IF

The following conventional tiered statistical tests were performed to select reliable IF specimen directions after AF demagnetization (Table 3). The screening test consisted of using Fisher (1953) statistics to determine the degree of specimen deviation from the sample mean. If the specimen direction diverges by more than 20° from the sample direction, then the specimen direction was rejected. Thus a homogeneous sample mean direction was formed from 2, 3, or 4 specimen directions.

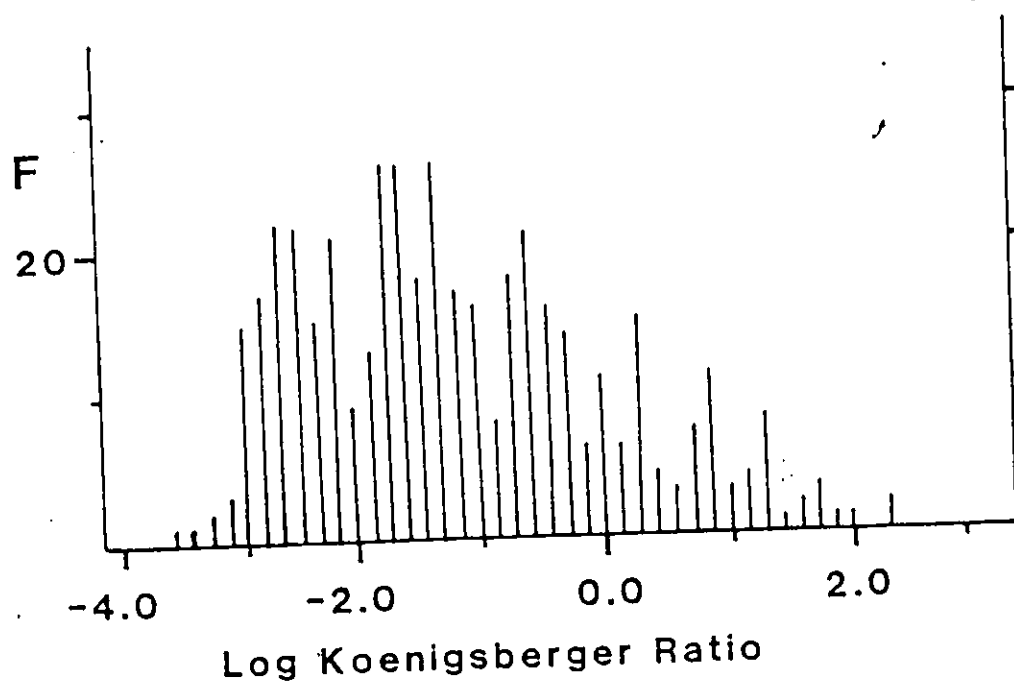


Fig. 20 Lognormal histogram of the Koenigsberger ratio (Q) for 491 HR specimens.

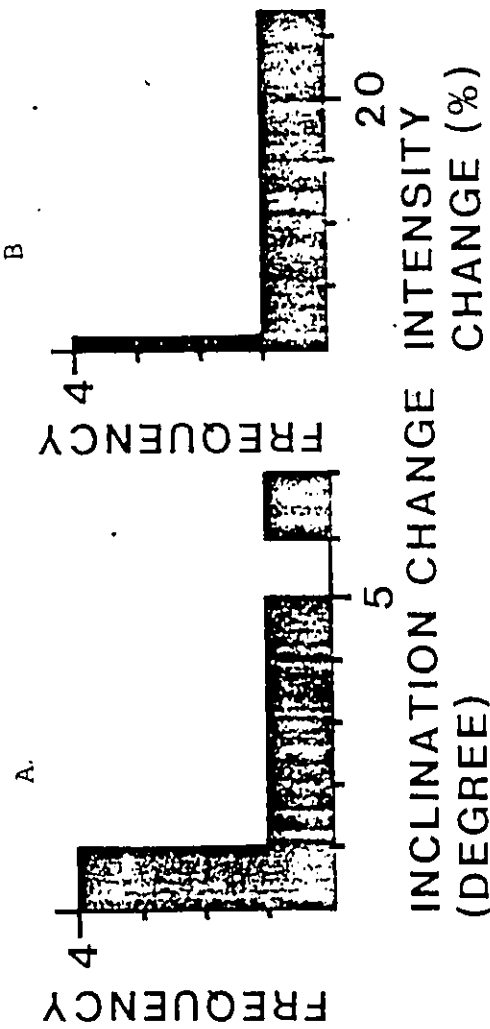


Fig. 21a Histogram of NRM inclination of HR specimens over four weeks

Fig. 21b Histogram of NRM intensity change of HR specimens over four weeks

In 17 of the 175 samples the intensity of magnetization was considered to be too low for reliable remanence measurement and so their data was rejected. A total of 10 samples gave a homogeneous direction, an additional 32 samples gave a homogeneous direction after 1 specimen was rejected. An additional 6 sample groups were found where two directions were recognized. Thus, of the original 175 samples, a total of 48 samples, or only 27%, yielded acceptable sample mean directions after screening tests.

4.5.2 Statistical Analysis of HR

The HR paleomagnetic remanence directions show a high degree of scatter. Thus screening of the data at the core level and at the site level was necessary to eliminate unstable and inhomogeneous directions. The homogeneous site mean directions for the HR were determined in a similar manner to the IF (Table 4). There are three steps by which a homogeneous site mean direction was determined: 1) core data were rejected if only one core specimen direction was available, 2) a core mean direction was accepted if the two core specimen directions diverged by $<20^\circ$, and 3) at least two core mean directions had to be acceptable to calculate a site mean direction.

In 117 of 291 cores the directions for the two specimens diverged more than 20° . These cores were considered

to be inhomogeneously magnetized and their data were rejected. In 20 of the remaining 174 cores, their data were rejected because the sole remaining direction was decided inadequate to represent the site. An additional 7 sites were rejected because there was only one acceptable core direction.

A total of 19 of the original 54 sites survived the screening tests and yielded acceptable site mean directions. In the 19 accepted sites, 7 are from metasediments (37%), 5 are from metavolcanics (26%), 5 are from quartz diorites (26%), and 2 are from diabase dikes (11%).

4.6 AF DEMAGNETIZATION OF IF

4.6.1 Pilot Specimens

In order to define the nature of the IF NRM, 58 representative specimens having typical NRM directions and intensities were selected from the 175 blocks for AF step demagnetization studies. The data for the 58 specimens were AF demagnetized up to 100 mT in 5, 10, 15, 20, 30, 40, 50, 60, 80, and 100 mT steps and were analyzed by: a) stability index analysis; b) vector-removed between successive steps; and, c) remanence direction stereocontour plots to determine the composition of the NRM. The paleomagnetic stability index (PSI) (Symons and Stupavsky, 1974) gives the rate of change of the remanence direction in mdeg/T during demagnetization and quanti-

tively measures the degree of success of the demagnetization treatment in isolating a stable remanence component. When the treatment isolates a remanence component, a direction 'end point' is reached at some demagnetizing field above which the direction remains constant and PSI approaches zero. In addition the vector removed between successive demagnetizing steps becomes parallel to the measured vector. In contrast for the paleomagnetically unstable specimens where the treatment fails to isolate direction changes between succeeding demagnetizing steps, the PSI remains high at all fields and the vector removed never becomes parallel to the measured vector.

On examining the pilot specimens, they appear to show the removal of unstable viscous remanence (VRM) components in the present steeply inclined Earth's field direction in the 20-30 mT steps (Fig. 22). Above 40 mT the PSI curves record an increasing rate of directional change from step to step as larger random anhysteritic remanence (ARM) components are progressively added by the demagnetization process.

The intensity decay curves (Fig. 23) support this interpretation. The same specimens show the rapid exponential intensity decay up to 30 mT as significant viscous components are removed and thereafter a linear intensity decay throughout the balance of the demagnetization pro-

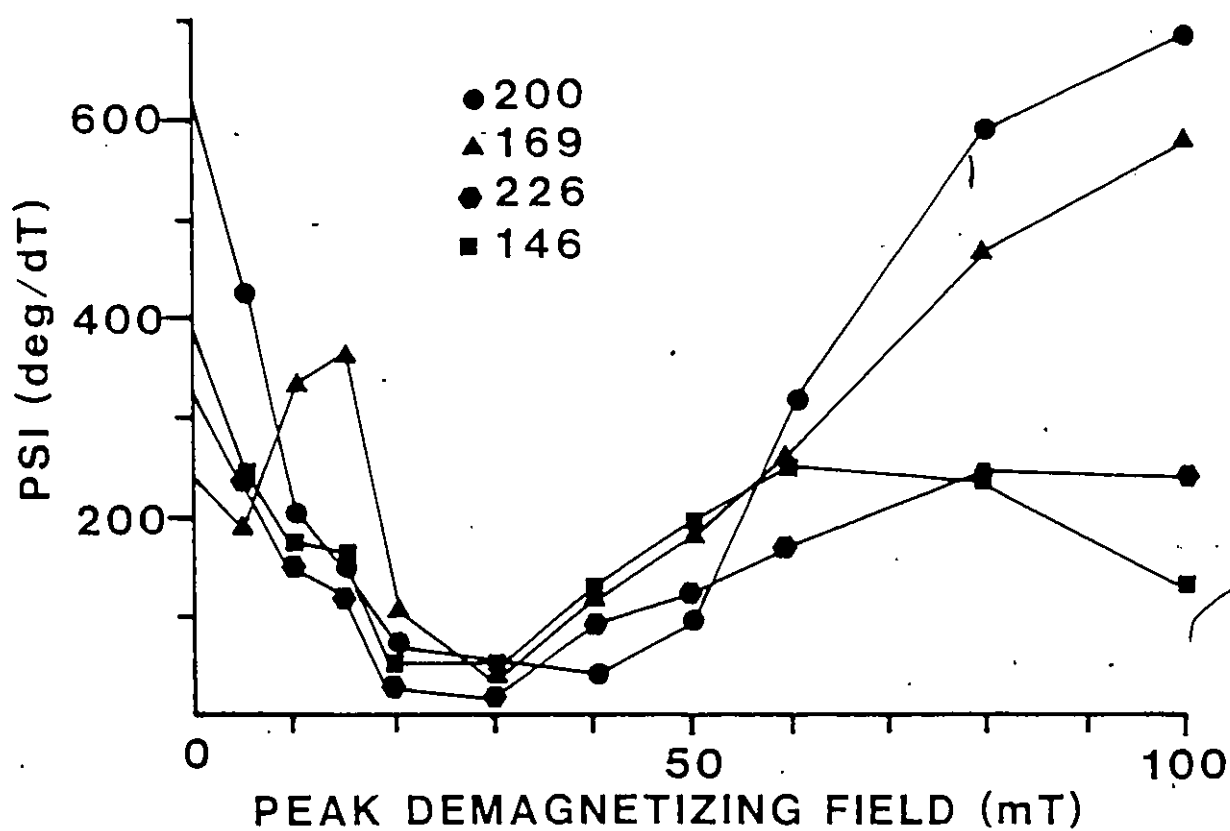


Fig. 22 IF AF demagnetization curve - paleomagnetic stability index for directional changes.

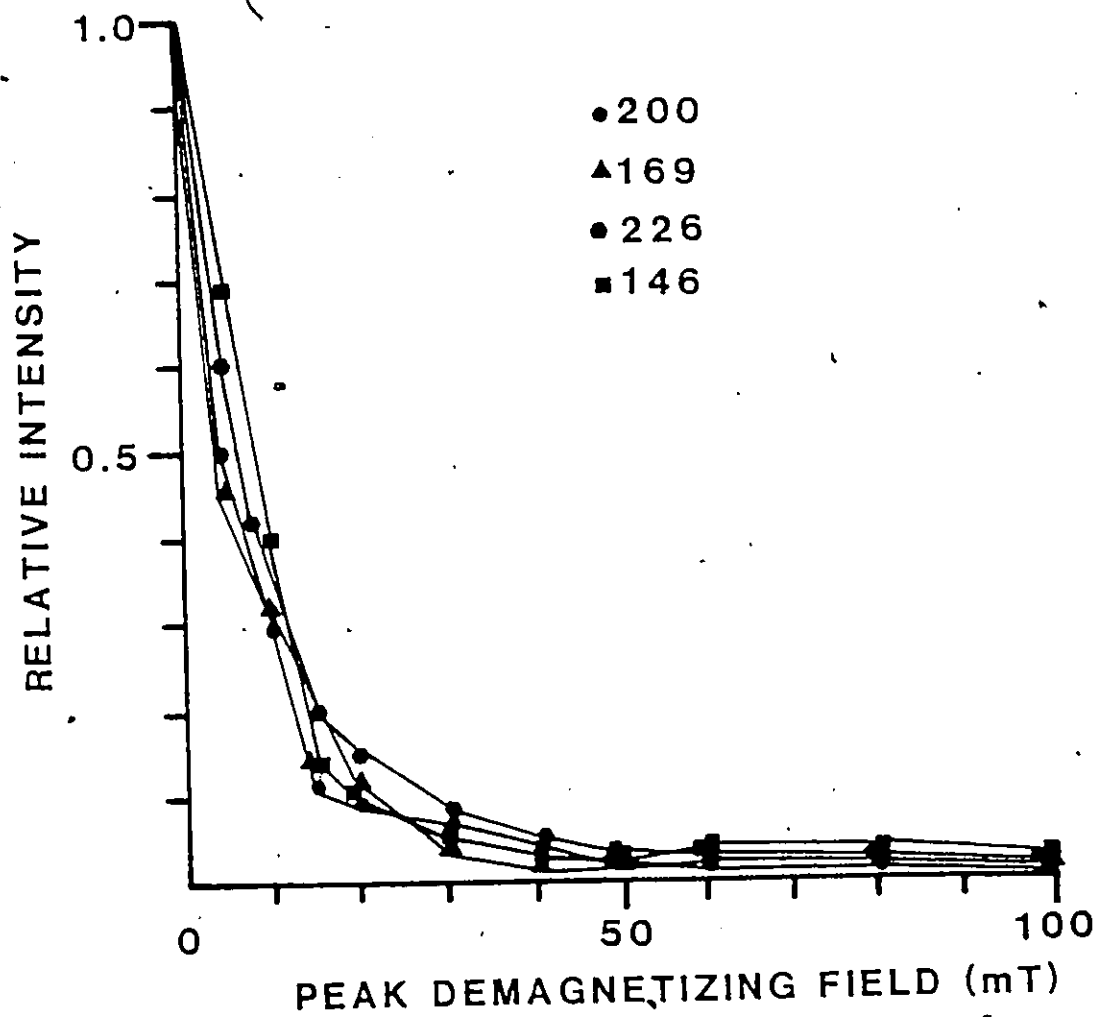


Fig. 23 IF AF demagnetization curve - relative intensity.

cess. All the specimens show 95% reduction in intensity between 0-30 mT and 99% intensity removed by 100 mT. The directional changes of representative specimens are shown in Fig. 24. The optimum cleaning field was selected by inspection of the PSI minima. In most cases, as shown by Fig. 25a, this field is in between 30-40 mT by which time the relative intensity (J_n/J_o) has been reduced to <10% of its original intensity (J_o) in most specimens (Fig. 25b).

4.6.2 REMAINING SPECIMENS

4.6.2a Conventional Analysis

After AF demagnetization at demagnetizing fields ranging from 30-40 mT, the four specimen directions per block were assigned unit weights and the block mean remanence directions and statistical precision (Fisher, 1953) were computed. Reliably magnetized blocks for interpretation were selected by requiring remanence homogeneity at the block level. A total of 48 accepted block mean directions (see 4.5.1 Statistical Analysis of IF) when plotted on a stereonet form a highly dispersed population and thereby indicate they carry a very complex remanence (Fig. 26).

4.6.2b Modal Analysis of the Paleomagnetic Data

When the NRM remanence of a rock unit is complex consisting of VRM, metamorphic overprints and the primary

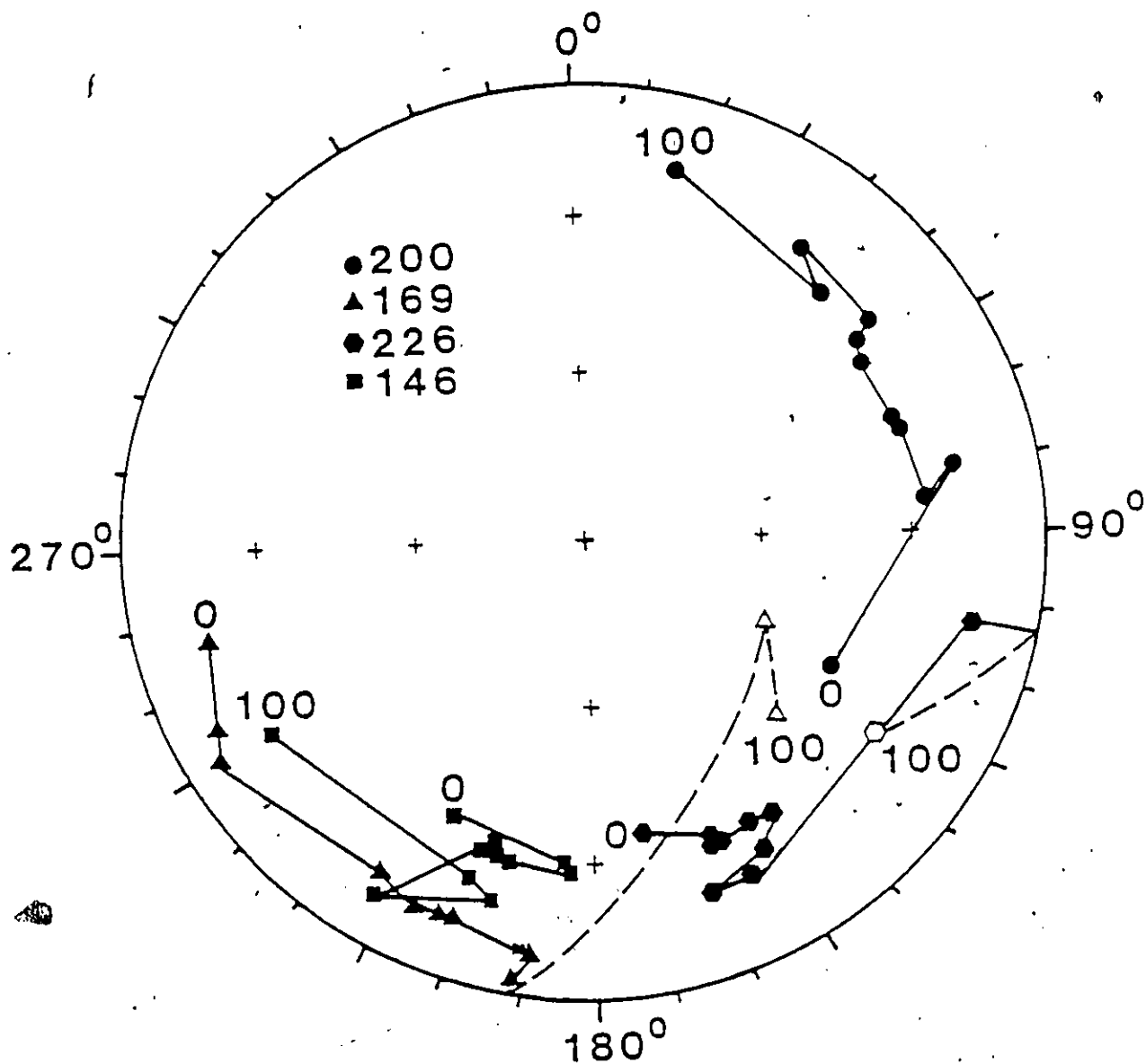


Fig. 24 Directional changes of AF demagnetization on an equal area projection for IF pilot specimens.

Note: Change in direction on progressive AF demagnetization in fields of 0, 5, 10, 15, 20, 30, 40, 50, 60, 80 and 100 mT, for IF pilot specimens. Solid (open) symbols indicate down (up) directions.

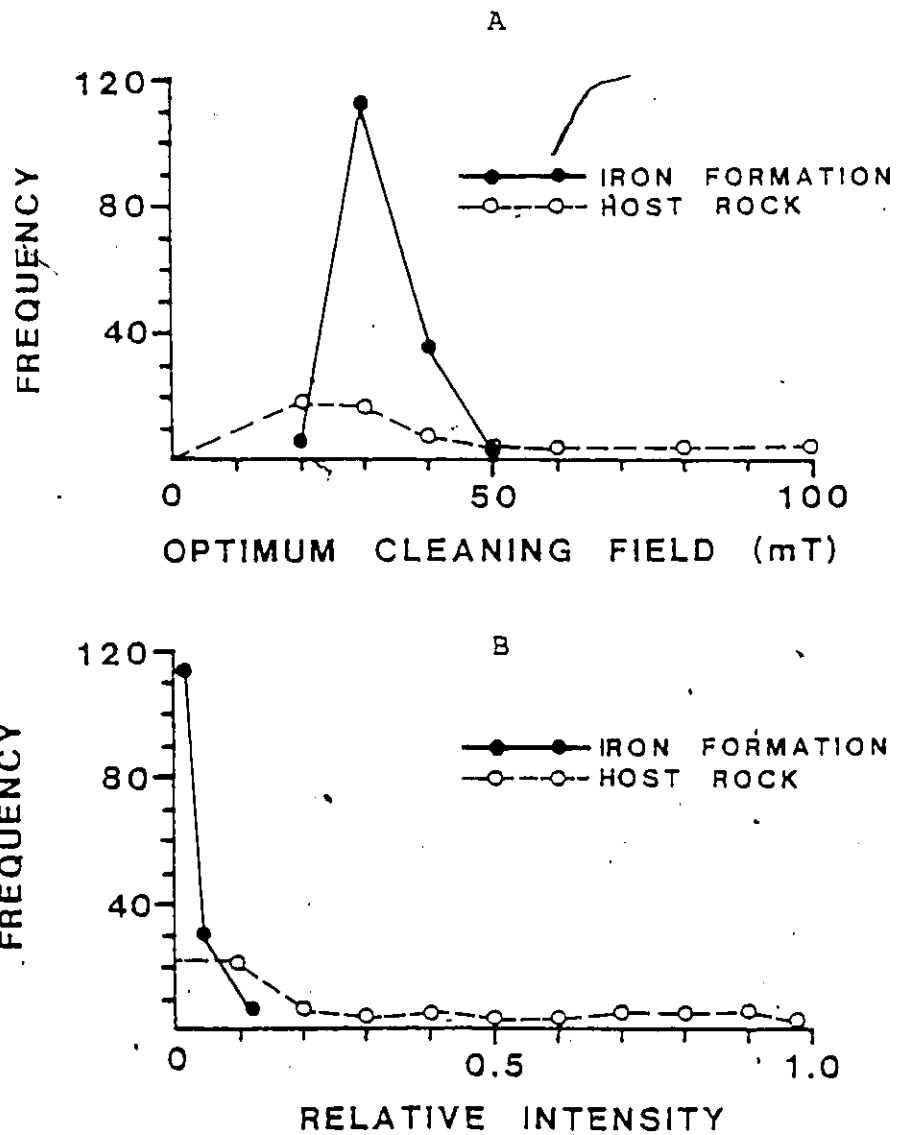


Fig. 25 (A) Plot of optimum AF cleaning field for IF and HR specimens.
 (B) Relative intensity of NRM after cleaning at optimum AF field.

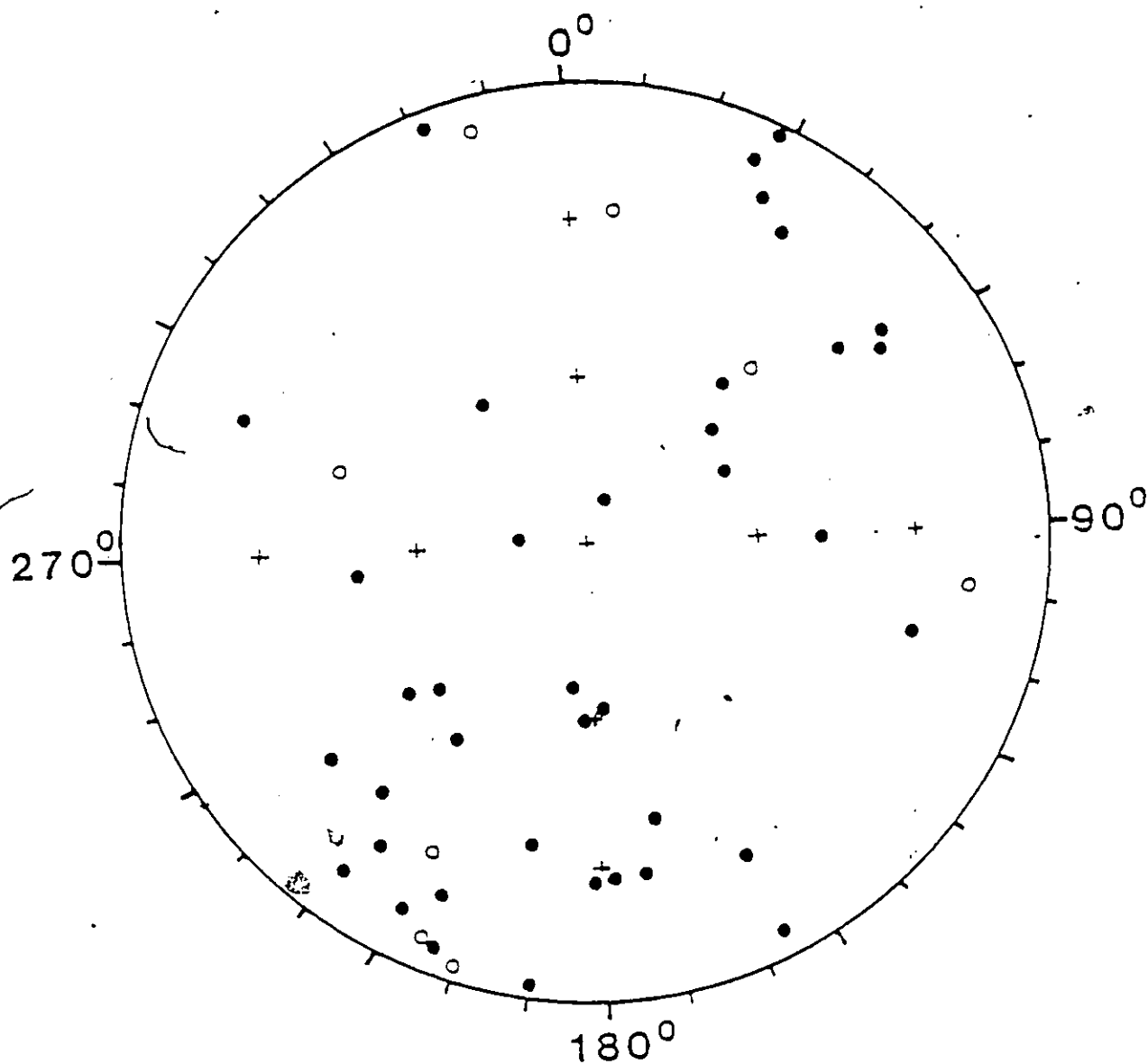


Fig. 26 IF AF cleaned site mean directions on an equal area projection.

Note: Solid (open) symbols indicate down (up) directions.

magnetization, and or when a remanence component is isolated in only a few specimens per site, a population level analysis (Symons and Stupavsky, 1981; Van Alstine, 1980) has been found to be successful for defining the components in this type of rock units.

The population level analysis is a single step screening of all specimens after a common treatment. The procedure is to plot the specimen directions on a stereonet with the positive down directions and the negative up directions separately. All the directions can be smoothed and contoured by using a Kamb's method (1959). The concentrations of directions identify the various remanence components present in the rock. The difference between this method and conventional point density percentage contours is that the smoothing area (A) depends on the number of directions (N). The contour intervals are in terms of the standard deviation (σ) and expected density (E) for the random sampling of N randomly directed vectors. Therefore, any anomaly outlined having $E + 2\sigma$ directions more than the number of expected for a random distribution of vectors will be highly significant especially if it is in one localized area of the stereonet (Kamb 1959). The mode of remanence component may be obtained from the anomaly maxima or by using Fisher statistics on those directions falling within a given anomaly contour. The smoothing method was performed on AF cleaned IF specimens that were: a) corrected for the bedding tilt and the plunge

of 30° SW, and b) uncorrected for folding. The AF IF specimens, after smoothing and contouring (Figs. 27, 27a, 28) form several statistically significant anomalies. The mode of each remanence component (anomaly) and its precision were calculated by selecting only those specimen directions which fall within the $E + 2\sigma$ contour and thus explicitly define the remanence component, and using these directions to compute the Fisher mean (= mode) and radius of circle of 95% confidence (=precision). This method gives essentially the same mode and precision as the more complex method of Van Alstine (1980). The anomalies, designated as E_1 , E_2 , E_3 , W_1 , W_2 , and W_3 , yielded mean directions which are given in Table 5.

4.7 FOLD TEST AFTER AF CLEANING

A non-conventional paleomagnetic fold test was performed by selecting only those specimen directions within an anomaly defined by the $E + 2\sigma$ contour. The specimen directions after correction for folding were compared with the uncorrected directions using the angular variance tests of Laroche (1969) and Watson (1956). In addition, tests of modal directions before and after fold corrections were made.

The angular variance test of Laroche (1969) compares the dispersion in remanence directions before and after fold

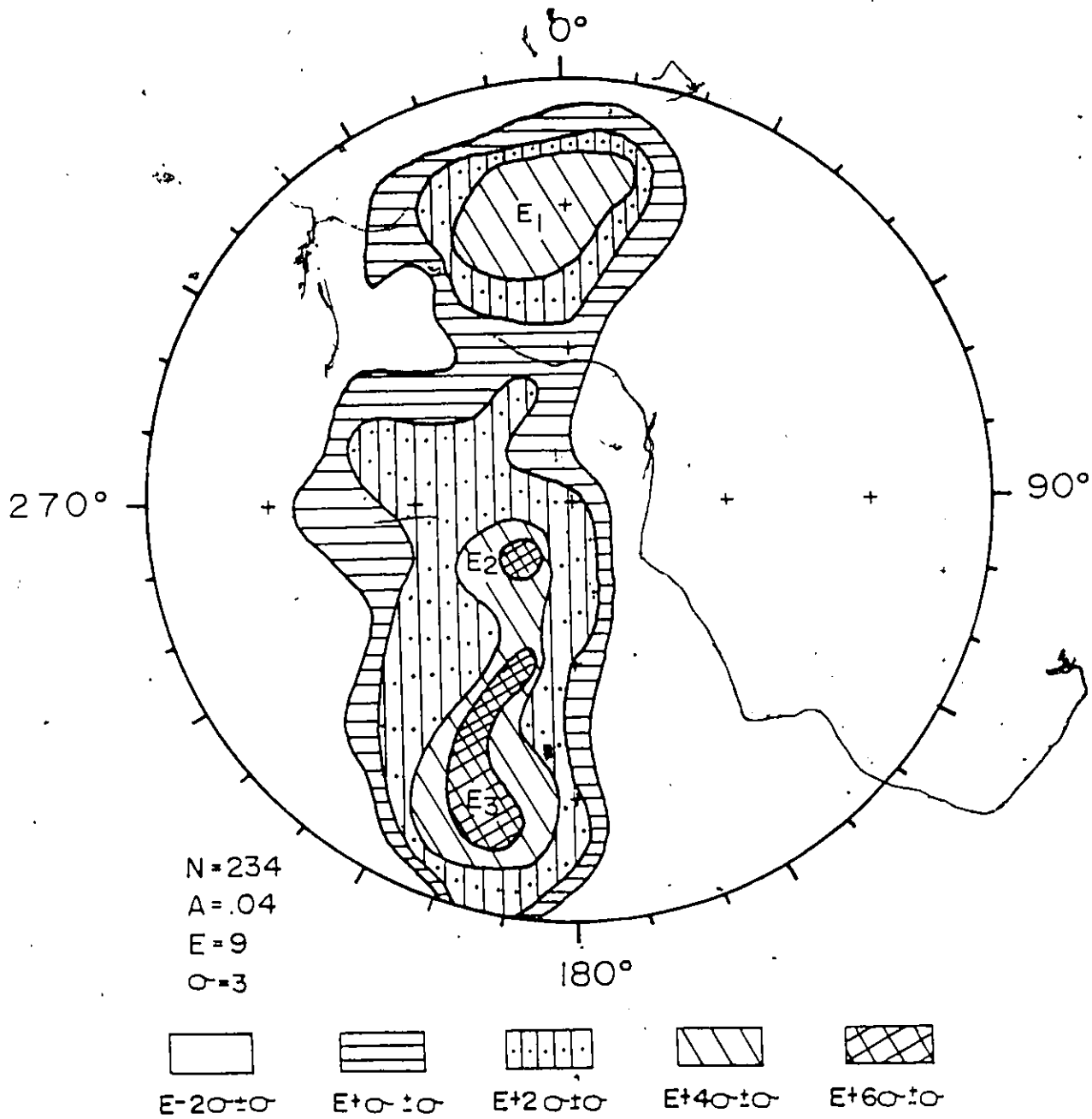


Fig. 27 Smoothing and contouring of AF cleaned IF specimens corrected for bedding tilt and plunge of fold (down direction; east limbs of east and west synclines)

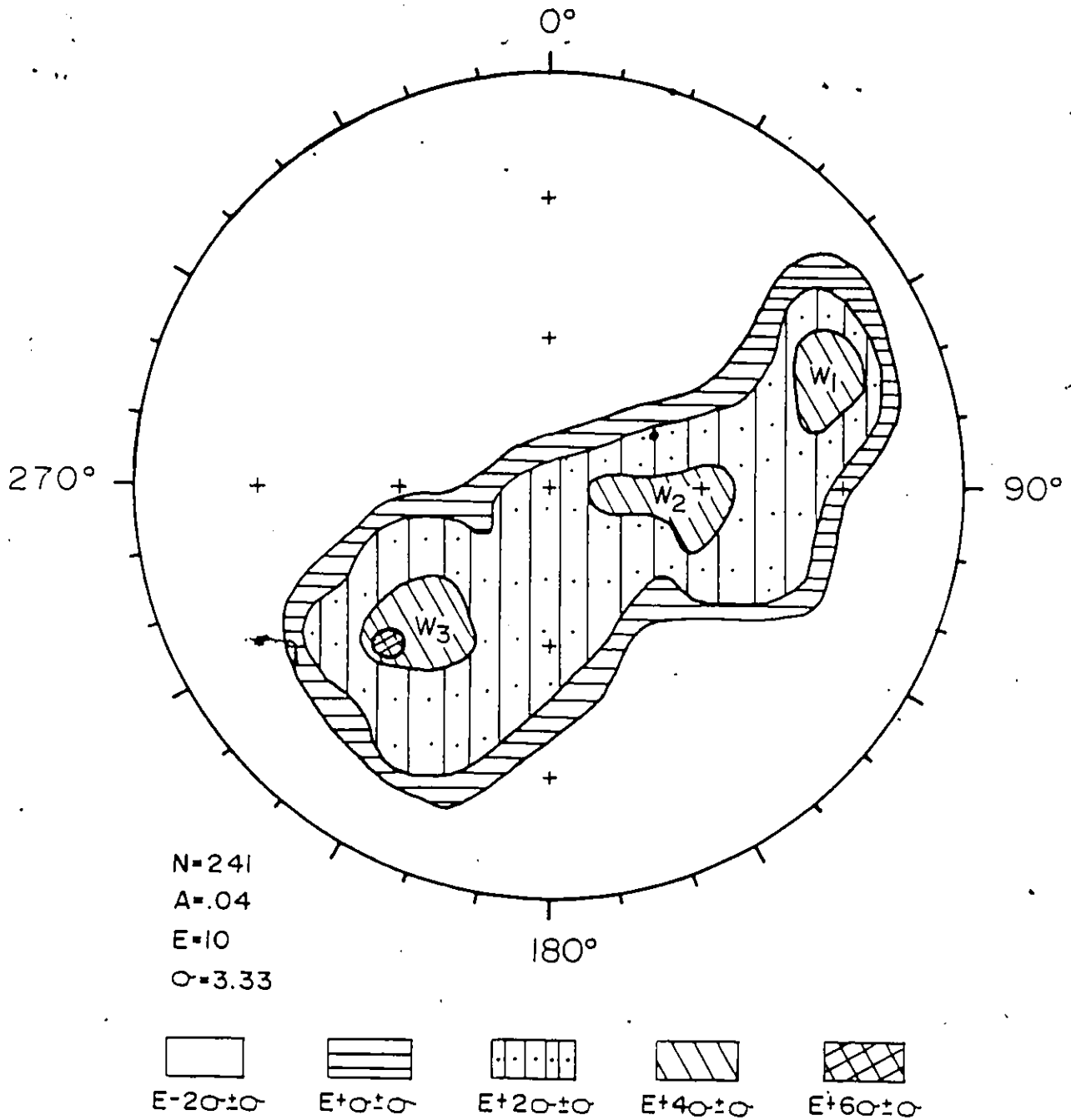


Fig. 27a Smoothing and contouring of AF cleaned IF specimens, corrected for bedding tilt and plunge of fold (down direction; west limbs of east and west synclines).

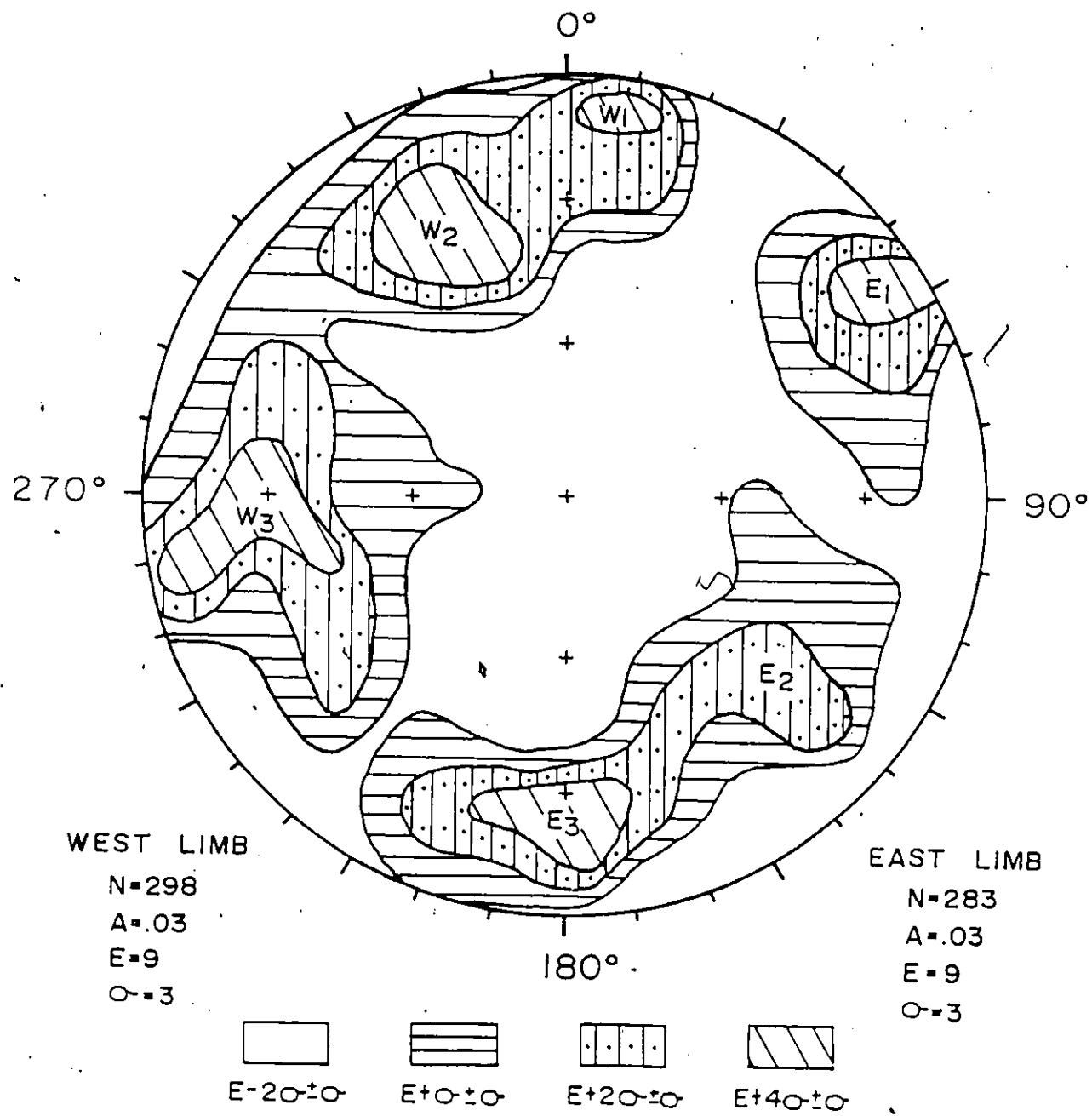


Fig. 28 Smoothing and contouring of AF cleaned IF specimens not corrected for bedding tilt and plunge of fold (down direction; east and west limbs of east and west synclines).

corrections. The variance ratios (ratio of precision parameters) is compared with the corresponding theoretical statistic: $F_2 (N_A - 1), 2 (N_S - 1), 0.05$. If $V > F$ then the two populations are significantly different in dispersion and hence probably reflect different conditions of remanence acquisition or removal. The second test of Watson (1956), computes the statistic:

$$F_C = (N-2) \left(\frac{R_1 + R_2 - R}{N - R_1 - R_2} \right)$$

where R is the length of the vector sum of the resultants of the R_1 and R_2 populations, and $N = (N_1 + N_2)$ is the total number of samples in the two populations. This is compared to the theoretical statistic: $F_2, 2(N - 2), 0.05$. If $F_C > F$, then the two populations define significantly different directions.

All the IF specimens falling within the $E + 2\sigma$ smoothing contours of the corrected and uncorrected direction anomalies (Figs. 27, 27a, 28) were compared and the summary of variance tests for east and west limbs is given in Table 5.

The tests for E_3 and E_1 are inconclusive because their variance ratios of 1.10 and 1.19 respectively are smaller than theoretical statistics of 1.39 and 1.42 at the 95% confidence level. The precision parameter, k ,

TABLE 5

Summary of Remanence Directions and Angular Variance Tests for Corrected Versus Uncorrected Anomalies of East (E) and West (W) Limbs of East-West Synclines

Group	Number of Specimen (N)	Length (R)	Decl. (deg)	Incl. (deg)	K	α_{95} (deg)	V	$F_{0.05}$	Result
Corrected E ₁	53	50.0	350.7	31.0	16.2	5.0	1.19	1.42	Inconclusive
Uncorrected E ₁	39	37.0	56.8	21.2	19.3	5.4			
Corrected E ₂	24	23.4	244.0	72.0	36.0	5.0	1.75	1.59	Prefolding
Uncorrected E ₂	33	31.4	132.4	32.0	20.05	5.7			
Corrected E ₃	57	54.6	201.5	29.0	16.8	4.7	1.10	1.39	Inconclusive
Uncorrected E ₃	48	45.0	188.4	24.5	15.3	5.4			
Corrected W ₁	20	20.0	72.0	24.4	64.0	4.1	2.79	1.65	Prefolding
Uncorrected W ₁	34	32.6	6.4	18.0	23.0	5.2			
Corrected W ₂	48	45.4	104.3	57.0	19.1	4.8	1.02	1.42	Inconclusive
Uncorrected W ₂	42	40.0	326.5	25.6	19.4	5.1			
Corrected W ₃	42	40.4	218.2	48.2	26.1	4.4	1.94	1.42	Prefolding
Uncorrected W ₃	62	57.1	267.7	27.3	13.5	5.1			

NOTES: R is the length of vector resultant; K is Fisher's (1953) precision parameter; α_{95} is the radius of 95% confidence level (Fisher 1953); V is the variance ratio of corrected and uncorrected populations; $F_{0.05}$ is the theoretical statistic $F_2(N_{corr}-1, 2(N_{uncorr}-1))$, 0.05 thereby setting the test at the 95% confidence level.

(Fisher, 1953) in both cases shows no significant difference in dispersion. Only the E_2 anomaly indicates that there is significant difference in the dispersion of directions between the corrected and uncorrected because the variance ratio of 1.75 is greater than the theoretical statistic of 1.59 at the 95% confidence level. In addition, the precision parameter is greater for corrected direction population showing that this population is less dispersed. Therefore, the remanence isolated in this anomaly is pre-folding.

Similarly the variance tests when applied to the west limb anomalies W_3 and W_1 indicate that their isolated remanences are pre-folding. In both cases their variance ratios 1.94 and 2.79 respectively are greater than the theoretical statistics of 1.42 and 1.65 at the 95% confidence level. Their k values are higher for corrected directions showing that their population are also less dispersed. The test for W_2 remains inconclusive.

The Fisherian analysis gives no clear picture of primary and secondary remanences isolated in east and west limbs. By this test one can notice that the anomaly in one limb which shows pre-folding remanence remains inconclusive to the corresponding anomaly of the other limb, although it would be expected to be the same for the same remanence components in both limbs. It was also noticed that each anomaly

carried primary remanence directions along with their secondary remanence directions thus resulting in hybrid directions, i.e., combined primary and secondary remanences. According to Van Alstine (1980), where distributions of vectors that are not symmetric about the mean, the computed vector means and other Fisherian statistics are of questionable geophysical significance. For skewed anomalies, the modal analysis method developed by Van Alstine (1980) gives a more characteristic measure of central tendency. The tendency toward skewness may result from either incomplete removal of secondary components of magnetization (Helsley, 1973) or by inaccurate determinations of the required tectonic corrections around complex microfolds. Therefore, keeping these two factors in mind, a modified graphical modal analysis was performed on the IF AF specimen directions by grouping corresponding anomalies from the east and west limbs to compare the corrected and uncorrected directions. Unlike the mean, the modes are identified as maxima in the resulting plot. For a truly Fisherian distribution, the mode is identical to the mean. Table 6 shows the anomalies designated A, B, and C components were tested for corrected and uncorrected directions. A modal graphical test was also performed by plotting and comparing corrected and uncorrected directions (Figs. 28, 29). The variance test for the A component indicates that

TABLE 6

Variance Tests for Corrected and Uncorrected Directions (Components of East and West Limbs are Combined)

Anomaly Combined	Designated Component	Number of Specimen (N)	Length (R)	Decl. (deg)	Incl. (deg)	K	α_{95}	V	F _{0.05}	Results
Corrected	A	64	64.42	118.05	71.29	8.40	6.10	4.44	1.31	Prefolding
E_2+W_2										
Uncorrected		75	35.83	359.42	70.51	1.89	17.29			
E_2+W_2										
Corrected	B	100	94.10	207.50	37.24	14.50	3.88	3.44	1.26	Prefolding
E_3+W_3										
Uncorrected		110	84.15	233.30	32.40	4.22	7.50			
E_3+W_3										
Corrected	C	72	59.30	11.98	34.56	5.26	8.03	1.48	1.31	Postfolding
E_1+W_1										
Uncorrected		72	63.70	33.05	21.51	7.77	6.37			
E_1+W_1										

NOTES: R is the length of vector resultant; α_{95} is the radius of 95% confidence (Fisher 1953); K is the Fisher's (1953) precision parameter; V is the variance ratio of corrected and uncorrected populations; F_{0.05} is the theoretical statistic $F_2(N_{corr}-1, 2(N_{uncorr}-1))$, 0.05 thereby setting test at the 95% confidence level.

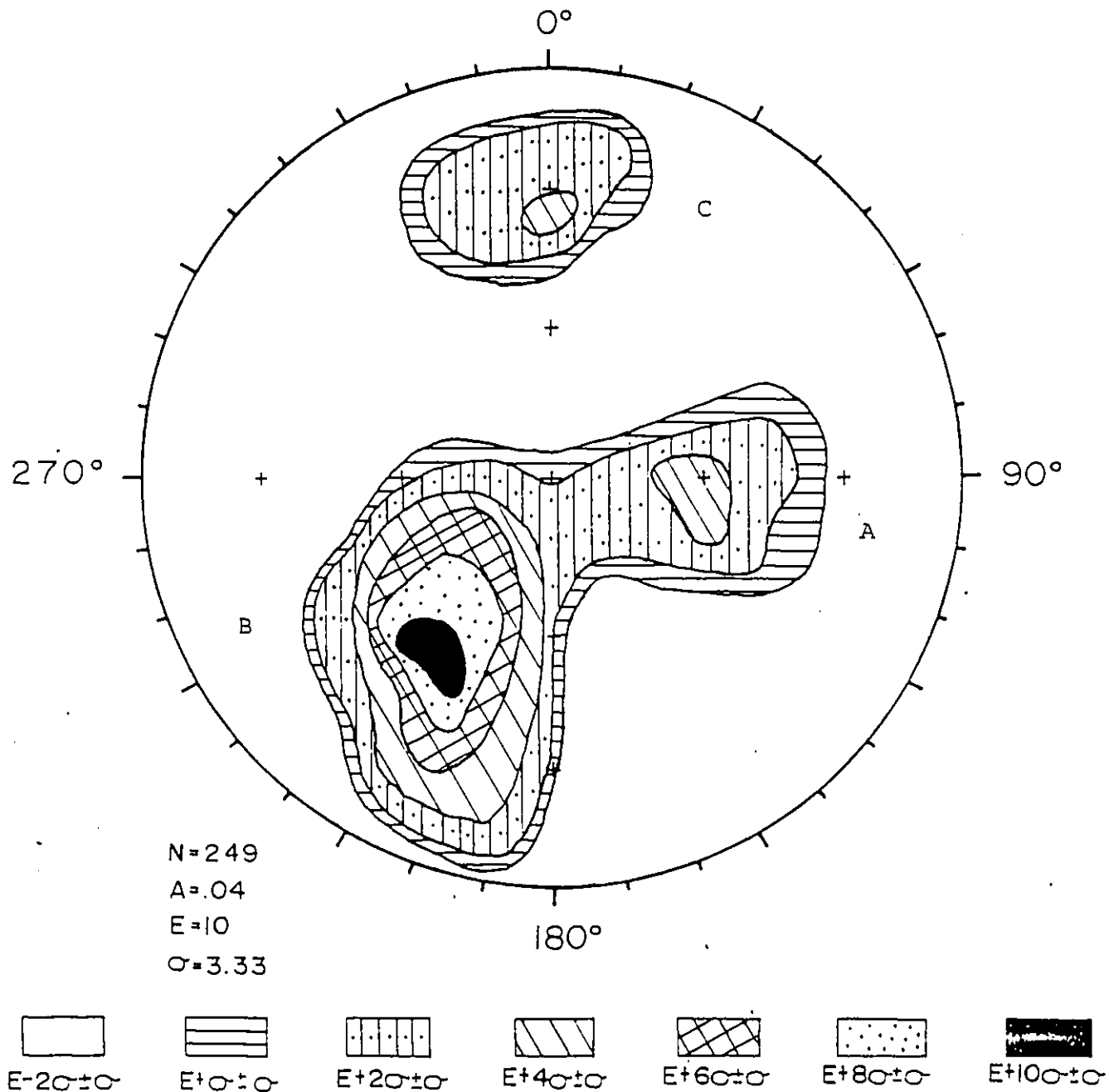


Fig. 29 Smoothing and contouring of AF cleaned IF specimens corrected for bedding tilt and plunge of fold (down directions; components of east and west limbs are combined).

there is significant difference in dispersion of direction because the variance ratio of 4.44 is far greater than the theoretical statistic of 1.31 at the 95% confidence level. In addition, the precision parameter, K , is greater for the corrected direction population showing that their population is less dispersed. Therefore the remanence isolated in this component is pre-folding. Similarly, the B component indicates significant difference in dispersion of direction because the variance ratio of 3.44 is far greater than the theoretical statistic of 1.26 at the 95% confidence level. Also, precision parameter, K , is greater for corrected direction population showing that their population is less dispersed. Therefore, the remanence isolated in this component is also pre-folding. On the other hand, the variance test for the C component shows that their remanence directions are post-folding. The variance ratio of 1.48 is greater than the theoretical statistic of 1.31 at the 95% confidence level, showing differences in dispersion of direction. In addition, the precision parameter for the uncorrected direction population is less dispersed. The reason for A component showing pre-folding remanence could be due to one of the following factors: 1) the A and B component directions show a girdle like distribution (Fig. 29), therefore it is difficult to say that these directions belong to A or B component directions in the girdle; or 2) the AF cleaning may have been unsuccessful in removing the

secondary component completely. Thus the directions in A component could have hybrid directions, i.e., primary remanence and unresolved secondary remanence. The graphical test (Figs. 28, 29) for A, B, and C components (corrected vs. uncorrected) are clearly indicative of a successful fold test, where all the uncorrected directions move toward a single corresponding corrected direction. The B component gives a very strong graphical indication of prefolding remanence in support of the variance fold test. When the uncorrected directions from the east and west limbs are corrected, they merge to form the single B component anomaly. The A and C uncorrected directions of both limbs also move toward a single corrected directions, but not as significantly as B component directions. This and girdle shaped anomaly for A and B components suggests that the A and C components are carrying some hybrid component directions.

4.8 THERMAL DEMAGNETIZATION OF IF PILOT SPECIMENS

A total of 48 representative specimens having typical NRM directions and intensities were selected from the 175 IF blocks, and these were thermally demagnetized in steps of 100, 200, 300, 400, 450, 500, 550, 575, 600, 625, and 650°C. The directional behaviour of the specimens were studied to determine the success of thermal demagnetization in isolating their stable remanence. All 48 specimens appear to isolate a single stable end point at 450° or

500°C. Above these temperatures they show random directional behaviours (Fig. 30). The thermal intensity decay curves (Fig. 31) show an initial drop in intensity up to 450°C as viscous or unstable remanent components are progressively removed, leaving the stable end points. Between 0°C - 450°C, the specimens show an 85-90% reduction in the intensity, but above 450°C they show an ~99% reduction in intensity. The PSI curves (Fig. 32) show an initial rate of directional change in the order of 50 mdeg/°C and decrease slightly as the stable directions are isolated. Thereafter the curves record an increasing rate of directional change giving values of as much as ~4300 mdeg/°C above 550°C as the randomly directed partial thermoremanent (pTRM) components are acquired and dominate the remanence response.

4.8a Modal Analysis of Pilot Specimens at 450°C, 500°C, and 550°C

All the directions, both corrected and uncorrected for the bedding and plunge of the fold, were plotted on stereonet, smoothed, and contoured by using Kamb's method (1959) (Figs. 33a, b). The modes of the resultant anomalies were obtained by anomaly maxima and by using Fisher statistics for those directions falling within a $E + 2\sigma$ anomaly contour. The summary of the remanence directions for corrected and uncorrected anomalies (components) are given in Table 7.

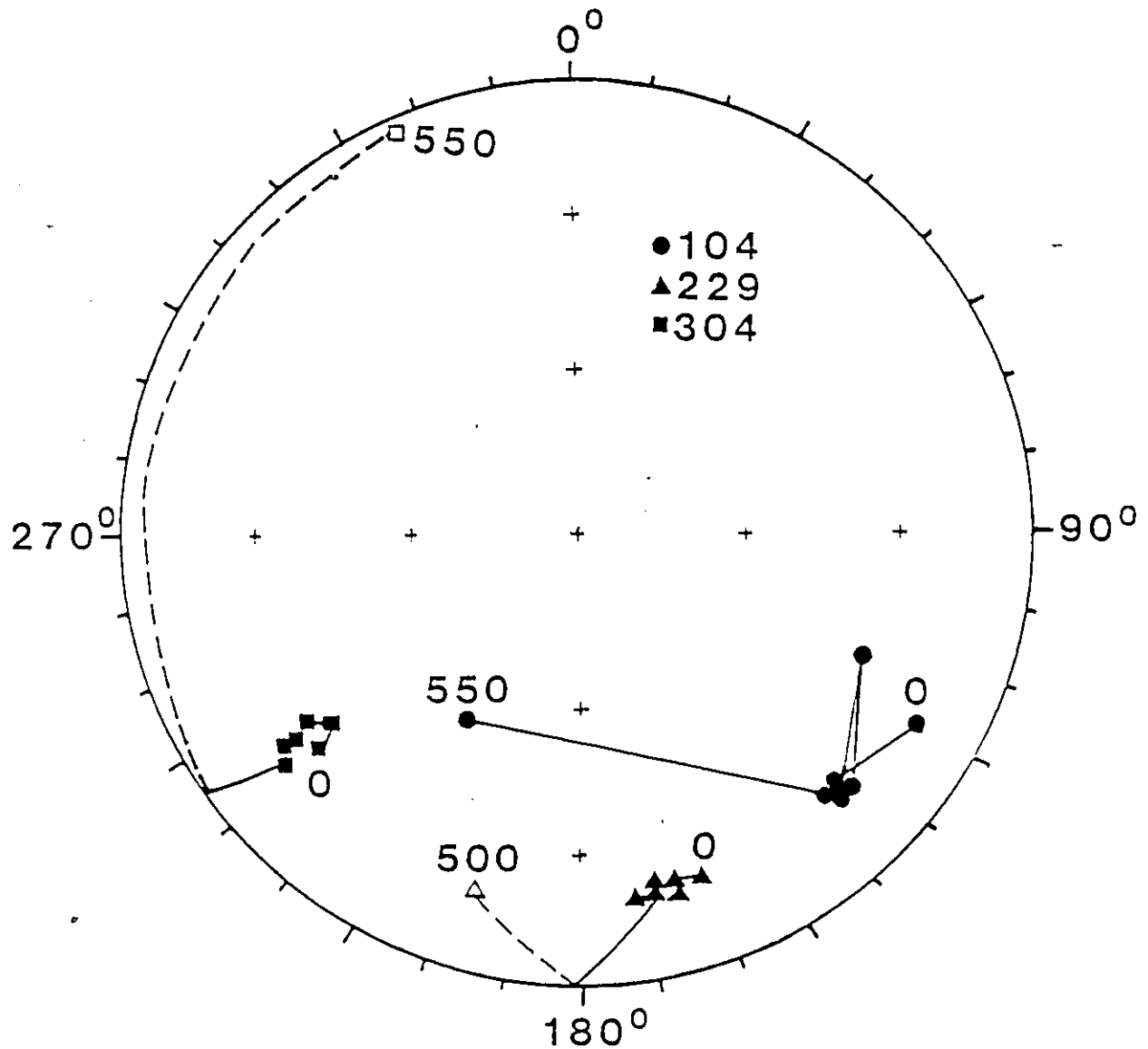


Fig. 30 Directional changes of thermal demagnetization on an equal area projection for IF pilot specimens.

Note: Change in direction on progressive thermal demagnetization at temperatures of 0, 100, 200, 300, 400, 450, 500 and 550°C, for IF pilot specimens. Directions at or above 550°C are not plotted because of their erratic directional behaviour. Solid (open) symbols indicate down (up) directions.

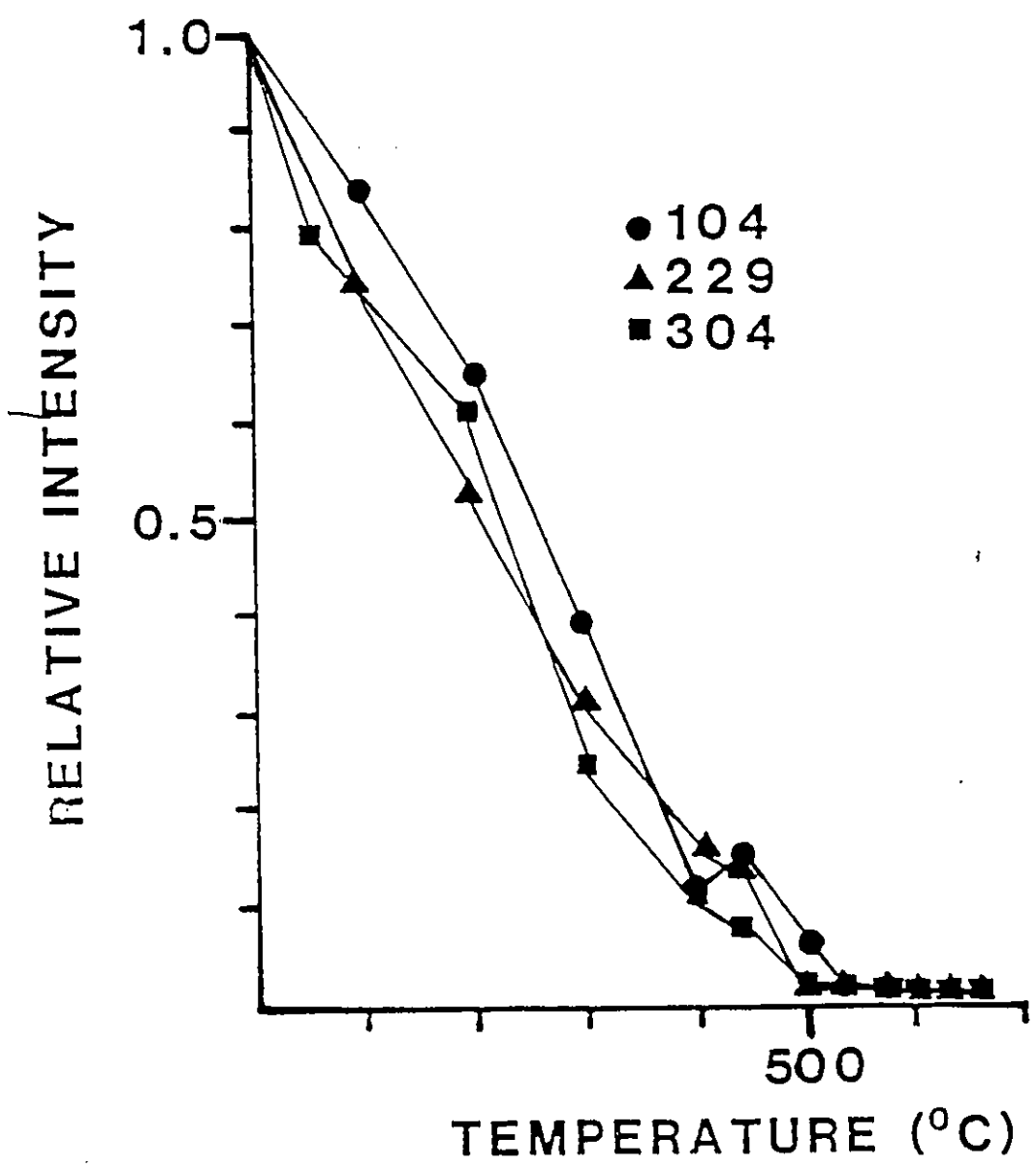


Fig. 31 IF thermal demagnetization curve - relative intensity.

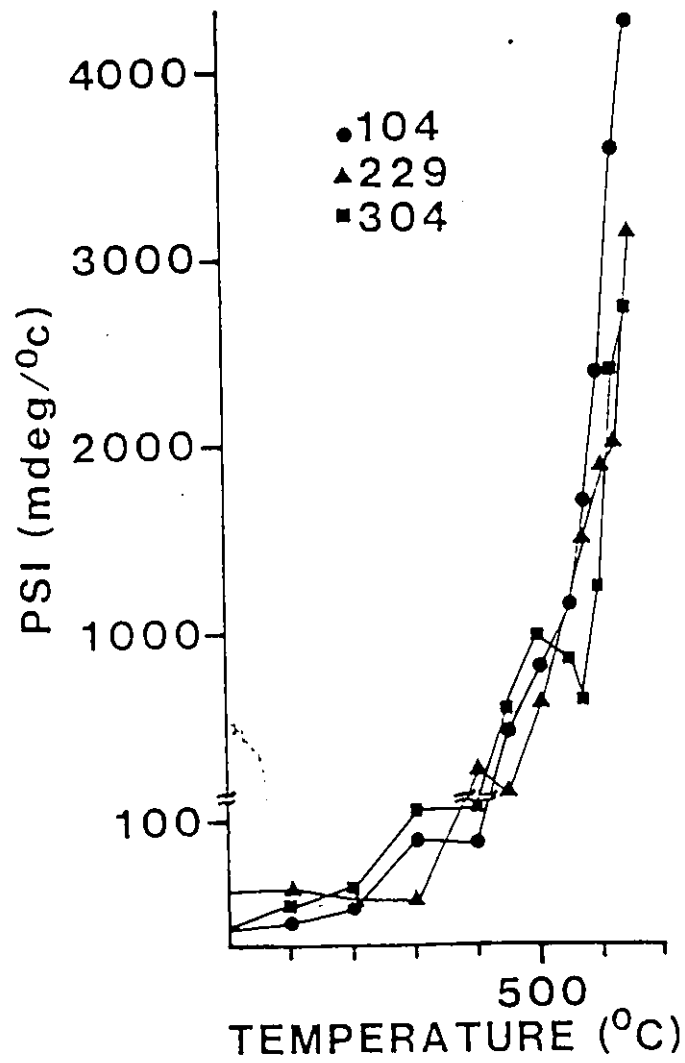


Fig. 32 IF thermal demagnetization curve-paleomagnetic stability index.

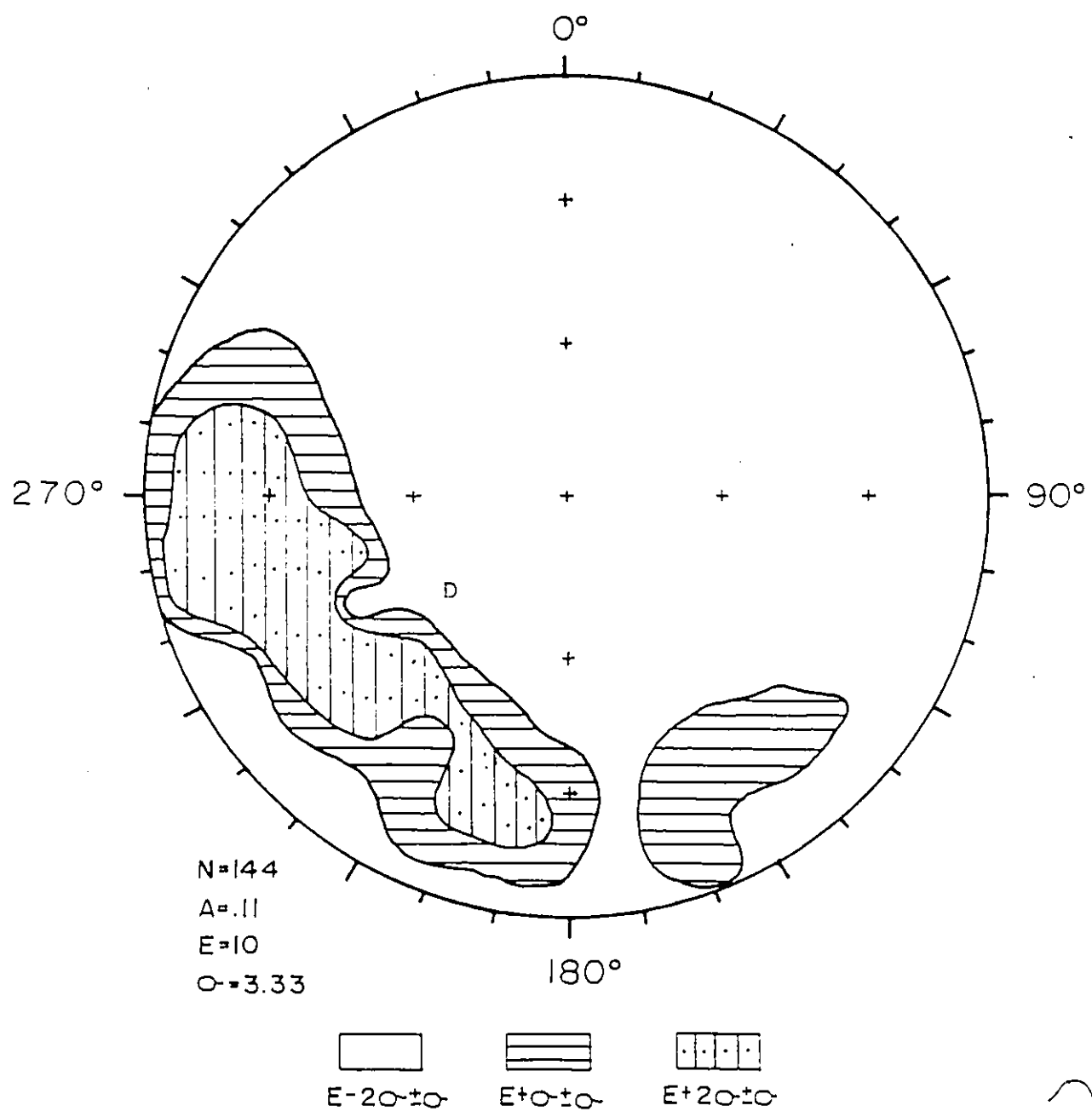


Fig. 33a Smoothing and contouring of thermally cleaned IF pilot specimens corrected for bedding tilt and plunge of fold (down direction).

Note: Smoothing and contouring is performed only on those directions which were demagnetized at 450, 500 and 550°C.

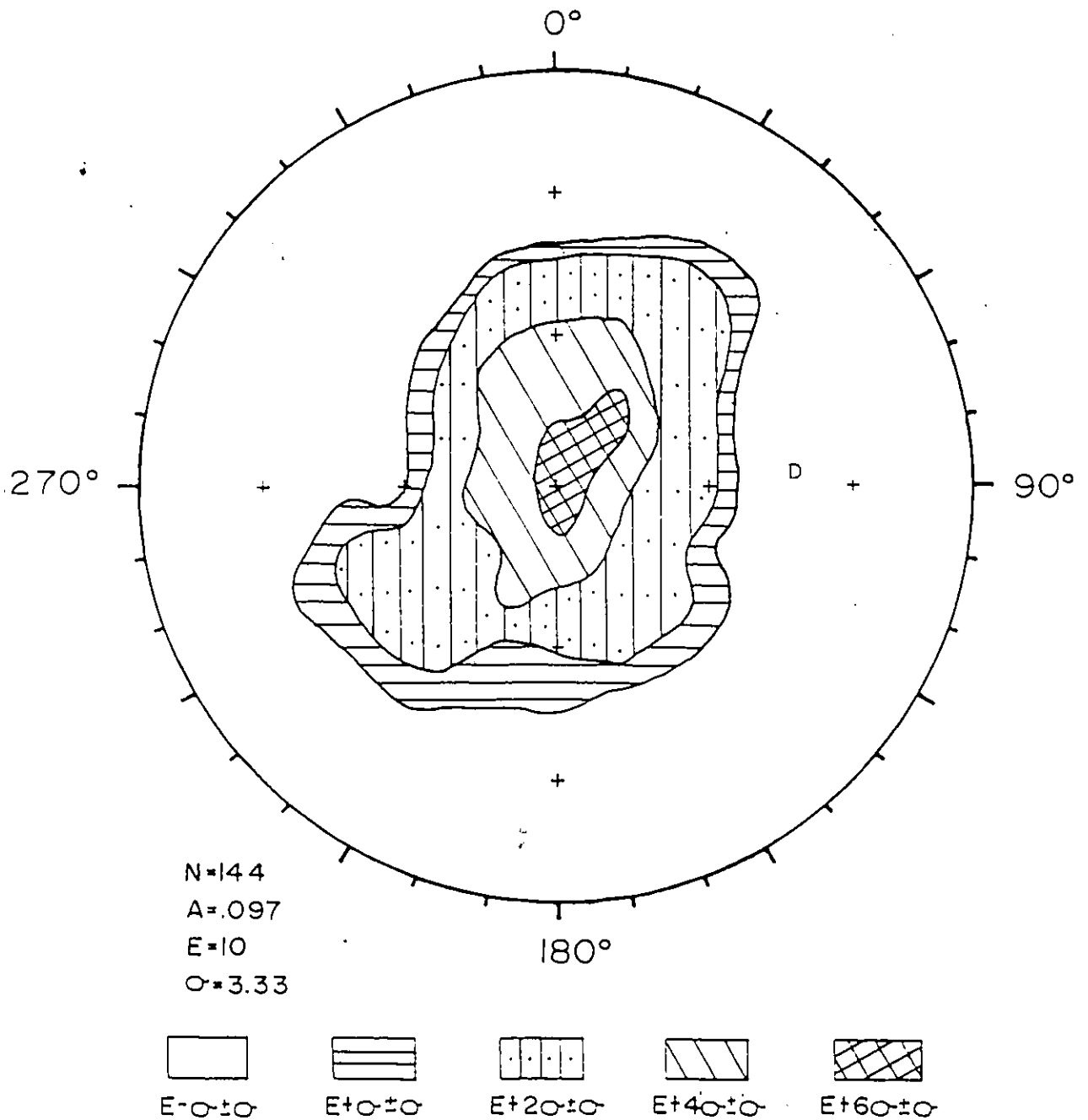


Fig. 33b Smoothing and contouring of thermally cleaned IF pilot specimens not corrected for bedding tilt and plunge of fold (down direction).

Note: Smoothing and countouring is performed only on those directions which were demagnetized at 450, 500 and 550°C.

4.8b Fold Test of Thermally Cleaned IF Pilot Specimens

A fold test was performed on the specimen directions corrected for bedding and plunge with the uncorrected directions using the angular variance test of Laroche (1969) and Watson (1956). The directions involved in this test are only these directions which were demagnetized at 450, 500, and 550°C. The result is summarized in Table 7. The variance test proved inconclusive because the variance ratio of 1.01 is smaller than the theoretical statistic of 1.24 at the 95% confidence level.

The graphical inspection of Figs. 33a,b, show that uncorrected anomaly is less dispersed at $E + 6\sigma \pm \sigma$ than the corrected anomaly $E + 2\sigma \pm \sigma$ which suggests that the remanence is postfolding (D component). But the inconclusive variance test prohibits any speculation about this postfolding remanence and suggests that it is invalid statistically.

4.9 AF DEMAGNETIZATION } OF THE HOST ROCK

4.9.1 Pilot Specimens

A total of 54 HR pilot specimens, one from each site, were AF step demagnetized up to 100 mT. The directional changes of representative specimens are shown in Fig. 34. The PSI curves (Fig. 35) show the absence of any significant viscous remanence. The low initial rate of directional change

TABLE 7

Summary of Remanence Directions and Fold Test for
1F Thermally Cleaned Pilot Specimens

Group	Number of Vectors (N)	Length (R)	Decl. (deg)	Incl. (deg)	K	α_{95}	V	$F_{0.05}$	Result
Corrected	144	49.49	249.09	9.63	1.57	16.07	1.01	1.24	Inconclusive
Uncorrected	144	53.06	214.38	71.85	1.58	15.45			

D

NOTE: R is the length of vector resultant

K is the Fisher's (1953) precision parameter

α_{95} is the radius of 95% confidence (Fisher 1953)

V is the variance ratio of corrected and uncorrected populations

$F_{0.05}$ is the theoretical statistic $F_2(N_{corr}-1), 2(N_{uncorr}-1)$, 0.05 thereby setting test at the 95% confidence level.

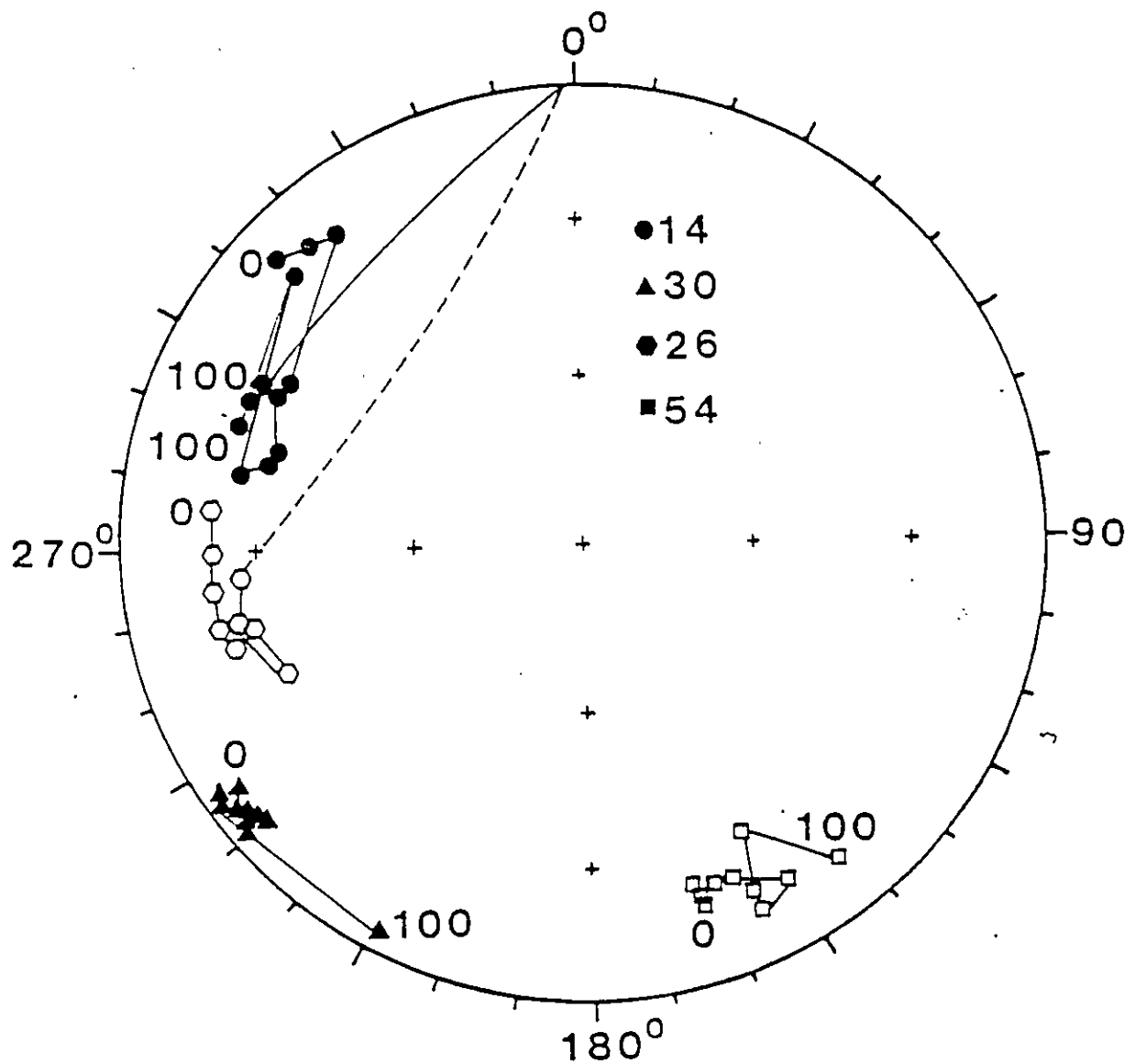


Fig. 34 Directional changes of AF demagnetization on an equal area projection for HR pilot specimens.

Note: Change in direction on progressive AF demagnetization in fields of 0, 5, 10, 15, 20, 30, 40, 50, 60, 80 and 100 mT, for HR pilot specimens. Solid (open) symbols indicate down (up) directions.

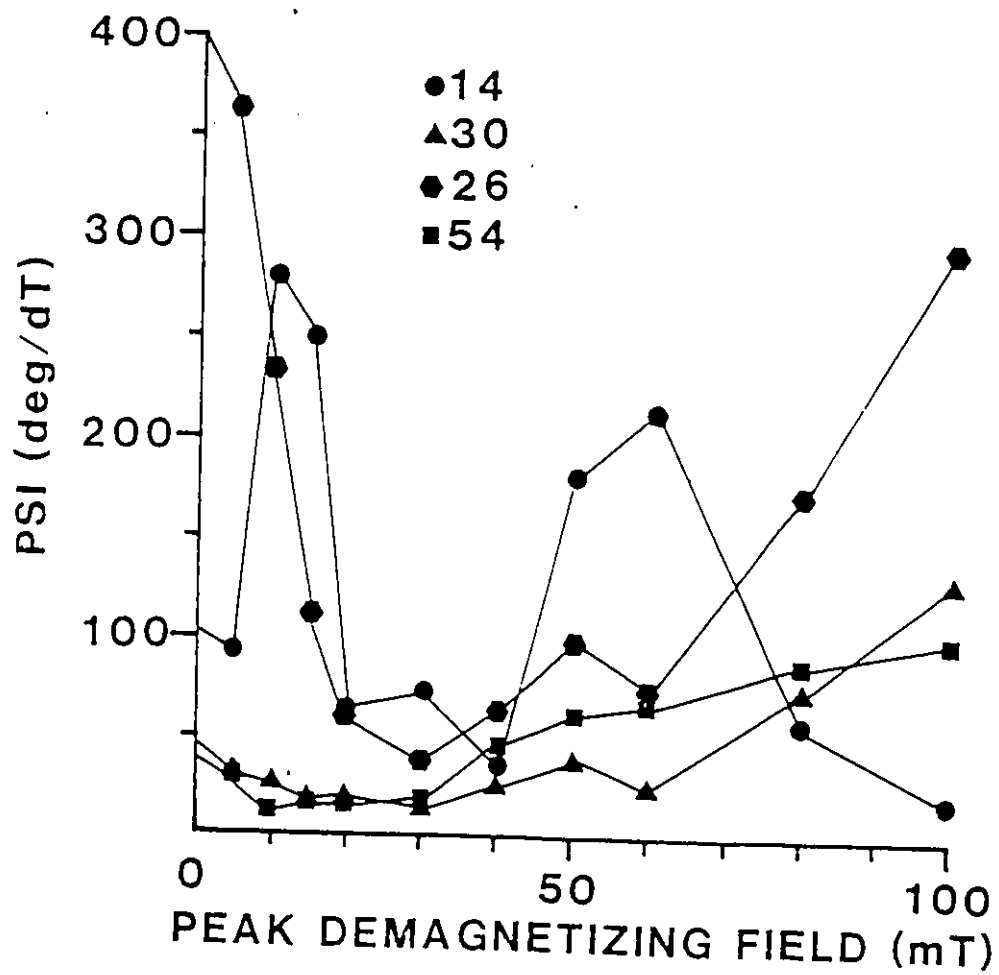


Fig. 35. HR AF demagnetization curve - paleomagnetic stability index for directional changes.

in the order of $<50 \text{ deg/T}$ remains about the same throughout the demagnetization process up to 40 mT. Above 40 mT the curves record an increasing rate of directional change from step to step as larger random ARM components are progressively added.

The intensity decay curves (Fig. 36) show a range of reduction rates for the pilot specimens. Between 0-15 mT, 50% of the specimens show an 80% reduction in the intensity, 25% show 50% reduction in the intensity, and remaining 25% show only a 5% reduction in the intensity. Most of the specimens show ~65% of their intensity removed by 50 mT and ~80% removed by 100 mT. The optimum cleaning field was selected by inspection of the PSI minima. In most cases, as shown by Fig. 25a, this field is less than 40 mT and the relative intensity of the stable remanence (Fig. 25b) ranges from 10-98% of the original intensity.

4.9.2 Remaining Specimens

4.9.2a Conventional Analysis

The remaining specimens from each site were AF demagnetized at their optimum field as selected above. After appropriate data screening (Table 4) the means were computed. A total of 19 accepted site mean (see 4.5.2 Statistical Analysis of the HR) directions when plotted on stereonet (Fig. 37), they form four poorly defined clusters, and they were designated as E, F, G, and H components. Of the

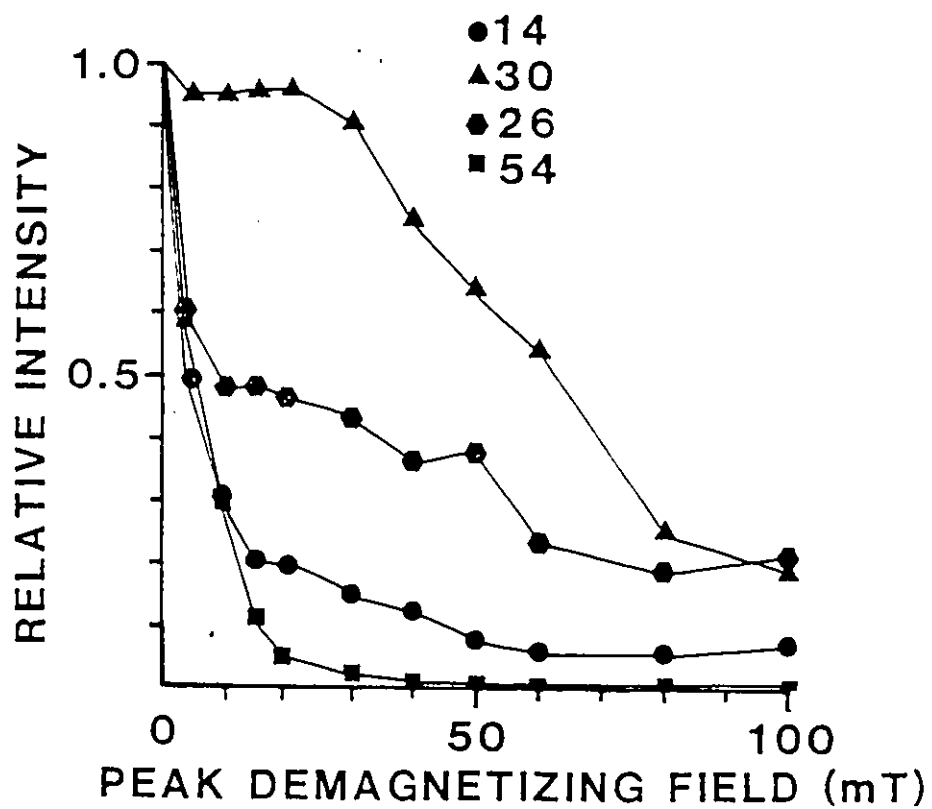


Fig. 36 HR AF demagnetization curve-relative intensity.

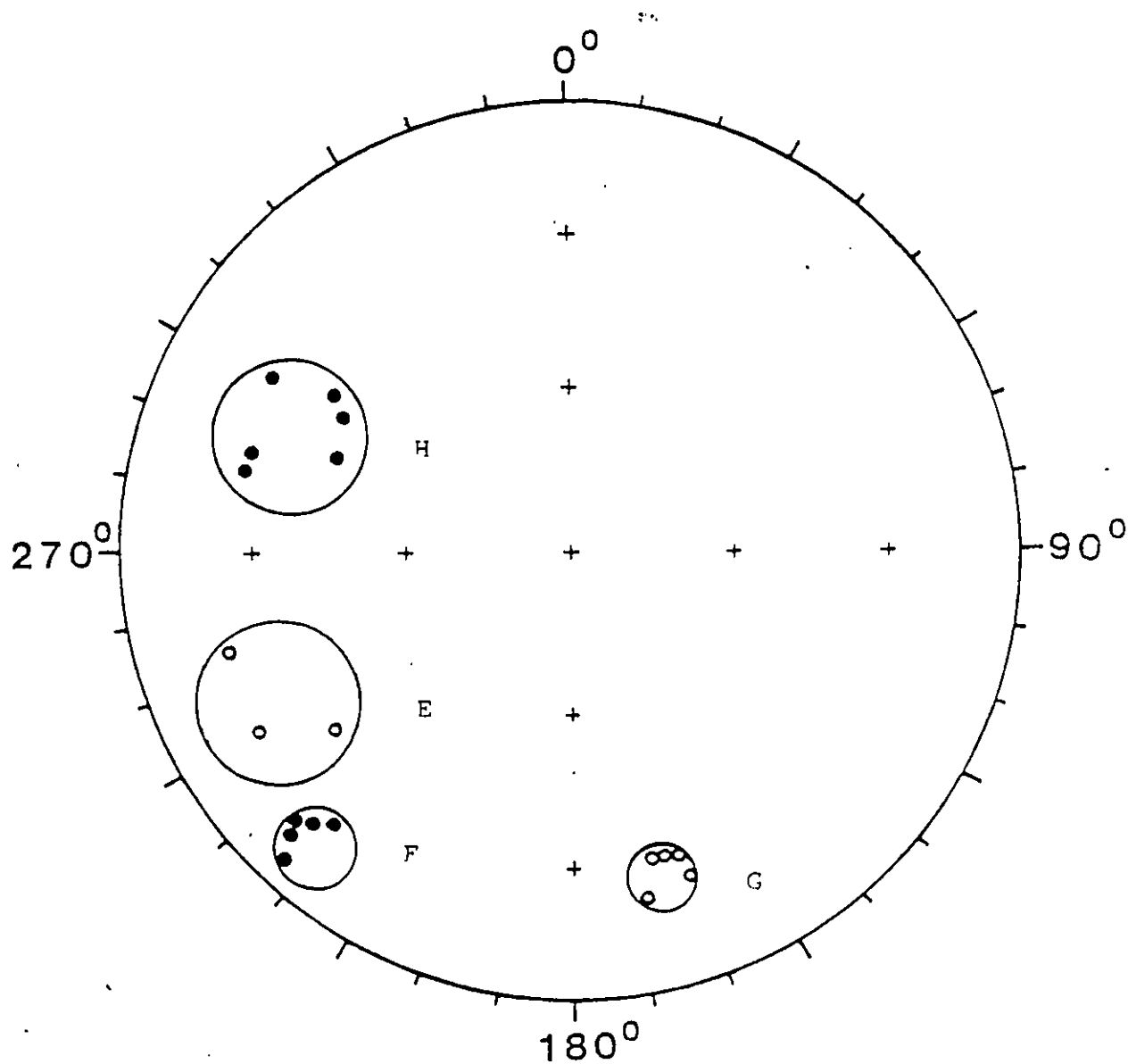


Fig. 37 HR AF cleaned site mean directions on an equal area projection.

Note: Mean direction of E, F, G, and H components with their circles of 95% confidence. Solid (open) symbols indicate down (up) directions.

19 accepted sites, three show the E component (239.9° , -30.0°), five show the F component (233.0° , 20.0°), five show the G component (166.0° , -23.0°), and six sites show the H component (293.0° , 28.0°). (Table 8). These four poorly defined components have low statistical significance because their remanence components were isolated only in a few specimens per site. Also, their confidence level at α_95 is fairly dispersed ($\sim 20^\circ$). They also appear to have very complex nature of remanence consisting of VRM, metamorphic overprint and primary magnetization. Therefore, it was decided to use a population level analysis (see 4.6.2b Modal Analysis of Paleomagnetic Data) of Symons and Stupavsky (1981), and Van Alstine (1980).

4.9.2b Modal Analysis of the Paleomagnetic Data

All the specimen directions, both corrected and uncorrected for the bedding tilt, were plotted on stereonet, smoothed, and contoured by using Kamb's method (1959). The AF HR specimens after smoothing and contouring form several statistically significant anomalies (Figs. 38a, b; 39a, b).

The mode of each remanence component (anomaly) and its precision were calculated by selecting only those specimen directions which fall within the E + 2 Contour. These directions were used to compute the Fisher mean (= mode) and radius of circle of 95% confidence (= precision). The anomalies designated E, F, G and H components yielded mean directions which are summarized in Table 8.

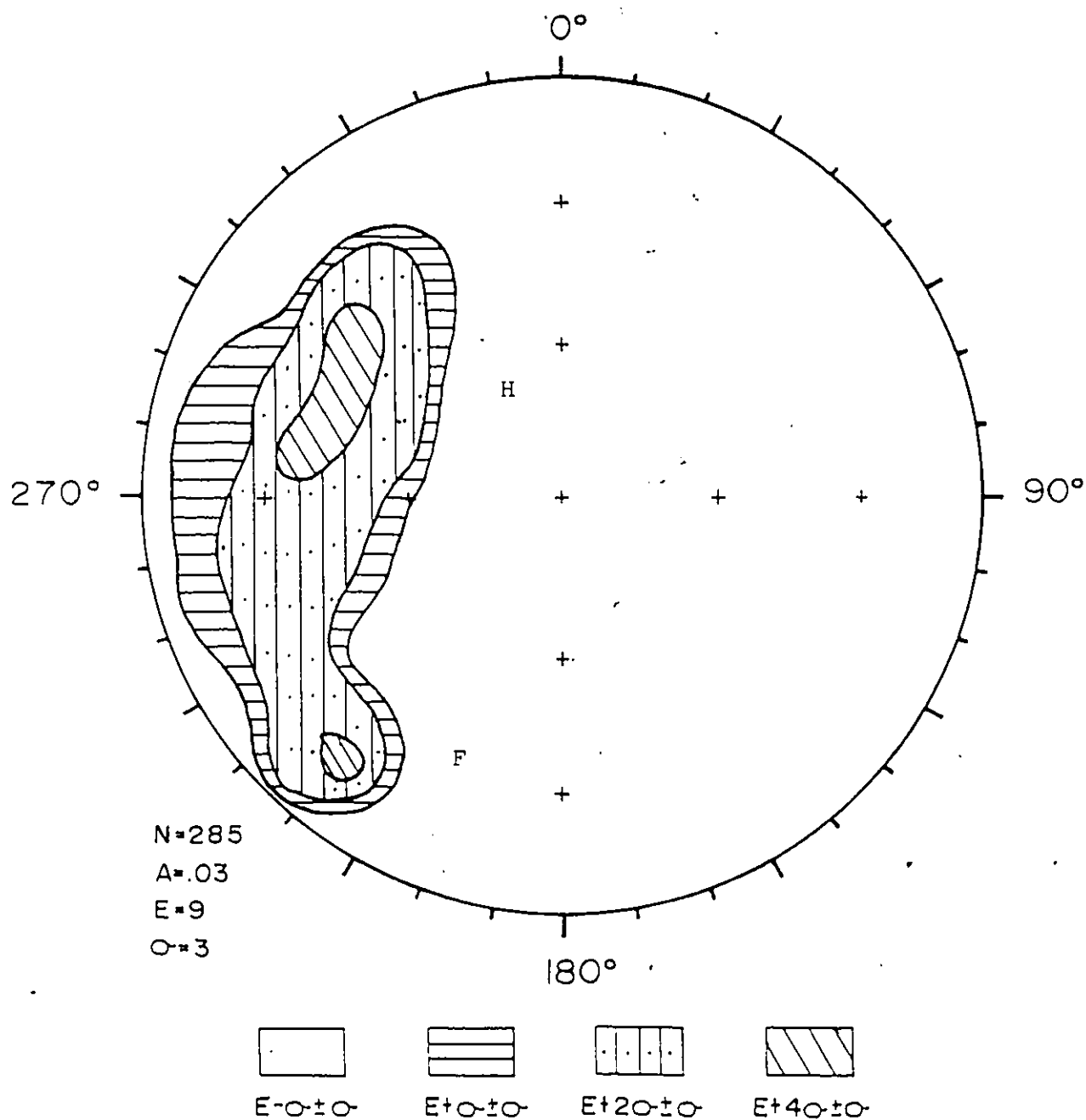


Fig. 38a Smoothing and countouring of AF cleaned HR specimens corrected for bedding tilt (down direction).

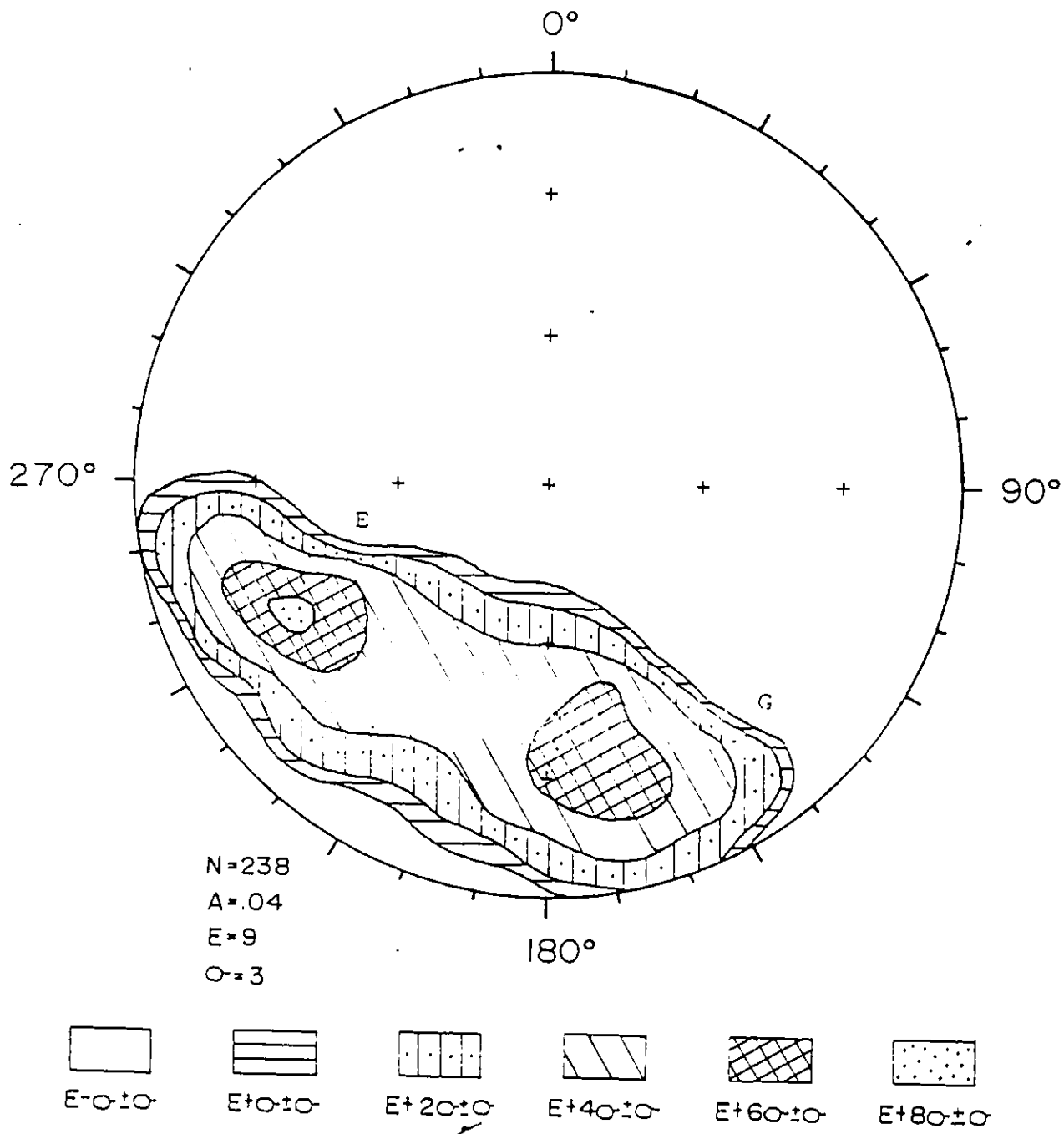


Fig. 38b Smoothing and contouring of AF cleaned HR specimens corrected for bedding tilt (up direction).

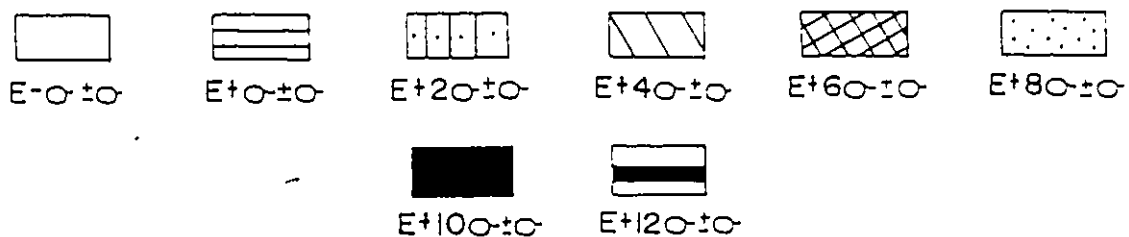
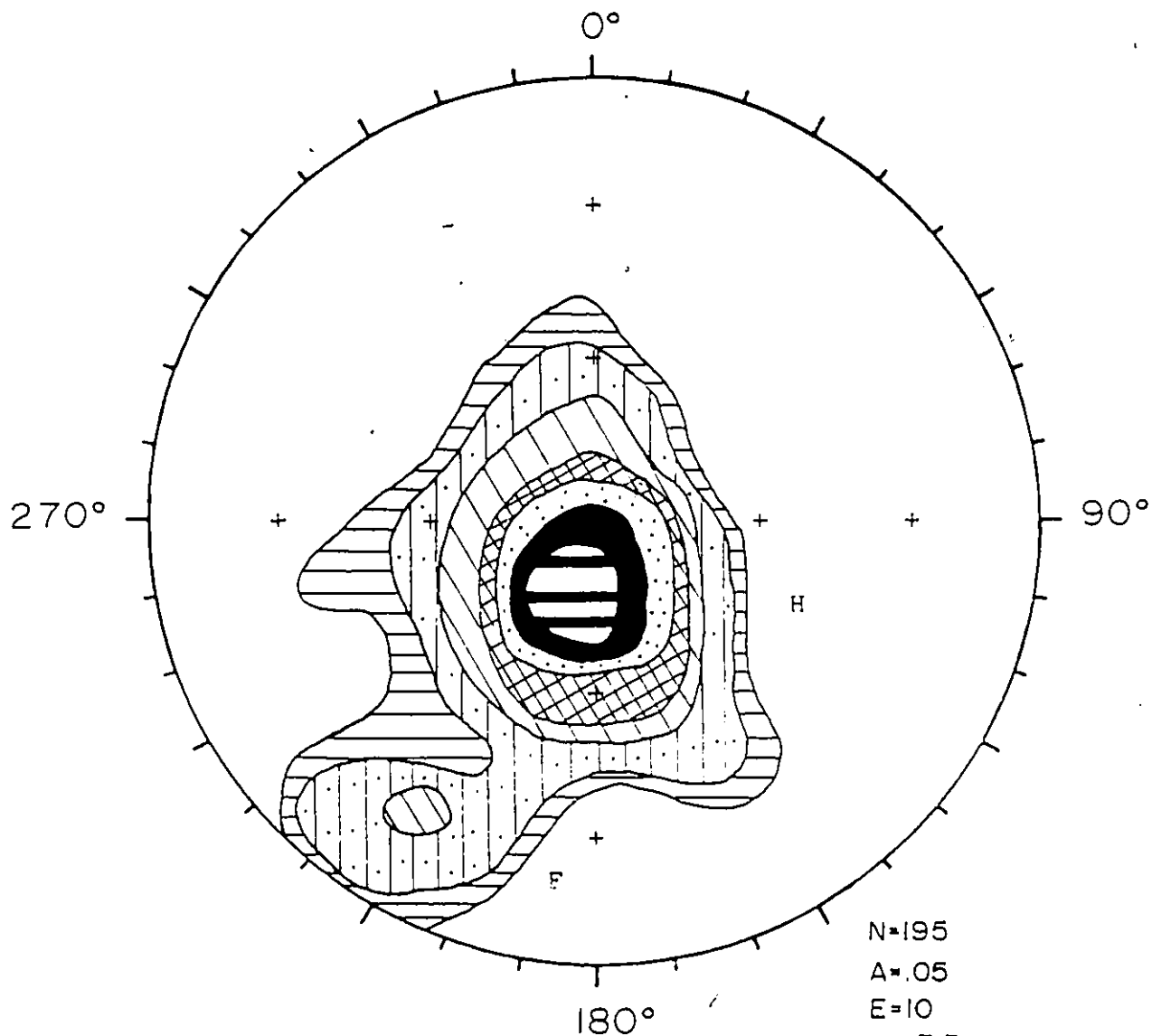


Fig. 39a Smoothing and contouring of AF cleaned HR specimens not corrected for bedding tilt (down direction).

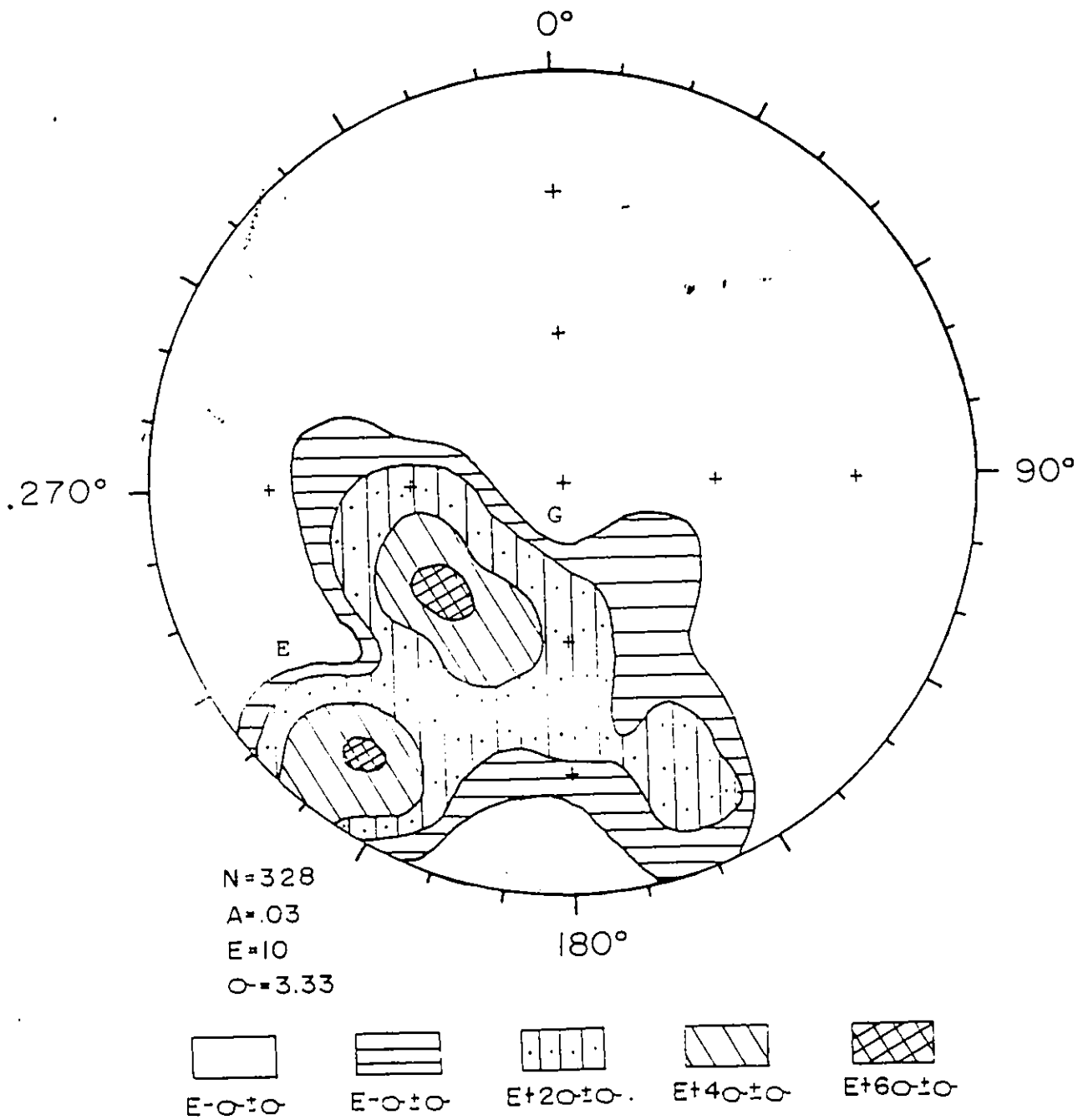


Fig. 39b. Smoothing and contouring of AF cleaned HR specimens not corrected for bedding tilt (up direction).

When unscreened and uncleaned NRM directions were plotted, contoured, and smoothed using the same technique as discussed earlier, they defined three well pronounced anomalies (Fig. 40), i.e., E, G, and H components. Their mean remanence directions are summarized in Table 8. The E, G, and H components directions, isolated by AF demagnetization are close to the original NRM directions. The F component is isolated by the AF cleaning process. Thus, AF demagnetization has been successful in isolating the F component.

4.9.3 Fold Test After AF Cleaning

A non-conventional fold test (see 4.7 Fold Test After AF Cleaning) was performed by grouping the specimens from a population within an anomaly. The specimen directions corrected for bedding tilt were compared with the uncorrected directions using the angular variance test of Larochelle (1969), and Watson (1956). The results are summarized in Table 9.

All the specimens falling within the $E + 2\sigma$ smoothing contour of the corrected and uncorrected directions (Figs. 39a, b; 39a, b) were compared. The variance tests for E, F, and G components showed that they are inconclusive because their variance ratios of 1.11, 1.05 and 1.50 are respectively smaller than their theoretical statistics of

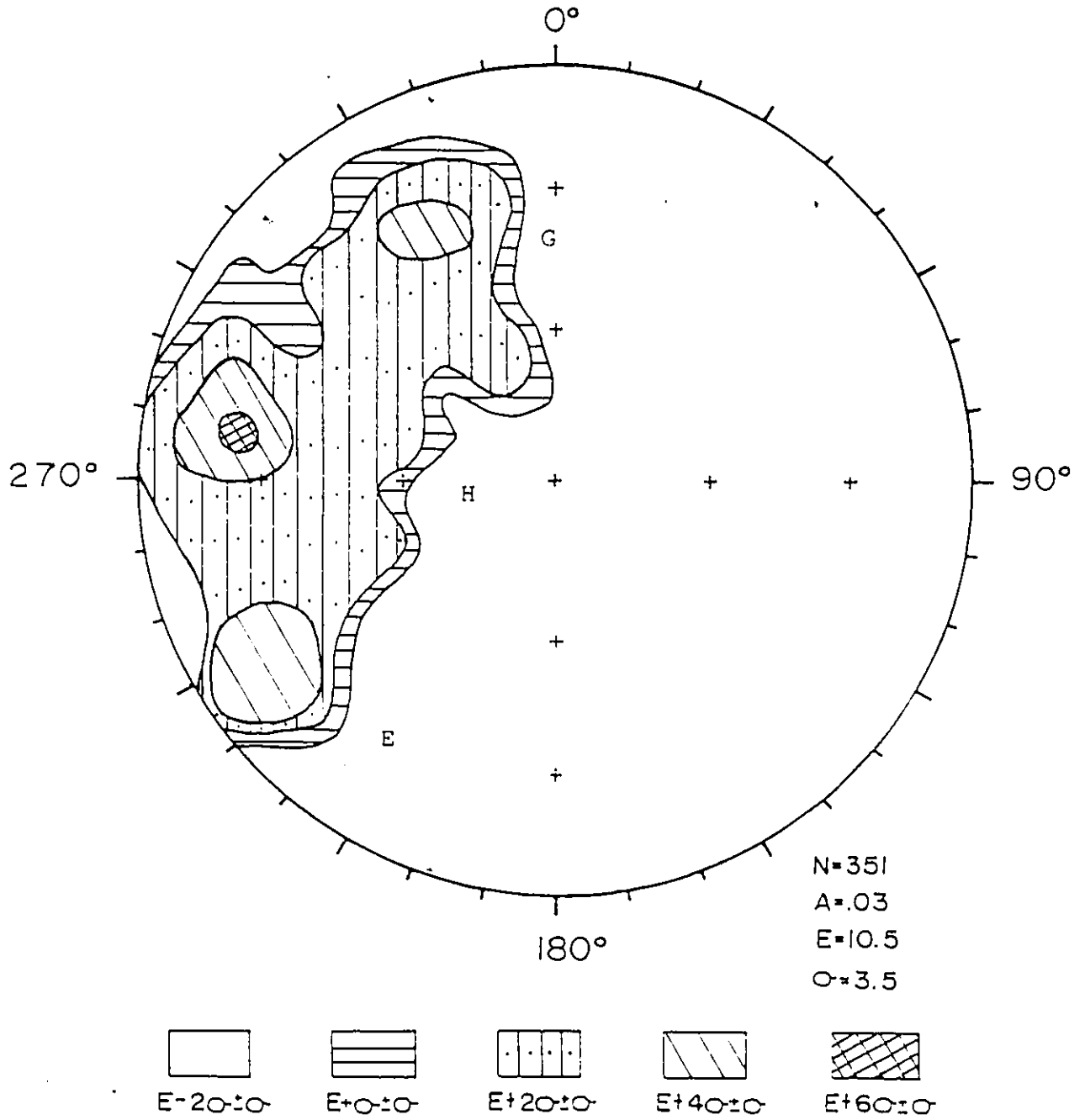


Fig. 40 Smoothing and contouring of NRM HR specimens not corrected for bedding tilt (down direction).

TABLE 8
Summary of Host Rock Remanence Directions

	Number of Specimen (N)	Length (R)	Decl. (deg)	Incl. (deg)	K	α_{95} (deg)
<u>INITIAL NRM</u>						
Population level analysis						
E	24	24.00	237.30	14.60	119.50	2.72
G	35	34.00	336.00	28.00	43.20	3.74
H	41	40.00	280.40	20.10	42.00	3.49
<u>AF DATA</u>						
i) Site mean						
E	3	3.86	239.95	-30.32	21.24	20.40
F	5	4.89	233.03	20.52	36.88	12.77
G	5	6.88	166.44	-23.21	48.58	8.75
H	6	5.67	293.34	28.52	15.41	17.62
ii) Population level analysis						
E	30	29.48	240.77	-27.90	56.50	3.53
F	19	19.79	225.81	14.20	88.44	3.49
G	50	28.29	164.15	-27.20	39.73	4.30
H	23	23.54	292.58	36.15	50.32	4.21
<u>THERMAL PILOTS</u>						
E	7	6.89	230.86	13.63	54.94	8.22
G	6	5.83	148.55	-23.02	29.29	12.59
H	8	6.93	277.71	12.62	86.76	6.52

NOTE: R is the length of vector resultant; K is the Fisher's (1953) precision parameter; α_{95} is the radius of 95% confidence (Fisher (1953)).

TABLE 9
Angular Variance Ratio Tests of Host Rock AF Data

	Number of Specimen (N)	Length (R)	Decl. (deg)	Incl. (deg)	K	α_{95}	V	$F_{0.05}$	Result
1. E component	corrected	29.48	240.77	-27.90	56.50	3.53	1.11	1.51	Inconclusive
	uncorrected	40.36	218.31	-11.98	62.77	2.84			
2. F component	corrected	19.79	225.81	14.20	88.44	3.49	1.05	1.87	Inconclusive
	uncorrected	10.88	215.79	14.71	80.98	5.10			
3. G component	corrected	28.29	164.15	-27.20	39.73	4.30	1.50	1.56	Inconclusive
	uncorrected	31.47	223.84	-54.86	58.26	3.36			
4. H component	corrected	23.54	292.58	36.15	50.32	4.21	2.32	1.55	Prefolding
	uncorrected	63.90	198.89	82.47	21.31	3.84			

NOTE: R is the length of vector resultant; K is Fisher's (1953) precision parameter; α_{95} is the radius of 95% confidence (Fisher 1953); V is the variance ratio of corrected and uncorrected populations; $F_{0.05}$ is the theoretical statistic $F_2(N_{corr}-1), 2(N_{uncorr}-1)$, 0.05 thereby setting test at the 95% confidence level.

1.51, 1.87, and 1.56 at the 95% confidence level. The test for H component indicates that there is a significant difference in dispersion of direction because the variance ratio of 2.32 is greater than the theoretical statistic of 1.55 at the 95% confidence level. In addition, the precision parameter, K, for the corrected direction population shows that their population is less dispersed. Therefore, the remanence isolated in the H component is pre-folding.

4.10 THERMAL DEMAGNETIZATION OF HR PILOT SPECIMENS

A total of 54 HR pilot specimens, one from each site, were thermally demagnetized up to 650°C. Of the 54 pilot specimens, only 46 (85%) survived to 650°C. Rejections were made on the basis of high PSI values and large random fluctuations in direction.

On examining the pilot specimens, they showed that they could be grouped into three populations (Fig. 41). The directional changes of representative specimens are shown in Fig. 42. The PSI curves (Fig. 43) show the low initial rate of directional change of <50 mdeg/°C throughout the demagnetization process up to 500°C. Above 500°C the curves record an increasing rate of directional change from step to step as larger random pTRM components are progressively added. The intensity decay curves (Fig. 44) show a very slow intensity decay for all the specimens

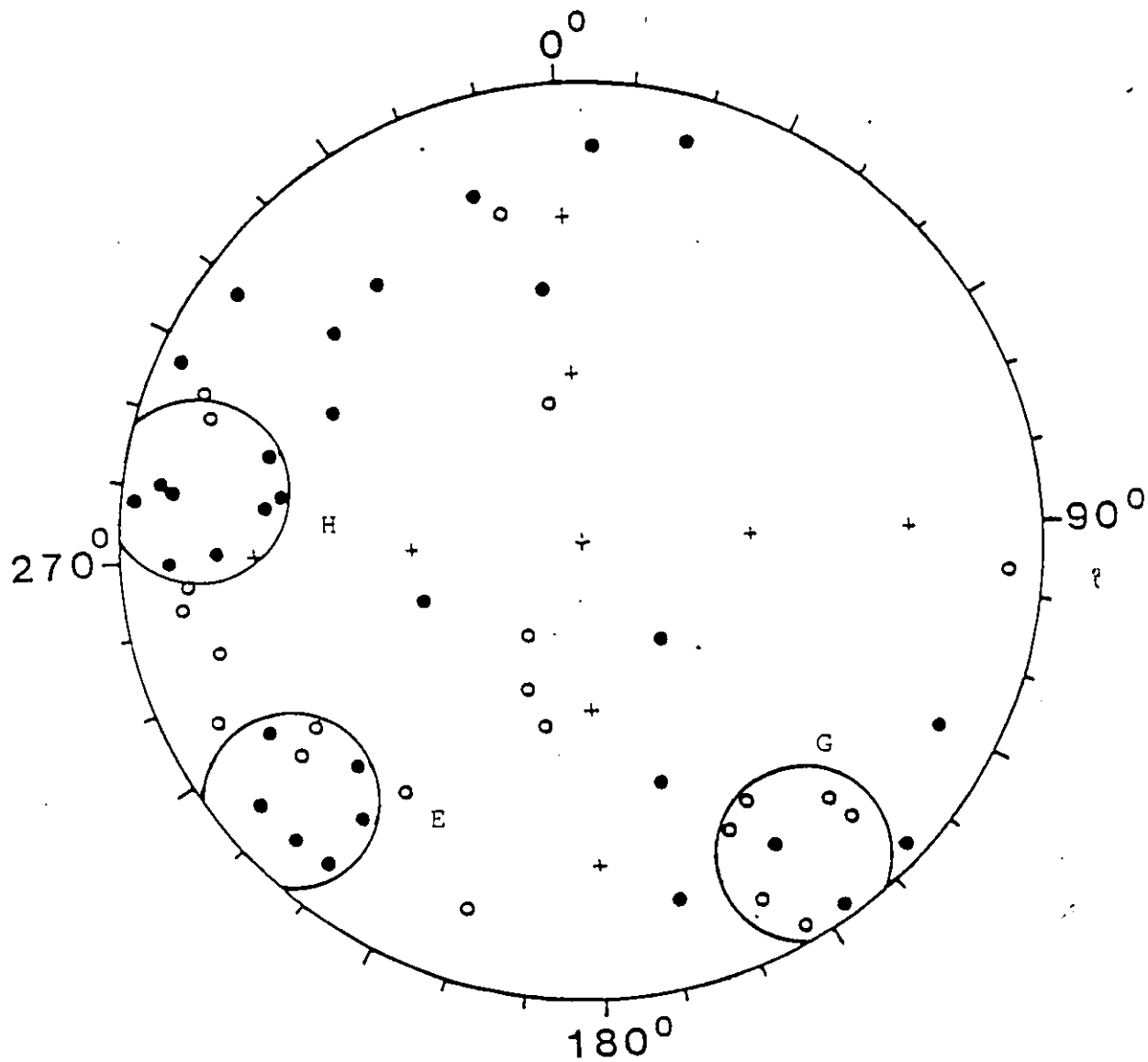


Fig. 41 HR thermally cleaned pilot specimen directions on an equal area projection.

Note: Mean direction of E, G, and H components with their circles of 95% confidence. Solid (open) symbols indicate down (up) directions.

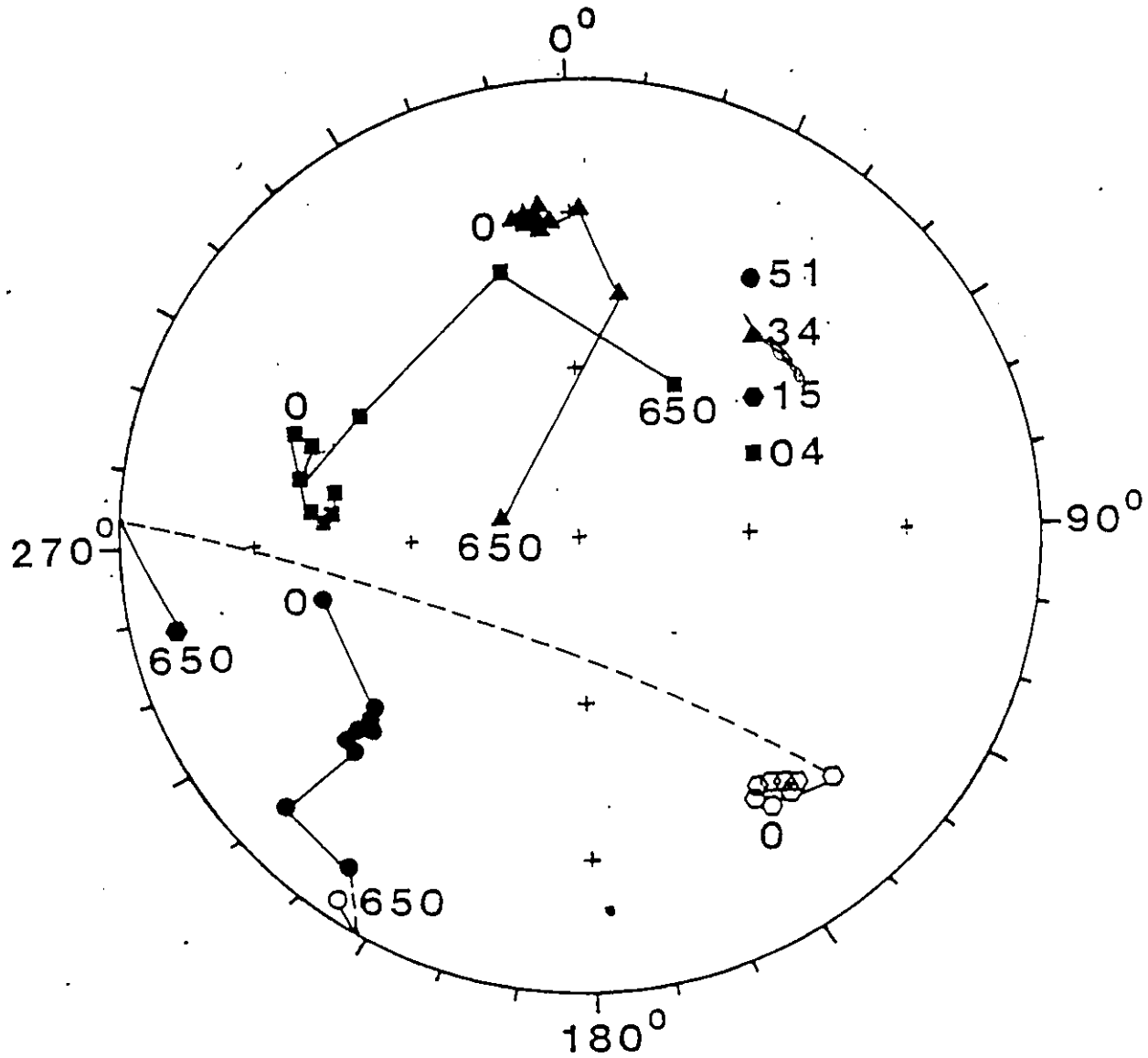


Fig. 42 Directional changes of thermal demagnetization on an equal area projection for HR pilot specimens.

Note: Change in direction on progressive thermal demagnetization at temperatures of 0, 100, 200, 300, 400, 450, 500, 550, 575, 600, 625, and 650°C for HR pilot specimens. Solid (open) symbols indicate down (up) directions.

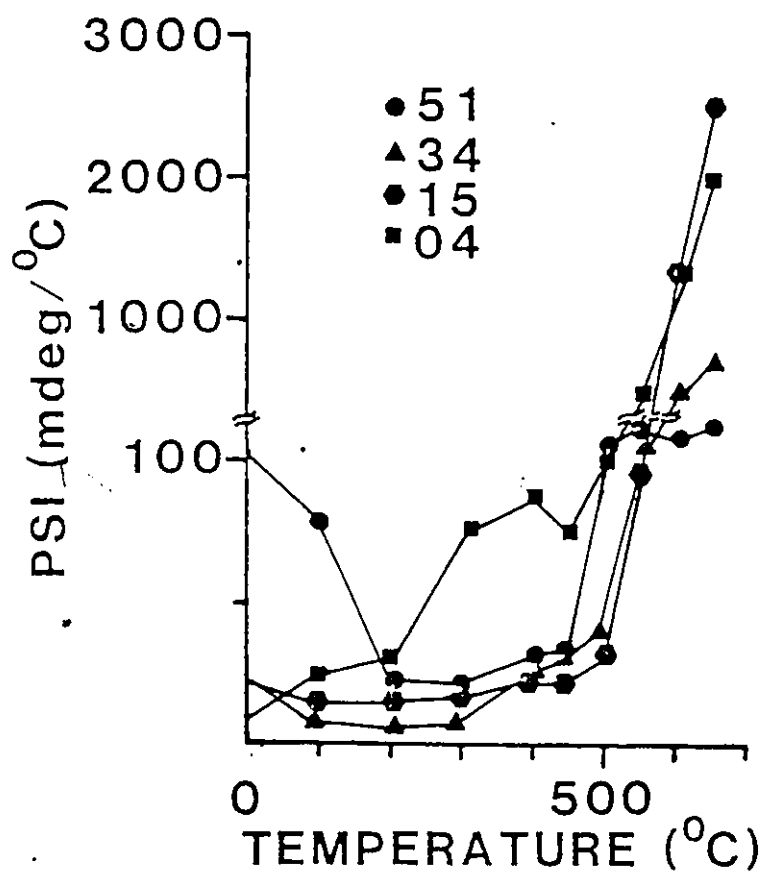


Fig. 43 HR thermal demagnetization curve - paleomagnetic stability index for directional changes.

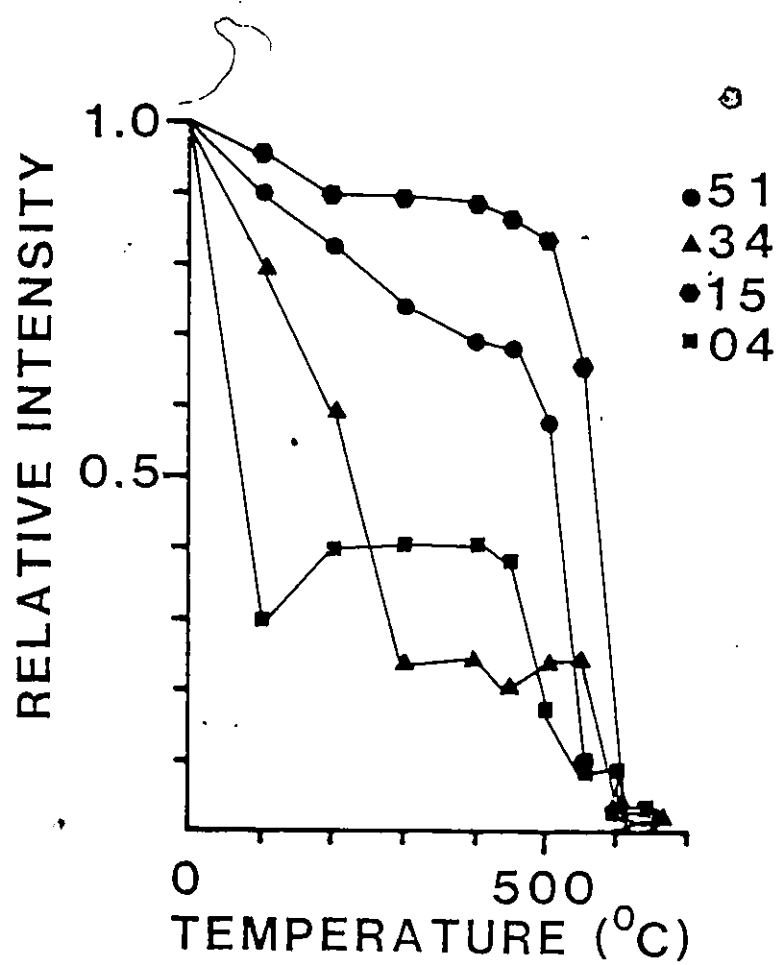


Fig. 44 HR thermal demagnetization curve-
relative intensity.

which might be caused by the presence of hematite or of single domain magnetite. Also they show a range of intensity reduction rates but all of them show ~98% of their intensity removed between 550°C to 600°C. When the surviving pilot specimens are plotted on a stereonet (Fig. 41) and grouped to compute their mean direction, they formed three poorly defined E, G, and H components. The summary of remanence directions of these components are given in Table 8. The remanence directions E, G, and H components that were isolated by thermal cleaning are in close agreement with E, G, and H components isolated by AF cleaning. The AF cleaned F component was not obtained by thermal cleaning process. Population level analysis of HR thermally cleaned pilot specimens was deemed inadequate because of the small number of specimens or vectors, i.e. 54.

4.11 DIKE-HR BAKED CONTACT TEST

On the intrusion of a dike, the HR near the contact is heated above the Curie temperatures of its magnetic minerals and it acquires the same remanence direction as the dike on cooling. The purpose of this contact test is two-fold:

(a) to provide information on the remanence stability of the HR, and

(b) to determine paleomagnetic age of dike intrusion.

Four basic dikes which range in size from 15 cm to 1 m

wide, intrude metavolcanics and quartz diorite in the study area. Their respective HR were sampled at a distance of ~50 m from the contact.

The AF cleaned mean remanence direction of the dikes, baked zones and HR are summarized in Table 10.

Dikes 7 and 32 indicate positive contact tests (Fig. 45a). Their remanence directions are similar to their corresponding baked zones and differ from the HR directions. This suggests that the remanence was acquired in the direction of dike near the contacts upon intrusion. Statistically different remanence directions are shown by HR in both cases which provides evidence that their remanence predate dike intrusion. Dikes 36 and 37 give similarly positive contact tests although the baked zone was not sampled (Fig. 45b). The paleomagnetic ages of the dike intrusions are discussed in the section 4.12 below.

4.12 PALEOMAGNETIC AGES OF THE ISOLATED REMANENT COMPONENTS

As previously discussed, the IF gives two stable pre-folding A and B components. The A and B components give apparent paleomagnetic ages (APA) that likely represent a primary and the secondary remanence respectively that IF acquired prior to deformation during Kenoran orogeny (Table 11). Figure 46 shows that the B component falls near the apparent polar wander-

TABLE 10
Results of Dike - HR Baked Contact Test

Site	Number of Specimens (N)	Length (R)	Decl. (Deg.)	Incl. (Deg.)	K	α_{95} (deg.)
07-dike	3	2.98	24.0	-42.8	96.84	12.6
07-baked zone	5	4.97	355.7	-44.0	118.98	7.0
05-HR (quartz diorite)	4	4.90	280.6	-34.6	39.43	12.0
32-dike	4	3.95	172.0	74.0	54.90	12.5
32-baked zone	2	2.00	170.7	73.5	240.60	16.0
32-part. baked zone	3	3.00	177.8	61.5	852.20	4.0
40-HR (metavolcanics)	4	3.93	203.0	27.0	43.50	14.0
42-HR (metavolcanics)	5	4.95	212.7	14.6	81.70	8.5
36-dike	5	4.93	223.0	-57.7	59.30	10.0
35-HR (quartz diorite)	5	4.93	246.0	-57.4	61.50	9.8
37-dike	3	2.93	286.0	-32.7	30.00	23.0
38-HR (quartz diorite)	7	7.90	255.0	-53.0	67.60	6.8

Notes: R is the length of vector resultant; K is the Fisher's (1953) precision parameter; α_{95} is the radius of 95% confidence (Fisher 1953).

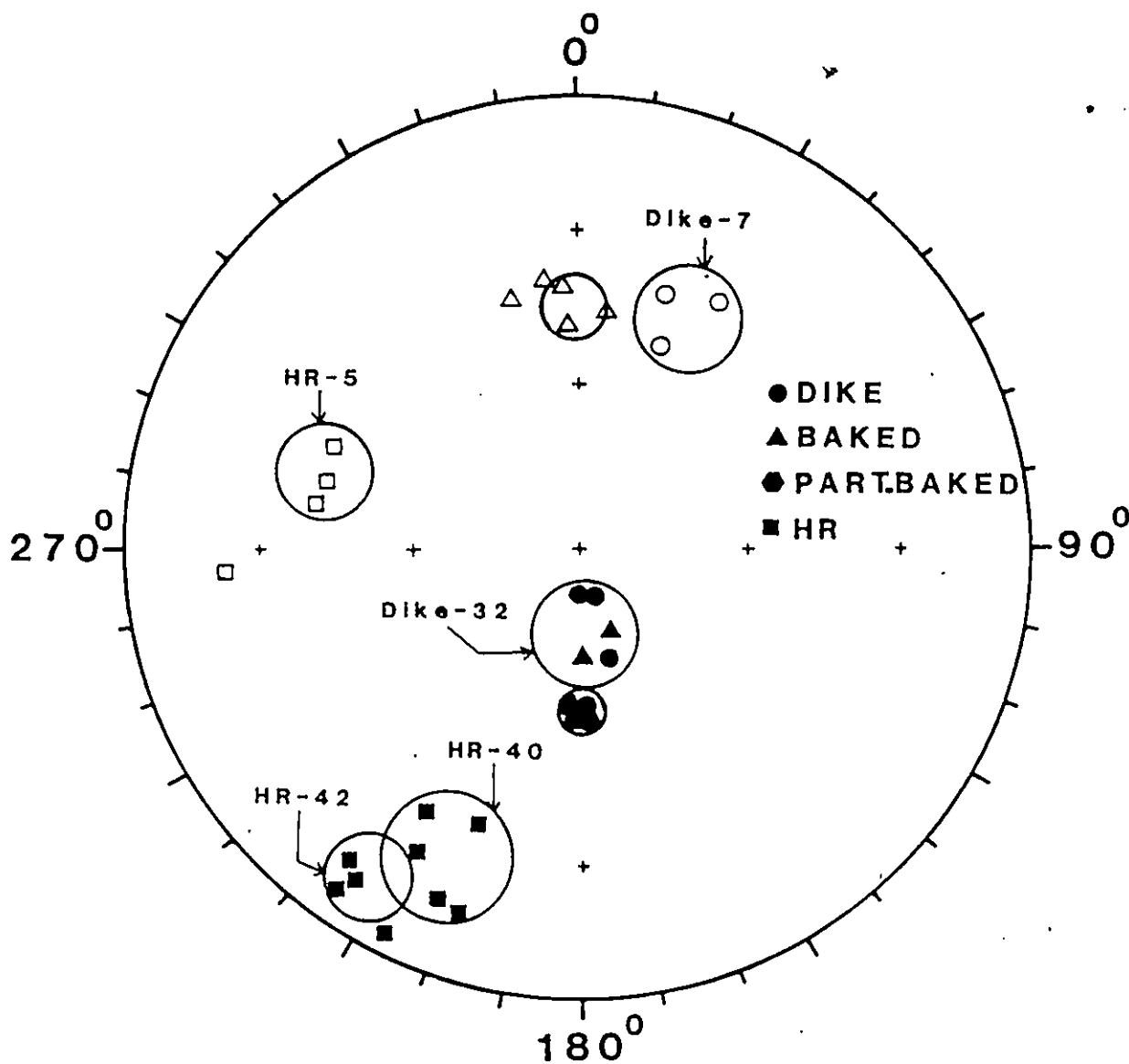


Fig. 45a Dike-HR baked contact test.

Note: Mean direction of dike, baked zone, partially baked zone and HR are shown with their circles of 95% confidence. Solid (open) symbols indicate down (up) directions.

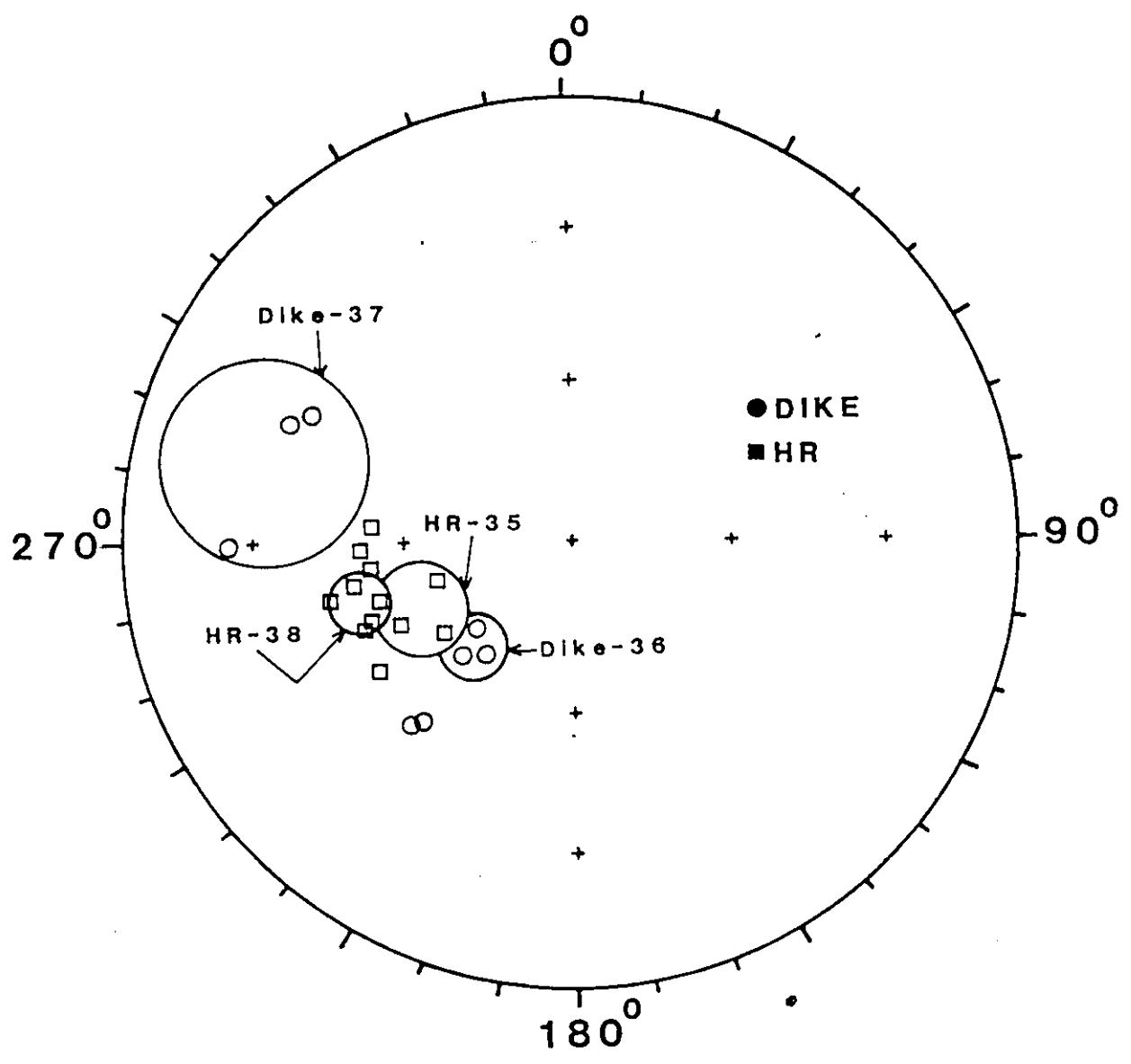


Fig. 45b Dike-HR baked contact test.

Note: Mean direction of dike and HR are shown with their circles of 95% confidence. Solid (open) symbols indicate down (up) directions.

TABLE 11
Paleomagnetic Pole Positions of the Griffith Mine

Group	Number of specimens (N)	Modal Directions				Paleomagnetic Pole Position				
		Length (R)	Decl. (deg)	Incl. (deg)	K	α_{95}	Long. ($^{\circ}$ W)	Lat. ($^{\circ}$ N)	d_p (deg)	d_m (deg)
<u>IF</u>										
A component	64	64.42	118.1	71.3	8.4	6.1	49.0	27.0	6.1	7.4
B component	100	94.10	207.5	37.2	14.5	3.9	300.0	14.5	2.6	4.5
C component	72	59.30	12.0	34.6	5.3	8.0	263.0	54.7	2.8	5.1
D component	144	53.06	214.4	72.0	1.6	15.5	112.8	21.2	24.0	27.0
<u>HR</u>										
E component	30	29.48	240.8	-28.0	56.5	3.5	349.8	29.8	2.1	3.9
F component	19	19.79	226.0	14.2	88.4	3.5	323.0	20.0	1.8	3.6
G component	50	28.29	164.2	-27.2	39.7	4.3	248.3	51.4	2.6	4.7
H component	67	63.90	200.0	82.5	21.3	3.8	100.0	36.5	2.9	4.9

NOTE: For the pole position the longitude and latitude are in degrees West (Long. $^{\circ}$ W) and North (Lat. $^{\circ}$ N) respectively, with d_p and d_m being the semi-axes of the oval of confidence along and perpendicular to the site-pole great circle.

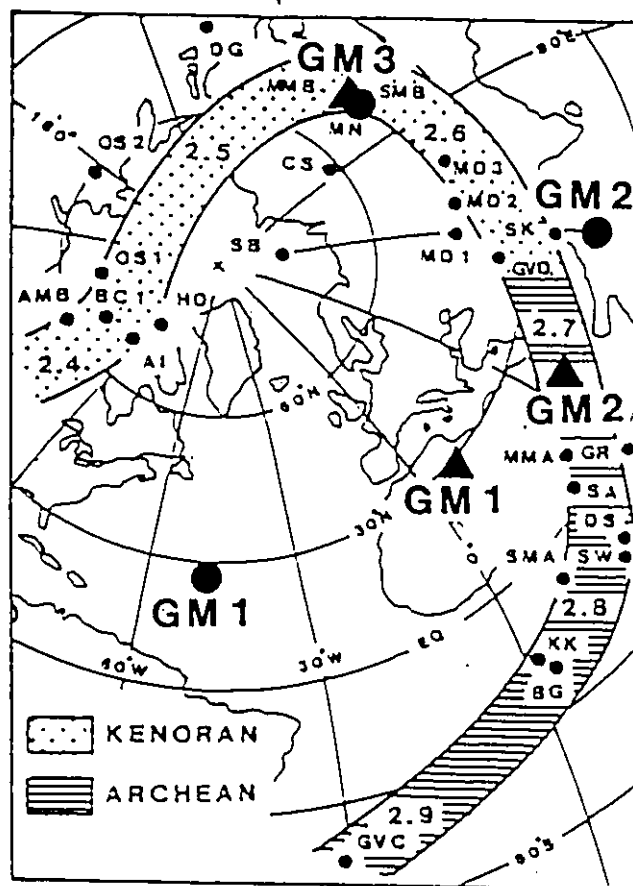


Fig. 46 Apparent polar wander (APW) curve (after Seguin, *et al.* 1982) showing the pole positions.

- indicates pole positions for iron formation.
- ▲ indicates pole positions for host rock.

ing (APW) path for this period (Seguin et al. 1982). Its location gives an APA of ~ 2.7 Ga. The oldest A component diverges significantly from A component poles of Sherman, Moose Mountain and Adams Mine IF. Microplate tectonics prior to the acquisition of the B components between various "greenstone belts" within the Superior Province may be an explanation for this discordance. The Griffith Mine is located within the Uchi greenstone belt whereas the other IF studied and pole positions for the APW path are derived from within the Abitibi greenstone belt. The paleomagnetic pole positions for the HR E and F components, for which the fold tests were inconclusive, fall at ~ 2.8 and ~ 2.7 Ga respectively near the APW path. These paleomagnetic ages are consistent within the range of 2.7 - 2.8 Ga for the radiometric dates of meta-volcanics and metasediments in the Confederation Lake area of Uchi greenstone belt near the study area (Nunes and Thurston, 1980).

The postfolding IF C component falls at ~ 2.6 Ga near the APW path. This remanence is thus likely a post-folding Kenoran orogenic remagnetization acquired when the Bruce Lake pluton was intruded into the volcanics. Significant IF baking is possible because there is evidence of partial melting from the baking effects of the Bruce Lake pluton in one localized eastern IF area (personal communication with Mr. Facca, Mine Geologist). The HR G component for which fold test was inconclusive gives a similar paleomagnetic age.

The paleomagnetic pole for the IF D and HR H component fall at ~ 2.0 Ga on the APW path of Irving (1979) (Fig. 47). This age is consistent with the postfolding D (=H) component indicated by the graphical fold test (Figs. 33a, b; 38a-39a). The postfolding nature is indicated by the fact that the uncorrected modal plots of the data defines the direction anomaly peak by $E + 12\sigma \pm \sigma$ contour for the HR and $E + 6\sigma \pm \sigma$ contour for the IF. In contrast, the directional anomaly peak after fold correction is defined by $E + 4\sigma \pm \sigma$ contour for HR and $E + 2\sigma \pm \sigma$ contour for IF. Thus clearly the uncorrected remanence data are significantly less dispersed. However, the 'modified' fold test for the modal plots where only remanence directions are selected that are enclosed with the $E + 2\sigma$ contour, indicates that the HR H component was acquired before folding. The IF D component shows that the fold test is inconclusive. Clearly this conclusion is incorrect and indicates that the 'modified' fold test does not always give correct conclusions. Obviously a more statistically justifiable fold test procedure needs to be developed for testing modal plots of paleomagnetic data.

The dike poles, except one, fall at or near the APW path of Irving (1979) (Fig. 48). Their locations suggest paleomagnetic ages ranging between ~ 1.7 to 1.9 Ga. These ages are consistent with ~ 1.9 Ga ± 50 Ma for the radiometric

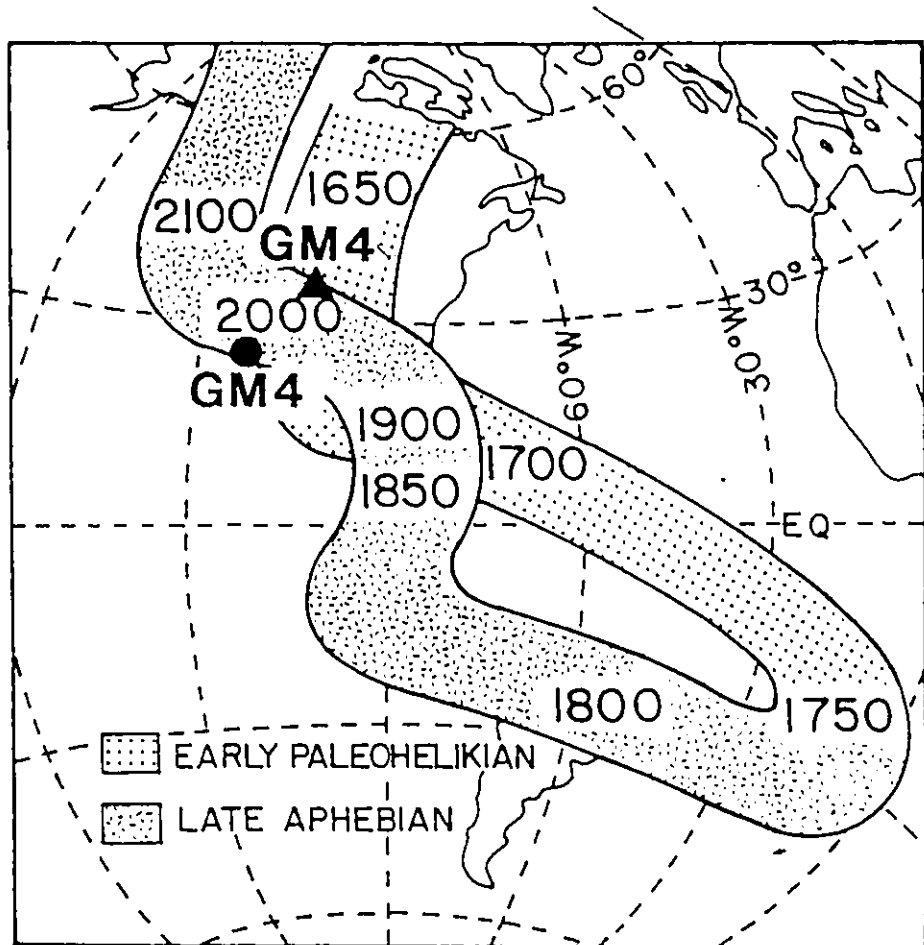


Fig. 47 Apparent polar wander (APW) curve (after Irving, 1979) showing pole positions

- indicates pole position for iron formation.
- ▲ indicates pole position for host rock.

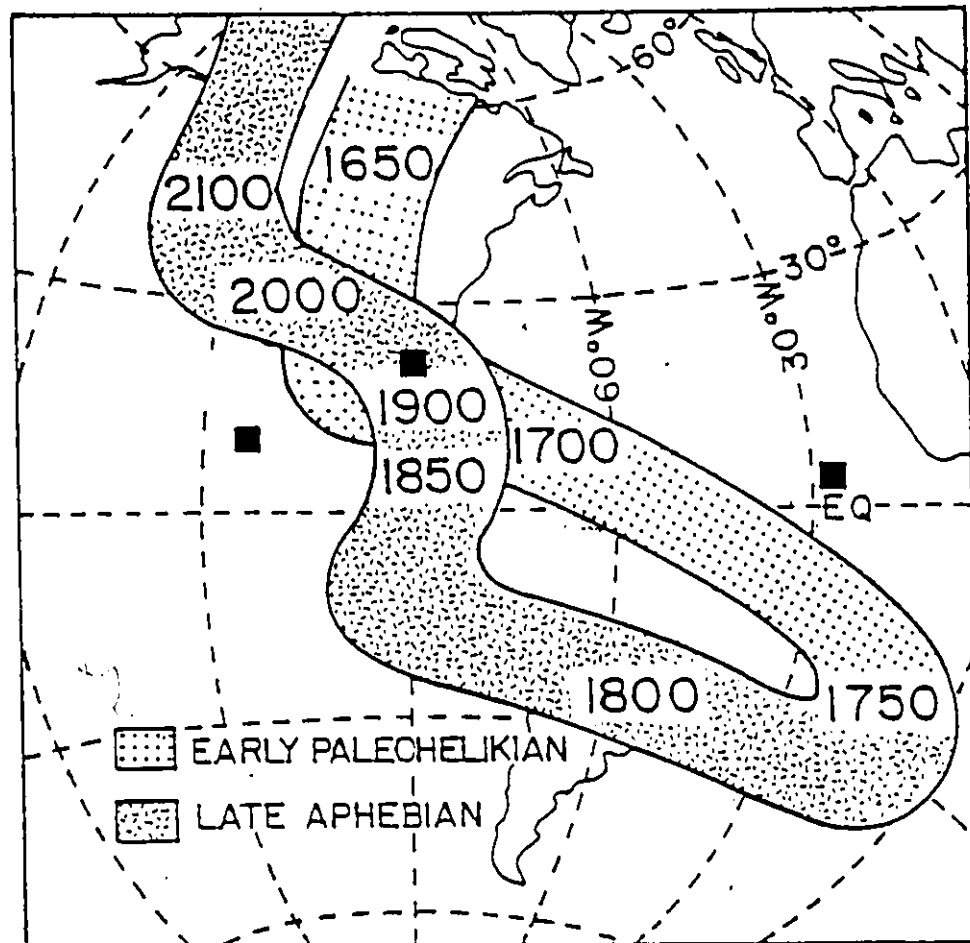


Fig. 48 Apparent polar wander (APW) curve (after Irving, 1979) showing pole positions for dike.

date of diabase dike in the English River Gneiss Belt (48.8°N, 94.1°W) near the study area (Wanless et al., 1968). Thus the dike remanence and probably the GM 4 (i.e., D and H components) component was possibly acquired when dikes intruded the HR during the Hudsonian orogeny.

4.13 MAGNETIC MODEL

4.13.1 Dipping Sheet of Infinite Strike Length

The computer model for the magnetic anomaly used in this study for the Griffith Mine IF uses dipping sheet equations for infinite strike length (Gay 1963) which include the following:

- 1) the EMF direction (5°, 78°) and intensity (60, 500 Y) (ODM-GSC 1960);
- 2) varied depth for the calculated curve (Fig. 49) until peak values agree for specified strike (N30°E), dip (85°E/W) and width (60 m);
- 3) the IF susceptibility (K_{\perp}) of 0.116 cgs/cm³;
- 4) the IF anisotropy of susceptibility of $K_{\parallel}/K_{\perp} = 1.45$;
- 5) a realistic demagnetizing factor of 2π (Gay 1963);
- 6) the NRM augmenting factor of 0.14 J_i or 14% increase (Strangway 1965); and
- 7) the terrain clearance of 147 m for the aeromagnetic anomaly.

The magnetic anomaly produced by the North pit is

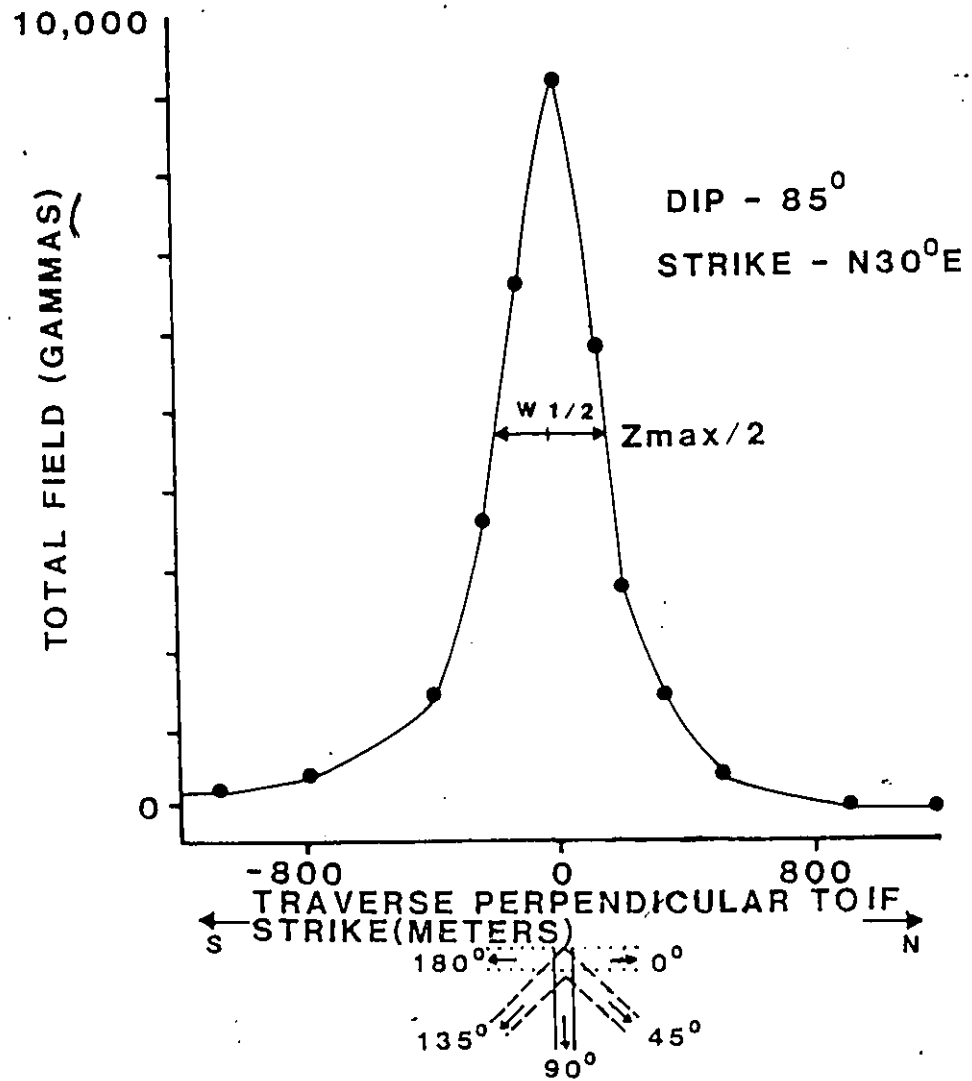


Fig. 49 Computed magnetic anomaly of IF at 147 m elevation (total field relative to background equal to zero).

used as an example of comparison between the theoretical and actual anomaly calculation. The computed peak anomaly for the North pit is 9,200 γ (Fig. 49). The measured peak value over the North pit is 70,000 γ . Subtraction of the background value of 60,500 γ gives a peak anomaly of 9,500 γ . Thus the calculated and measured peak value agrees to within 3%. This suggests that the best fitting model for this IF is infinite strike length of finite depth extent. The width of 60 m represents only high grade ore zone which was measured directly from the pit map. The observed and computed half-width ($W_{1/2}$) anomaly values, used as a depth extent for the North pit are 145 and 177 m respectively. Thus the calculated and observed $W_{1/2}$ agrees to within 18% from the height of the aircraft. Similar anomaly curves were found in the Sherman Mine (Symons and Stupavsky, 1979), Moose Mountain Mine (Symons, et al., 1980) and Adams Mine (Symons et al., 1981). Summary and comparison of the magnetic properties of the four deposits are shown in Tables 12a, b. Calculated and measured $W_{1/2}$ and peak anomaly values for the North and South pits are given in Table 13.

TABLE 12a

Summary and Comparison of Magnetic Properties of the Iron Formation at the Sherman, Moose Mountain, Adams and Griffith Mines

	Sherman	Moose Mountain	Adams	Griffith
1. Metamorphic grade	low greenschist	upper greenschist amphibolite	mid greenschist	upper green-schist amphibolite
2. Magnetic susceptibility k_{\perp} to bedding plane, k_{\perp} (cgs/cc)	0.096	0.110	0.065	0.116
3. Anisotropy of magnetic susceptibility, k_{11}/k_{\perp}	1.60	1.75	1.62	1.45
4. NRM remanence				
Magnetite	2.5×10^{-2}	4.8×10^{-2}	1.21×10^{-2}	2.1×10^{-2}
Hematite	4.0×10^{-6}	3.9×10^{-6}		
5. Koenigsberger ratio, Q	0.46	0.63	0.67	0.66
6. Effective Q, $Q_e = R/N \cos \theta$	0.22	0.24	0.14	0.14
7. AF demagnetized remanence (N and R components combined)	(170°, 0.1°, 5°)Pr (96°, -7°, 9°)Pr	(4°, 5°, 8°)Pr (81°, 6°, 6°)Pr (278°, 78°, 17°)Pr	(256°, 7°, 3°)Pr	(208°, 37°, 4°)Pr (118°, 71°, 6°)Pr (12°, 35°, 8°)Pr (214°, 72°, 15°) I

NOTE; Remanence directions given as (Decl., Incl., α_{95}). Pr = pre-folding at 95% confidence level; pt = post folding at 95% confidence level; I = inconclusive fold-test; *thermally cleaned inconclusive fold test. For details of the results listed, see text.

TABLE 12b

Summary and Comparison of Magnetic Properties of the Host Rock at the
 Sherman, Moose Mountain, Adams and Griffith Mines

	Sherman	Moose Mountain	Adams	Griffith
1. Magnetic susceptibility \perp bedding plane, k_{\perp} (cgs/cc)	4.9×10^{-5}	5.0×10^{-5}	2.35×10^{-4}	3.6×10^{-4}
2. NRM remanence (emu/cc)	2.94×10^{-6}	1.99×10^{-6}	5.97×10^{-6}	1.47×10^{-5}
3. Koenigsberger ratio, Q	0.104	0.063	0.013	0.051
4. AF demagnetized remanence (N and R components combined)	(168°, 9°, 8°)Pr (84°, 4°, 15°)I	(3°, 5°, 35°)I (82°, 3°, 28°)I	(305°, 79°, 4°)I (190°, 54°, 4°)I	(241°, -28°, 3°)I (226°, 14°, 3°)I (164°, -27°, 4°)I (200°, 82°, 4°)Pt

NOTE: Remanence directions given as (Decl., Incl., α_{95})

Pr = Prefolding at 95% confidence level; I = Inconclusive fold test; Pt = Post folding at 95% confidence level. For details of the results listed, see text.

TABLE 13
Summary of Aeromagnetic Response of IF

Pit	Strike (deg.)	Dip (deg.)	Width (m)	Peak Aeromagnetic Response @ 147 m			
				(γ) Observed		Computed	
				Peak Value	$W_{1/2}$	Peak Value	$W_{1/2}$
North	30	85	60	9,500	145	9,200	177
South	27	85	75	12,500	161	11,414	169

NOTE: Observed response from Map 861G Bruce Lake, Ontario (ODM-GSC 1960).

CHAPTER V

CONCLUSION AND RECOMMENDATIONS

From the preceding discussion, a number of conclusions can be drawn:

1. The close agreement between the Griffith Mine magnetic parameters and those of the Sherman, Moose Mountain, and Adams Mine (Tables 11a, b) suggests that the genesis of the four ore bodies was similar.

2. The similarity of magnetic characteristics for the four Algoma-type banded IF suggests, therefore, that the values may be representative of Algoma-type IF as a whole and may be used in magnetic anomaly computation for exploration purposes.

3. For anomaly interpretation purposes the HR NRM can be omitted because the induced magnetization of the IF is ~2170 times greater.

4. If the IF NRM directions were entirely aligned with the Earth's field, then the remanence would increase the induced anomaly by 66%. Thus the remanence intensity and direction may be important factors.

5. The close agreement between observed and expected anomalies is achieved using a model of infinite depth extent.

6. The present explorational rationale of only using the most intense vertical magnetizations as targets for examination is insufficient and unjustified.

7. A more logical approach to exploration is outlined:

(a) Locate potential area of interest from regional geology,

(b) determine regional strike and dip,

(c) using realistic values of susceptibility, anisotropy, demagnetization, remanence and depth, compute the type curves for the aeromagnetic anomaly for a number of thicknesses and depth extent.

(d) match observed magnetic anomalies with type curves, and,

(e) use detailed mapping and diamond drilling to put restraints on thickness, depth of burial and depth extent.

8. AF demagnetization of the IF results in the isolation of two pre-folding and one post-folding remanence component. The pre-folding A component is directed at $(118^\circ, 71^\circ)$, and the B component at $(208^\circ, 37^\circ)$. The post-folding C component is directed at $(12^\circ, 35^\circ)$.

9. Thermal demagnetization of the IF results in the isolation of an additional post-folding D component at $(214^\circ, 72^\circ)$ that is indicated by graphical fold test.

10. These components are different from those isolated at the Sherman, Moose Mountain, and Adams Mine IF after bedding tilt and plunge correction for fold. This is expected because this IF comes from the Uchi greenstone belt whereas the others come from the Abitibi belt.

11. AF demagnetization of HR results in the isolation of E, F, G, and H components. The E component is directed at (241°, -28°), the F component at (226°, 14°), the G component at (164°, -27°), and the H component at (200°, 82°).

12. The inferred paleomagnetic pole position for the IF A component is 49°W, 27°N ($d_p = 6^\circ$, $d_m = 7^\circ$), B component is 300°W, 14°N ($d_p = 3^\circ$, $d_m = 4^\circ$), C component is 263°W, 55°N ($d_p = 3^\circ$, $d_m = 5^\circ$), and D component is 113°W, 21°N ($d_p = 24^\circ$, $d_m = 27^\circ$). The A, B, and C components are based upon smoothing and contouring of AF demagnetization data at the population level. The D component is based upon smoothing and contouring of thermal demagnetization data at the population level. The A and B components give the apparent paleomagnetic ages (APA) that likely represent a primary and the secondary remanence respectively that IF acquired prior to deformation during Kenoran orogeny. The B component falls near the APW path. Its location gives an APA of ~2.7 Ga. The A component pole diverges significantly from the A component poles of

Sherman, Moose Mountain and Adams Mine IF. Microplate tectonics prior to the acquisition of the B components between various "greenstone belts" within the Superior Province may be an explanation for this discordance.

The Griffith Mine is located within the Uchi greenstone belt whereas the other IF studied and pole positions for the APW path are derived from within the Abitibi greenstone belt. The C component gives an age of ~2.6 Ga and likely associated with the intrusion of Bruce Lake pluton. The D component gives an age of ~2.0 Ga and is, perhaps, related to a post-Kenoran event.

13. The inferred paleomagnetic pole position for the HR E component is 350°W , 30°N ($d_p = 2^{\circ}$, $d_m = 4^{\circ}$), F component is 323°W , 20°N ($d_p = 2^{\circ}$, $d_m = 4^{\circ}$), G component is 248°W , 51°N ($d_p = 3^{\circ}$, $d_m = 5^{\circ}$), and H component is 100°W , 36°N ($d_p = 3^{\circ}$, $d_m = 5^{\circ}$). The paleomagnetic ages for these poles are similar to those obtained for IF.

14. The inferred paleomagnetic pole position for dike 7 is 116°W , 11°N ($d_p = 2^{\circ}$, $d_m = 4^{\circ}$), dike 32 is 89°W , 21°N ($d_p = 20^{\circ}$, $d_m = 23^{\circ}$), and dike 37 is 27°W , 4°N ($d_p = 15^{\circ}$, $d_m = 26^{\circ}$). The paleomagnetic ages for these poles ranging between ~1.7 to 1.9 Ga and is likely associated with the Hudsonian orogeny.

APPENDIX I

Computer Program for the Calculation of the
Magnetic Anomaly Over a Thin Sheet of
Infinite Strike and Depth Extent


```

0041 U=U-KFM
0042 DOTX=SIGN(U, DOTX)
0043 U=ABS(TOPY)
0044 KLA=AMOD(U, DT(2))
0045 U=U-KEN
0046 TOPY=SIGN(J, TOPY)+DT(2)
0047 DXP=10.20(1)
0048 DO 17 I=1,11
0049 XP(I)=0.01X+LUAT(I-1)+DXP
0050 WRITE(6,101)
0051 DY2=.51*DT(2)
0052 DO 22 JJ=1,51
0053 IF JJ=1
0054 DO 100 J=1,101
0055 A(J)=BLK
0056 YN=TOPY-FLUAT(1)+DT(2)
0057 DO 18 J=1,N
0058 IF (ABS(YN-Y(J))-GT.DY2) GO TO 18
0059 L=1+IFIX(.5+X(J)-DOTX)/DT(1)
0060 A(L)=C
0061 CONTINUE
0062 IF (MOD(I,5).EQ.0) GO TO 20
0063 WRITE(6,102) (A(J),J=1,101)
0064 GO TO 22
0065 WRITE(6,103) YH, (A(J),J=1,101)
0066 CONTINUE
0067 WRITE(6,104) (XP(I),I=1,11)
0068 PRINT,3
0069 PRINT,3
0070 WRITE(6,105) XHAX, XMIN, YMAX, YMIN, DT(1), DT(2)
0071 RETURN
0072 FORMAT(1H1, 10X, 20HPLOT RANGE 100 LARGE )
0073 FORMAT(1H1, 12X, 1HP, 10(9X, 1HP)/12X, 103(1HP))
0074 FORMAT(12X, 1HP, 101A1, 1HP)
0075 FORMAT(1X, 1HP, 3HP, 101A1, 2HP)
0076 FORMAT(12X, 10J(1HP)/4X, 11(9X, 1HP)/5X, 11(4X, F6.0))
0077 FORMAT(1X, 12X, 7HP, 2X, 7HP INCR =, F6.0, 2X, 7HP INCR =, F7.0//)
0078 EN
0079 END

```

FEU.1.2X, 01YMF

```

0001 DIMENSION V(100),Y(100),VD(100),NAME(40)
0002 DIMENSION VII(100),YI(100),YIT(100)
0003 FORMAT(4F10.0)
0004 DIMENSION X(50)
0005 FORMAT(40A2)
0006 FORMAT(F6.1,5F6.1,F10.7,2F6.1)
0007 FORMAT(110,12J11,TOTAL FIELD IN GAMMA5*INCLINATION+ANOMALY+STRIKE
0008 1+DIP+*V.DITH(H)+DEP(H)+CIRCS DIP MS*PARALLEL DIP MS+*RATIO
0009 2+
0010 4 FORAAI(110,5X,F8.1,13X,F6.1,14X,F6.1,F6.1,14X,F6.1,5X,F10.7
0011 1,5X,F10.7,3X,F7.3)
0012 PI=57.296
0013 READ1,NAME
0014 READ2,RINT1,RINCL1,STR,DIP,I,Z,S,R,U
0015 IF(RINT1)7,7,H
0016 RS=R+S
0017 S=S*(1,0+U)
0018 R=R+S
0019 RINCL=RINCL/PI
0020 STR=STR/PI
0021 DIP=DIP/PI
0022 RINCL=ATAN(TAN(RINCL)/SIN(STR))
0023 RINT=RINT1+SIN(RINCL)/SIN(STR)
0024 R=KINC-DIP
0025 H=ATAN(TAN(U)/H*(1.0+12.500*S))
0026 AMPLE=2.0*H*INT*(+COS(U)/Z+COS(H))
0027 AMPLE=AMPLE*SIN(S)
0028 H=41
0029 DUSI=1.14
0030 A=1
0031 Y(I)=(A-1.0)*B.0-60.0
0032 PSI=ATAN(Y(I)/Z)
0033 VV=COS(PSI)*(R+COS(PSI)*COS(H))+SIN(PSI)*SIN(H)
0034 VVII=COS(PSI)*(COS(PSI)*SIN(H))-R*SIN(PSI)*COS(H)
0035 V(I)=AMPLE*VV
0036 VII(I)=AMPLE*VVII
0037 Y(I)=V(I)*SIN(RINCL)+VII(I)*COS(RINCL)
0038 YI(I)=V(I)*SIN(RINCL)-VII(I)*SIN(RINCL)
0039 YIT(I)=SQR(Y(I)*Y(I)+YI(I)*YI(I))*ORIN(YIT(I))
0040 X(I)=V(I)
0041 CONTINUE
0042 STR=PI*STR
0043 DIP=PI*DIP
0044

```

```

0042 R(INC1)=PI*R(INC1)
0043 Q4=Q
0044 PRINT3
0045 PRINT4,R(NT1),R(INC1),STR,DIP,T,Z,S,NR,Q0
0046 PRINT501
0047 PRINT10,Y(1),Y(2),Y(3),Y(4),Y(5),Y(6),Y(7),Y(8)
0048 PRINT10,X(1),X(2),X(3),X(4),X(5),X(6),X(7),X(8)
0049 PRINT61
0050 PRINT10,Y(9),Y(10),Y(11),Y(12),Y(13),Y(14),Y(15),Y(16)
0051 PRINT10,X(9),X(10),X(11),X(12),X(13),X(14),X(15),X(16)
0052 PRINT61
0053 PRINT10,Y(17),Y(18),Y(19),Y(20),Y(21),Y(22),Y(23),Y(24)
0054 PRINT10,X(17),X(18),X(19),X(20),X(21),X(22),X(23),X(24)
0055 PRINT61
0056 CALL PL013(Y,TT,N)
0057 GO TO 9
0058 CALL EXIT
0059 STOP
0060 END

```

```

0042
0043
0044
0045
0046
0047
0048
0049
0050
0051
0052
0053
0054
0055
0056
0057
0058
0059
0060

```

REFERENCES

- BMDP-77, 1977. Biomedical computer programs P-series, Univ. Calif. Press, Berkley, Los Angeles, London, 215 p.
- Bruce, E. L., 1924. Geology of the upper part of the English River Valley. Ont. Dept. Mines, V. 33, 4, pp. 1-11.
- CDM, 1961. Isoclinic, isogonic and isodynamic charts, Canada. Can. Dept. Mines Tech. Surveys.
- Christie, K. W., and Symons, D.T.A., 1969. Apparatus for measuring magnetic susceptibility and its anisotropy. Geol. Surv. Canada, Paper 69-41, 10 p.
- Cisowski, S. M., and Fuller, M., 1978. The effects of shock on the magnetism of terrestrial rocks. J. Geophys. Res., V. 83, No. B7, pp. 3444-3447.
- Fisher, R. A., 1953. Dispersion on a sphere. Proc. Royal Soc. London, Series A, 217, pp. 295-305.
- Gay, S. P., 1963. Standard curves for interpretation of magnetic anomalies over long tabular bodies. Geophysics, V. 28, pp. 161-200.
- Helsley, C. E., 1973. Data selection and reliability of pole positions. Trans. Am. Geophys. Un., 54, p. 249.
- Irving, E., 1979. Paleopoles and paleolatitudes of North America and speculations about displaced terrains. Can. J. Earth Sci., V. 16, pp. 669-694.
- Kamb, W. B., 1959. Ice petrofabric observations from the Blue Glacier, Washington, in relation to theory and Experiment. J. Geophys. Res., V. 64, pp. 1891-1909.
- Larochelle, A., 1969. L'application de la statistique au paléomagnétisme. Geol. Surv. Can., Paper 68-59, pp. 1-19.
- Nunes, P. D., and Thurston, P. C., 1980. An absolute age framework for the stratigraphy of the Uchi-Confederation Lakes Metavolcanic-Metasedimentary belt, District of Kenora, Ont.. Ont. Geol. Surv., Misc. Paper 92, pp. 15-23.

- ODM-GSC., 1960. Bruce Lake, Kenora District, Ontario. Ont. Dept. Mines - Geol. Surv. Canada. Aeromagnetic Series, Map 861G, Scale 1 inch to 1 mile. Survey flown 1959.
- ODM-GSC., 1965. Lac Seul, Ontario. Ont. Dept. Mines - Geol. Surv. Canada. Aeromagnetic Series, Map 7123G, scale 1 inch to 4 miles. Survey flown 1960-1961.
- Quick, A. W., 1981. Component magnetization of the Iron Formation and deposits at the Adams Mine, Kirkland Lake, Ontario; unpublished M.Sc. thesis, University of Windsor, 118 p.
- Schelske, J. E., 1970. Mining at Griffith Mine. Can. Min. Mett. Bull., (CIM) Bull. for Nov., pp. 1279-1282.
- Seguin, M. K., 1976. Are Precambrian iron formations suitable for paleomagnetic studies? *Annales de Géophysique*, V. 32, pp. 327-324.
- Seguin, M. K., Sharma, K.N.M., Woussen, G., Seymour, K. St., Symons, D.T.A., 1982. Paleomagnetism of the Archean volcanism and proterozoic dikes in La Grande Rivière area of Nouveau, Québec. Submitted for publication in *Can. J. Earth Sci.*
- Shapiro, V. A., and Ivanov, N. A., 1966. Dynamic remanence and the effect of shock on the remanence of strongly magnetic rock. *Dokl. Akad. Nauk SSSR*, 173, pp. 6-8.
- Shklanka, R., 1968. Iron deposits of Ontario. Ont. Dept. Mines, Mineral Resources Circular, No. 11, p. 342.
- Shklanka, R., 1970. Geology of the Bruce Lake Area, District of Kenora, Ontario. Ont. Dept. Mines, Report 82, pp. 1-25.
- Stockwell, C. H., McGlynn, J. C., Emslie, R. F., Sanford, B. V., Norris, A. W., Donaldson, J. A., Fahrig, W. F., and Currie, K. L., 1976. Geology of the Canadian Shield; in *Geology and Economic Minerals of Canada*, Part A. Geol. Surv. Canada, Report No. 1, pp. 47-51.
- Strangway, D. W., 1965. Interpretation of the magnetic anomalies over some Precambrian dikes. *Geophysics*, V. 30, pp. 783-796.
- Symons, D.T.A., 1966. A paleomagnetic study on the Gunflint, Mesabi and Cayuna iron ranges in the Lake Superior region. *Econ. Geol.*, V. 61, pp. 1336-1361.

- Symons, D.T.A., 1967. Paleomagnetic evidence on the origin of the Marquette and Steep Rock hard hematite and goethite deposits. *Can. J. Earth Sci.*, V. 4, pp. 1-20.
- Symons, D.T.A., and Stupavsky, M., 1974. A rational paleomagnetic stability index. *J. Geophys. Res.*, V. 79, No. 11, pp. 1718-1720.
- Symons, D.T.A., and Stupavsky, M., 1979. Magnetic characteristics of the Iron Formation near Temagami, Ontario. *Ont. Geol. Surv., Misc. Paper 87*, pp. 133-147.
- Symons, D.T.A., and Stupavsky, M., 1980. Magnetic Anomaly type curves and paleomagnetism of the Algoman-type Iron Formation near Temagami, Ontario. *Ont. Geol. Surv., Misc. Paper 93*, pp. 215-219.
- Symons, D.T.A., Walley, D.S., and Stupavsky, M., 1980. Component magnetization of the Algoman iron formation and host rocks, Moose Mountain Mine, Ontario. *Ont. Geol. Surv., Misc. Paper 93*, pp. 198-214.
- Thurston, P.C., and Breaks, F. W., 1978. Metamorphic and tectonic evolution of the Uchi-English River subprovince; in *Metamorphism in the Canadian Shield*. *Geol. Surv. Canada, Paper 78-10*, pp. 49-62.
- Van Alstine, D. R., 1980. Analysis of the modes of directional data with particular reference to paleomagnetism. *Geophys. J. R. Astron. Soc.*, 61, pp. 101-113.
- Walley, D. S., 1980. Component magnetization of the Iron Formation and deposits at the Moose Mountain Mine, Capreol, Ontario; unpublished M.Sc. thesis, University of Windsor, 137 p.
- Wanless, R. K., Stevens, R. D., Lachance, G. R., and Rimsaile, J.Y.H., 1968. Age determinations and geological studies. *Geol. Surv. Canada, Report 8*.
- Watson, G. S., 1956. Analysis of dispersion on a sphere. *Monthly Notices Roy. Astron. Soc. London, Geophys. Suppl.*, No. 7, pp. 153-159.

VITAE AUCTORIS

\ Born: October 1, 1951, in Lucknow, Utter Pradesh, India.

Education:

High School:

Mumtaz Higher Secondary School, Lucknow, Utter-
Pradesh, India.

Intermediate College:

Shia Intermediate College, Lucknow, Utter Pradesh,
India.

University:

University of Lucknow, Lucknow, Utter Pradesh, India.
Bachelor of Science, 1971.

Aligarh Muslim University, Aligarh, Utter Pradesh,
India.

Master of Science in Geology, 1973.

Special Paper: Glaciology.

University of Windsor, Windsor, Ontario, Canada.

Master of Science in Geology, 1982.

Thesis topic: Component Magnetization of the Iron
Formation and Deposits at the Griffith
Mine, near Red Lake, Ontario. 1982.